In Vitro NMR Study of Magnetization Exchange at Low Field and Proteoglycan-Depletion at High Field in Articular Cartilage

by

Ghada Ahmed Khouqeer

A thesis
presented to the University of Waterloo
in fulfillment of the
thesis requirement for the degree of
Doctor of Philosophy
in
Physics

Waterloo, Ontario, Canada, 2016

AUTHOR'S DECLARATION

I hereby declare that I am the sole author of this thesis. This is a true copy of the thesis, including any required final revisions, as accepted by my examiners.

I understand that my thesis may be made electronically available to the public.

ABSTRACT

In Vitro NMR Study of Magnetization Exchange at Low Field and Proteoglycan Depletion at High Field in Articular Cartilage

Magnetization exchange between different spin reservoirs, or spin groups, in cartilage tissue is an important aspect of the use of Magnetic Resonance Imaging (MRI) in the early detection of osteoarthritis (OA). A low field (Larmor frequency of 30 MHz) NMR study of relaxation times in bovine articular cartilage was undertaken with the aim of elucidating details about magnetization exchange in this tissue.

A key element of successful multi-site exchange modeling is the availability of a sufficient number of apparent relaxation parameters to model the intrinsic multi- site exchange scenario. Two-Dimensional (2D) time domain NMR spin-lattice relaxation experiments in the laboratory frame (T_1 experiments) and the rotating frame ($T_{1\rho}$ experiments) were performed in articular cartilage, which allows for effective extraction of relaxation parameters from the composite NMR response from the heterogeneous cartilage tissue. 2D inversion recovery T_1 experiments using non-selective excitation and monitor pulses as well as selective excitation and non-selective monitor pulses were used.

The 2D relaxation results for each of the above experiments were then analysed for exchange by comparing the experimentally observed parameters to the apparent parameters, calculated from a set of intrinsic parameters, which were adjusted until a reasonable match was realized. In this multi-experiment approach the exchange results from one experiment can be used to corroborate the exchange results from another experiment.

In order to circumvent the considerable masking effect that the bulk water has on effective proton NMR characterization of cartilage macromolecular components, the above 2D relaxation-exchange analysis approach also was applied to bovine cartilage tissue in which H_2O was replaced with D_2O, as well as cartilage tissue in which the bulk water was frozen, so as to allow for the selective saturation of the ice proton magnetization. Combining relaxation times and magnetization exchange analyses results from the four cases, natural cartilage at 3^oC and -10^oC as well as deuterated cartilage at 3^oC and -10^oC, a 4-site exchange scenario involving water, proteoglycan (PG) and two collagen spin reservoirs, was arrived at for cartilage tissue. Approximate rates for magnetization exchange between macromolecule spins and water spins as well as for inter-macromolecule magnetization exchange are presented.

In addition, the present results have clearly demonstrated that at -10^oC, at which temperature the bulk water in the tissue is frozen, the collagen proton magnetization in the tissue exhibit a similar relaxation behavior as seen at 3^oC; *i.e.*, the collagen proton magnetizations do not appear to be appreciably affected by the freezing phase transition.

Loss of PG is an important indicator of early OA. An ideal MRI scheme for OA detection can be envisioned to involve the direct detection of the degradation of PG with progression of the disease, while at the same time monitoring the collagen content, which is not significantly affected by early OA and can be used as internal reference. In this part of the thesis, first, high field (Larmor frequency of 500 MHz) Magic Angle Spinning (MAS) NMR was used to monitor the changes in the PG spectra of the articular cartilage with dehydration, and with PG-degradation (using trypsin). Second, articular cartilage samples

were modified enzymatically to achieve different PG-depletion levels using the trypsin enzyme and then chemical shift imaging (CSI) was used to obtain the PG spectra and a static spectral experiment was performed to measure the broad collagen spectra. The ratio of the PG spectral area to that of the collagen spectral area defines PG content relative to collagen content. As the collagen content does not change appreciably for early OA, this approach provides a relative PG content, which is expected to be useful for *in vivo* OA detection.

ACKNOWLEDGEMENTS

I would like to thank my supervisor, Professors H. Peemoeller, for his guidance, motivation, encouragement, knowledge and support which he provided during my PhD program at his lab at the University of Waterloo.

I would like to thank Dr. Claude Lemaire for his help and guidance and assistance with the 500 MHz machine, and his helpful discussions.

I'm much appreciative to my colleague Joshua Crone for his help and kindness.

I would like to thank Imam Mohammad Ibn Saud University and the Saudi Government for granting me a full scholarship throughout my PhD program.

Words alone cannot express the thanks I owe to my husband Mazin. All I have achieved would not have been possible without the help and continuous support I have received from him.

I am heartily thankful to my children, Loujaine, AbdulAziz, Omar, Anan and Mohamed for giving me happiness and joy and being patient.

I am forever indebted to my parents, sister and brothers for their love, concern, and encouragement when it was most required.

Table of Contents

List of Figures

List of Tables

Chapter 1
Introduction

Articular cartilage (AC) tissue is a smooth, connective tissue made up mainly of collagen, proteoglycans and water [1-4]. AC is a complex tissue that works as a shock absorber and provides smooth surfaces for articulating joints. Unlike most tissues, AC has limited ability to repair itself due to the presence of only a relatively small number of chondrocytes (~ 5 % by volume). Chondrocytes are the only cells found in cartilage and are responsible for maintaining the cartilage matrix (collagen fibers and proteoglycans (PG)). With a view towards development of effective treatment protocols for osteoarthritis (OA), schemes for the early detection of OA are being sought after. Ideally such schemes should be noninvasive. Considerable literature exists on the development of early osteoarthritis (OA) detection schemes using noninvasive Magnetic Resonance Imaging (MRI) techniques. In addition, the dynamic and structural aspects of the macromolecular components of cartilage have been studied intensively over the last several decades using Nuclear Magnetic Resonance (NMR).

Although the macromolecular elements (largely PG at early stages) of articular cartilage tissue degrade as OA progresses, for practical reasons clinical MRI schemes typically monitor the tissue's bulk water proton relaxation behavior, which only indirectly reports on macromolecular degradation. A critical, missing link in this approach is an in-depth knowledge of a) the changes in PG behavior as detectable by magnetic resonance (MR) and b) the details of the pathway between PG and the bulk water that communicates relaxation information between the two. A first step towards elucidating (a) and (b) is to gain

insight into the dynamics and MR relaxation of the macromolecular components (PG and collagen) as well as bound water*, which are expected to play a key role in (b).

In this work, results from proton NMR relaxation experiments at a Larmor frequency of 30 MHz in deuterated and natural AC, both above and below freezing temperatures are reported. Deuteration allows detailed examination of the macromolecular proton NMR relaxation, while freezing the bulk water permits targeted study of the non-freezable, bound water. The magnetization exchange details and intrinsic relaxation parameters of the different components of the AC system have been ascertained through detailed two-dimensional NMR time domain relaxation measurements, combined with modeling of exchange modified relaxation in this tissue. This type of study requires relaxation measurements involving different time scales. To this end spin-spin relaxation times (T_2) as well as spin- lattice relaxation times at high field (T_1) and low field ($T_{1\rho}$) were studied and analyzed for exchange contributions.

A key aspect of early OA detection is sensitivity. Typical relaxation approaches do not monitor PG directly, but rather monitor changes in PG (degradation), with OA progression, indirectly by measuring changes in relaxation parameters of water protons. Here a technique that determines the PG/collagen ratio from a direct measurement of PG in cartilage and relating the PG content to collagen content as an internal reference is proposed. To demonstrate this technique, 500 MHz Magic Angle Spinning (MAS) NMR experiments, static NMR experiments, and Chemical Shift Imaging (CSI) experiments were performed in

*Bound water commonly is considered to be strongly associated with a (macromolecular) surface such that its dynamics are slowed down and restricted by orders of magnitude, and its freezing point is depressed by several degrees.

articular cartilage tissue, enzymatically degraded to various degrees. This PG/collagen ratio determination technique can be adapted to MRI in vivo measurements and shows potential for the early detection of OA.

The second chapter of this thesis introduces NMR basics, including the Zeeman, dipole-dipole, and chemical shift interactions. This chapter discusses the connection between NMR parameters and molecular dynamics as well as exchange in biological materials. In addition, the MAS and CSI techniques are introduced.

The third chapter is a review of bovine articular cartilage components and properties. This chapter also covers some of the literature of NMR of cartilage. Specifically, NMR and MRI studies of structural and dynamical aspects, as well as enzymatic modifications of PG in the cartilage tissue, are emphasized.

Chapter four explains the experimental and analysis methods for low field (30 MHz) and high field (500 MHz) NMR experiments, including sample preparations, and details of pulse sequences.

In the first part of chapter 5 the low field (30 MHz) NMR relaxation results are presented and discussed in terms of magnetization exchange models. In the second part of this chapter the high field (500 MHz) results are presented with a focus on the detection of changes in AC with degradation, by referring the changes to collagen content as an internal reference.

The conclusions are presented in chapter six.

Chapter 2
Nuclear Magnetic Resonance (NMR)

2.1 NMR Interactions

A nuclear spin, with magnetic moment $\boldsymbol{\mu}$, in a sample, can be subject to a number of different interactions [5-8]. These interactions can involve coupling between $\vec{\mu}$ and magnetic fields external to the sample, as well as such fields internal to the sample (produced by electrons and other nuclear spins). Within the context of this work each of the applicable interactions is best described by a Hamiltonian, $\mathcal{H}_{interaction}$. This study utilizes proton (^{1}H) NMR for which the NMR Hamiltonian can be expressed as the sum of applicable interaction Hamiltonians

$$\mathcal{H} = \mathcal{H}_Z + \mathcal{H}_J + \mathcal{H}_D + \mathcal{H}_{CS} \quad , \tag{2.1}$$

where $\boldsymbol{\mathcal{H}}_{\mathrm{Z}}$ is the Zeeman interaction, $\boldsymbol{\mathcal{H}}_{\mathrm{J}}$ is the J coupling, $\boldsymbol{\mathcal{H}}_{\mathrm{D}}$ is the dipole-dipole interaction, and $\boldsymbol{\mathcal{H}}_{\mathrm{CS}}$ is the chemical shift interaction. In a magnetic field of 2.5 T, typical magnitudes of these interactions, in Hz, are as follows: Zeeman ~ 10^8, Dipole- Dipole ~10^3, Chemical Shift ~ 10^3, and the J- Coupling ~ 10. Only the magnitudes of the Zeeman and chemical shift interactions depend directly on the magnitude of the external magnetic field.

The J coupling is orders of magnitude smaller than the other interactions of equation 2.1, and is not considered further in this work. In strong fields, the Zeeman interaction, which is responsible for the precession of the spins, is generally the dominant interaction. The interactions $\mathcal{H}_D \; and \; \mathcal{H}_{CS}$ can provide information on structure and dynamics of the

molecular system in which the spin system is imbedded. Each of the interactions $\mathcal{H}_Z$, $\mathcal{H}_D$ and $\mathcal{H}_{CS}$ are discussed further below.

2.1.1 Zeeman Interaction and Precession

Zeeman interaction occurs when a magnetic moment $\boldsymbol{\mu}$ is placed in a magnetic field $\boldsymbol{B_o}$, for which the energy of interaction is

$$E = -\boldsymbol{\mu} \cdot \boldsymbol{B_o} \ . \tag{2.2}$$

For a nucleus, quantum mechanics dictates that μ can take on discrete, quantized values only. If the magnetic field (B_o) lies along the *z*-axis, the Zeeman Hamiltonian of the nucleus is given by

$$\mathcal{H}_z = -\boldsymbol{\mu} \cdot \boldsymbol{B_o} = -\gamma \hbar B_o I_z \ , \tag{2.3}$$

where I_z is the z-component of the spin operator and γ is the gyromagnetic ratio defined as ratio of magnetic moment μ to the spin angular momentum $I\hbar$, with $I \equiv$ spin quantum number and $\hbar \equiv$ Plank's constant. The spin's eignstates are specified through the magnetic quantum number m, and have energies $E_m = -\gamma \hbar B_o m$ with $m = I, I-1, \ldots, -I$. In this study proton NMR is being used and for protons $I = ½$, so that in a magnetic field they can have either spin up ($m = +1/2$) or spin down ($m = -1/2$). The transition between these two energy states can be observed by the absorption or emission of radiant energy

$$\Delta E = \hbar \omega_o = \gamma \hbar B_o \ , \tag{2.4}$$

where ω_o is the Larmor frequency.

Technically, in the NMR experiment resonant transitions, from the lower to the higher energy level, are achieved by applying a time-dependent magnetic field oscillating, perpendicular to the main static field, at radio frequency (RF),

$$\omega = \omega_o = \gamma \hbar B_o \quad . \tag{2.5}$$

The time-dependent Hamiltonian describing this process is

$$\mathcal{H}_{perturbation} = -\boldsymbol{\mu} \cdot \boldsymbol{B_1} = -\gamma \hbar B_{1x} I_x cos(\omega t) \, , \tag{2.6}$$

where $\boldsymbol{B_1}$ is the RF field, with amplitude B_{1x}, along the *x*-axis in the rotating frame, and I_x is the correspondent spin transition operator between the two states.

2.1.2 Dipole-Dipole Interaction and Nuclear Spin Relaxation

Consider two spins with magnetic moments $\boldsymbol{\mu_1}$ and $\boldsymbol{\mu_2}$ and the interaction energy between them given by

$$E = \frac{\boldsymbol{\mu_1} \cdot \boldsymbol{\mu_2}}{r^3} - \frac{3(\boldsymbol{\mu_1} \cdot \boldsymbol{r})(\boldsymbol{\mu_2} \cdot \boldsymbol{r})}{r^5} \quad , \tag{2.7}$$

where $\boldsymbol{r}$ is the radius vector from $\boldsymbol{\mu_1}$ to $\boldsymbol{\mu_2}$. The interaction between N spins can be expressed by the dipolar Hamiltonian (Slichter, 1996)[6],

$$\mathcal{H}_D = \frac{1}{2} \sum_{j=1}^{N} \sum_{k=1}^{N} \left[\frac{\boldsymbol{\mu_j} \cdot \boldsymbol{\mu_k}}{r_{jk}^3} - \frac{3(\boldsymbol{\mu_j} \cdot \boldsymbol{r_{jk}})(\boldsymbol{\mu_k} \cdot \boldsymbol{r_{jk}})}{r_{jk}^5} \right] \quad , \tag{2.8}$$

where the $\boldsymbol{\mu}$**'s** are now the operators $\boldsymbol{\mu_i} = \gamma_i \hbar \boldsymbol{I_i}$**.** The dipolar Hamiltonian for a pair of spins, after transforming from Cartesians to spherical polar coordinates, can be written as:

$$\mathcal{H}_D = \frac{\gamma_1 \gamma_2 \hbar^2}{r^3}\{A + B + C + D + E + F\} \ , \tag{2.9}$$

where

$$\left.\begin{aligned} A &= I_{1z}I_{2z}(1 - 3cos^2\theta) \\ B &= -\frac{1}{4}(I_1^+ I_2^- + I_1^- I_2^+)(1 - 3cos^2\theta) \end{aligned}\right\} \quad \Delta E = 0 \ ,$$

$$\left.\begin{aligned} C &= -\tfrac{3}{2}(I_1^+ I_{2z} + I_{1z} I_2^+)\sin\theta\cos\theta e^{-i\varphi} \\ D &= -\frac{3}{2}(I_1^- I_{2z} + I_{1z} I_2^-)\sin\theta\cos\theta e^{i\varphi} \end{aligned}\right\} \quad \Delta E = \hbar\omega_o \ , \tag{2.10}$$

$$\left.\begin{aligned} E &= -\tfrac{3}{4} I_1^+ I_2^+ sin^2\theta e^{-2i\varphi} \\ F &= -\frac{3}{4} I_1^- I_2^- sin^2\theta e^{2i\varphi} \end{aligned}\right\} \quad \Delta E = 2\hbar\omega_o \ ,$$

with $I^+$and I^- being the raising and lowering operators. The A and B terms are known as secular terms of the dipolar Hamiltonian with zero energy transfer between spins and the lattice. The A term, together with the coupling constant ($\propto \frac{1}{r^3}$), can be thought of as representing a static z-component of the local magnetic fields produced by the other magnetic moment. B is the flip-flop term involving mutual spin flips of the two spins. Terms A and B are responsible for dephasing of the spins due to dipole-dipole interactions. All other terms C, D, E, and F are known as non-secular terms of the dipolar Hamiltonian and involve energy exchange between spins and the lattice. The C and D terms correspond to one quantum transition, while the E and F terms correspond to two quantum transitions.

In this thesis nuclear spin relaxation plays an important role and the following presents a brief summary of relaxation relations being considered later in the Results and Discussion chapter.

The time evolution of the magnetization along the z-direction, M_z (t), can be ascertained by finding $\frac{d<I_z>(t)}{dt}$, where $<I_z>$ is the expectation value of I_z. Abragam [5] gives that for two identical spins I

$$\frac{d < I_z >}{dt} = -\frac{1}{T_1}[< I_z > - < I_z >_0] \quad , \tag{2.11}$$

where $<I_z>_0$ is the expectation value of I_z at thermal equilibrium and T_1 is the spin-lattice relaxation time. Within the present context lattice implies all non-spin degrees of freedom; e.g., motional modes of molecules carrying the spins. It can be shown [5] that

$$\frac{1}{T_1} = \frac{3}{2}\gamma^4\hbar^2 I(I+1)[J^1(\omega) + J^2(2\omega)] \quad , \tag{2.12}$$

where $J^{|q|}(|q|\omega)$ are the spectral density functions, which are a measure of the power available for transitions through $J^{|q|}(|q|\omega)d\omega$. The parameter q takes on values 0 (corresponding to A + B of equation 2.9), ± 1 (corresponding C or D of equation 2.9), and ± 2 (corresponding to E or F of equation 2.9).

The spectral density functions are the Fourier transforms of the autocorrelation function, $G^{(q)}(\tau)$, defined as $< F^{(q)}(x(t))\, F^{*(q)}(x(t+\tau)) >$, where x is a lattice coordinate, τ is a time interval, and F is a spin-lattice interaction, such as dipole-dipole interaction. The

brackets < > denote ensemble average. In effect the correlation function measures how a parameter, such as x, at time $t + \tau$, is correlated to its value at time t. Assuming a random Markovian process for the x-coordinate, the correlation function can be written as,

$$G^{q}(\tau) =< |F^{q}|^2 > e^{-\frac{\tau}{\tau_c}} \quad , \tag{2.13}$$

where τ_c is the correlation time characterizing the time scale of the motion. Then, the Fourier transform of the correlation function leads to the following expression

$$J^{|q|}(|q|\omega) =< |F^{|q|}|^2 > \frac{2\tau_c}{1 + (|q|\omega)^2\tau_c^2} \quad . \tag{2.14}$$

Considering rigid molecules for which the internuclear distance is constant, it can be shown that combining equations 2.12, and 2.14 leads to the following spin-lattice (longitudinal) relaxation rate $R_1 = 1/T_1$, given by [5]

$$\frac{1}{T_1} = C\left[\frac{\tau_c}{1 + \omega^2\tau_c^2} + \frac{4\tau_c}{1 + 4\omega^2\tau_c^2}\right] \quad , \tag{2.15}$$

where C is the interaction strength between the nuclei and is given by

$$C = \frac{2}{5r^6}\gamma^4 I(I + 1) \quad .$$

The time evolution of M_x can be ascertained from [$<I_z>$ (t)]. Abragam [5] gives

$$\frac{d < I_x >}{dt} = -\frac{1}{T_2} < I_x > \quad ,$$

where the spin-spin (transverse) relaxation rate $R_2 = 1/T_2$, is given by

$$\frac{1}{T_2} = \frac{C}{2}\left[3\tau_c + \frac{5\tau_c}{1 + \omega^2\tau_c^2} + \frac{2\tau_c}{1 + 4\omega^2\tau_c^2}\right] \quad . \tag{2.16}$$

In the spin-lattice relaxation time (T_{1x}) experiment in the rotating frame a low-power RF field $\boldsymbol{B_1}$ (t) is applied at resonance, perpendicular to $\boldsymbol{B_0}$. If we assume that $\boldsymbol{B_1}$ is applied along the *x*-axis in the rotating frame then the magnetization M_x in the rotating frame will decay along the *x*-axis with a relaxation rate $1/T_{1x}$, which for two identical spins on a rigid molecule, is given by [9]

$$\frac{1}{T_x} = \frac{C}{2}\left[\frac{3\tau_c}{1+4\omega_1^2\tau_c^2} + \frac{5\tau_c}{1+\omega^2\tau_c^2} + \frac{2\tau_c}{1+4\omega^2\tau_c^2}\right] \quad . \tag{2.17}$$

Considering Arrhenius behavior, the correlation time τ_c will have a temperature dependence given by,

$$\tau_c = \tau_0 e^{E_a/k_B T} \quad , \tag{2.18}$$

where E_a is the activation energy and k_B is Boltzmann's constant. Figure 2.1 shows plots of T_1, T_2 and T_{1x} as function of 1000/T for a bulk water molecule. It may be noted that expressions 2.15 and 2.16, for two identical spins on a rigid molecule undergoing isotropic motion (single correlation time), were first derived by Bloembergen, Purcell and Pound (1948) and are commonly referred to as the BPP relaxation time expressions [9, 10].

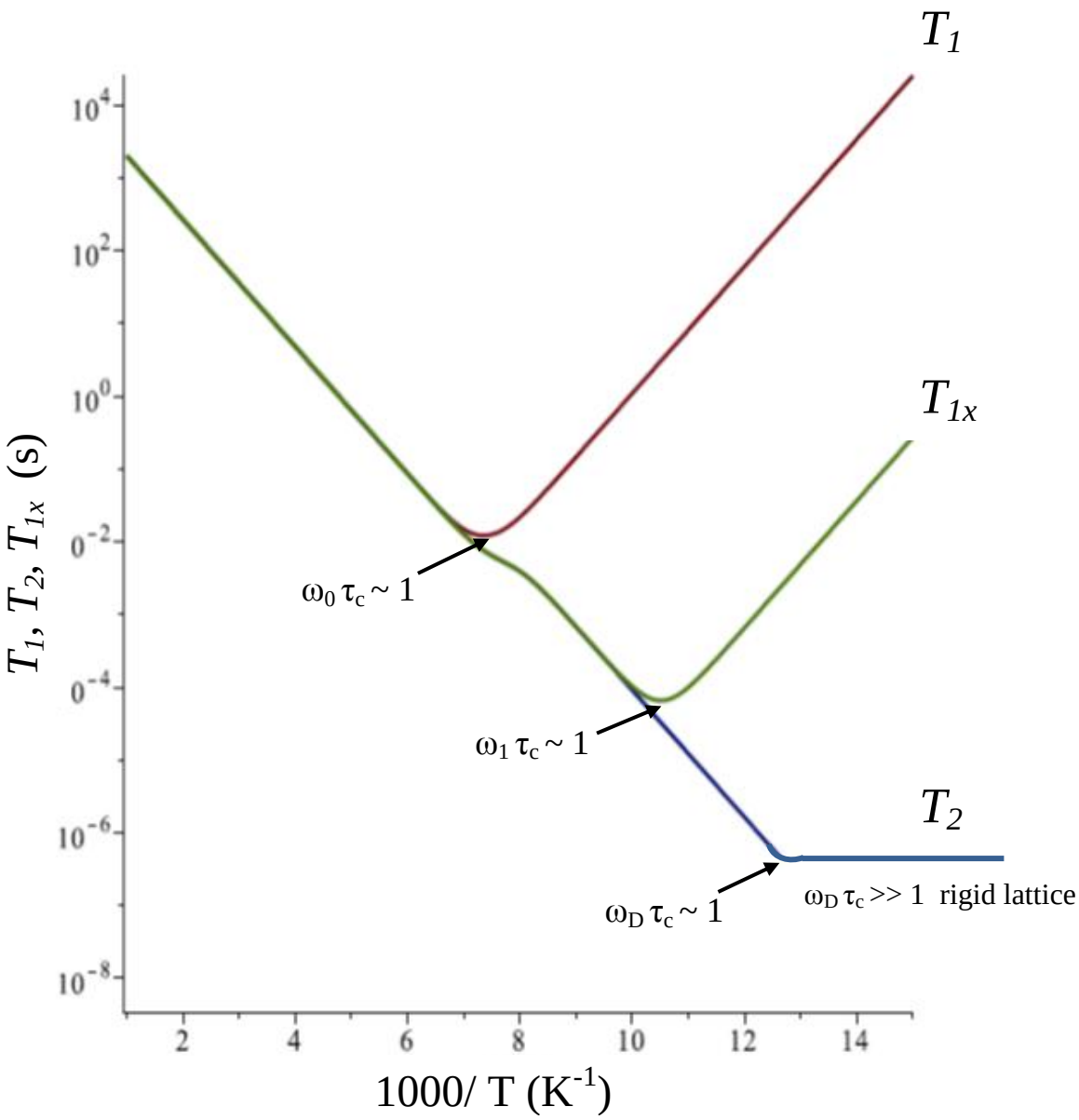

Figure 2.1 Behavior of bulk water proton relaxation times T_1, T_2 and T_{1x} as a function of inverse temperature. ω_D is the dipolar frequency.
Adapted from N. Bloembergen, E. M. Purcell, R. V. Pound " Relaxation Effects in Nuclear Magnetic Resonance Absorption" [10].

2.1.3 Chemical Shift Interaction and the Chemical Shift

If a molecule is placed in an external magnetic field $\boldsymbol{B_0}$, the field will induce currents in the electron cloud of the molecule. The resulting induced magnetic field, internal to the molecule, opposes the external field, so that the net field seen by the molecule's nuclei is less than $\mathbf{B_o}$; i.e., the nuclei are shielded. Then, to achieve resonance at a frequency $\omega_0 = \gamma \mathbf{B_o}$ (case where zero induced field exists), the applied field needs to be increased. Or, if the applied field is kept fixed at $\boldsymbol{B_o}$, the frequency of the RF excitation needs to be decreased. The effective (local) magnetic field, experienced by the nucleus, is given by

$$\boldsymbol{B_{eff}} = \boldsymbol{B_0} + \boldsymbol{B_{induced}} = (1 - \sigma)\boldsymbol{B_0} \quad , \tag{2.19}$$

where σ is a shielding parameter.

This means that the local resonance frequency is $\nu = \nu_0(1 - \sigma)$. The chemical shift scale δ is arrived at by using a reference sample (often tetramethylsilane (TSM), Si $(CH_3)_4$) with its resonance frequency $\nu_{reference}$:

$$\delta\ (ppm) = \ 10^6 \frac{\nu_{sample} - \nu_{reference}}{\nu_{reference}} \quad . \tag{2.20}$$

Fig. 2.2 gives the proton chemical shift ranges for various functional groups. It may be noted that the chemical shielding parameter σ signifies an absolute shift in local field, relative to its value in the absence of any induced field. For $\sigma << 1$, we can also write

$$\delta\ (ppm) = 10^6\left(\sigma_{reference} - \sigma_{sample}\right).$$

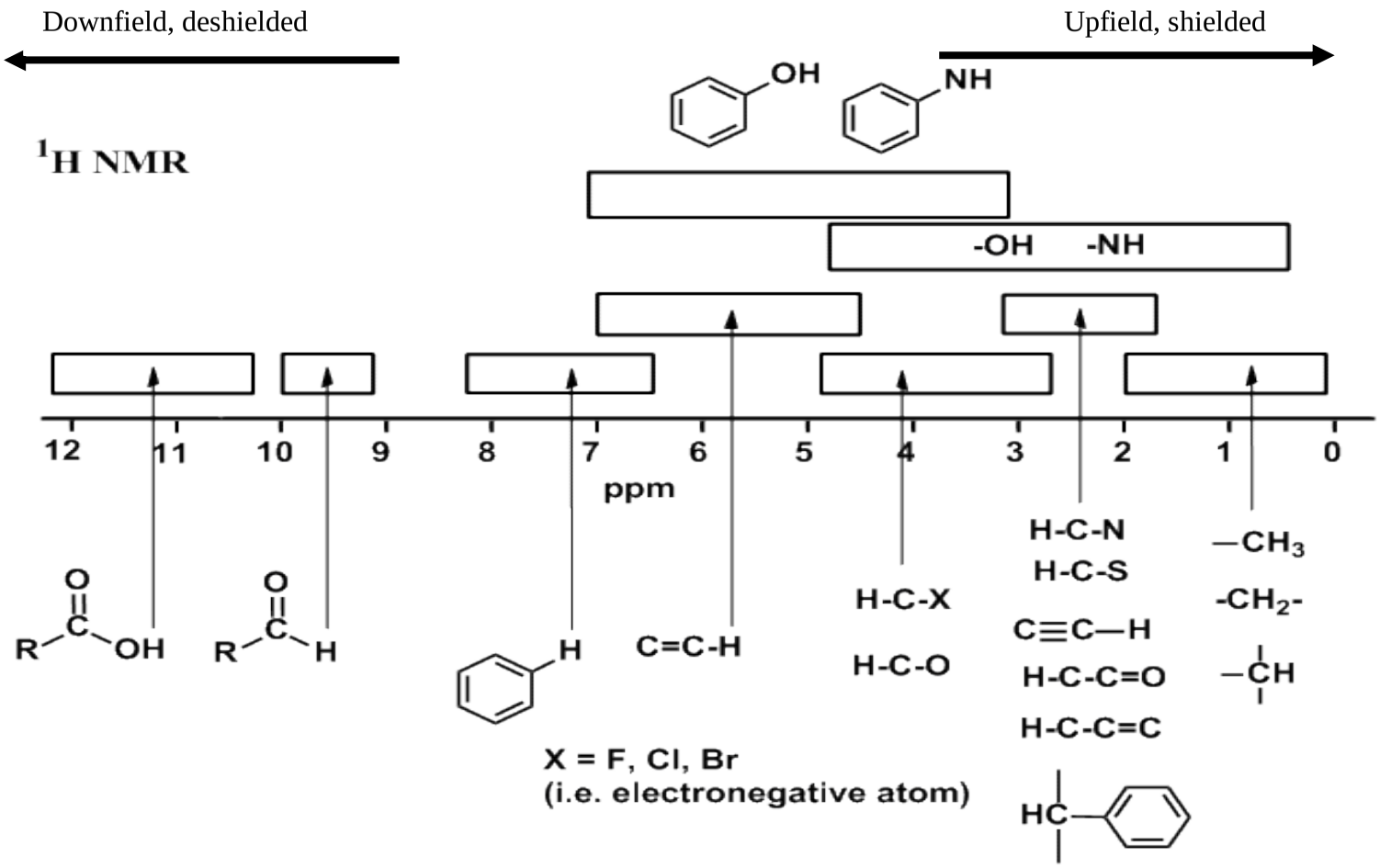

Figure 2.2 Proton NMR chemical shifts (δ in ppm) for common functional groups. This diagram was presented by Dr. Ian Hunt. [http://www.chem.ucalgary.ca/courses/351/Carey5th/Ch13/ch13-nmr-3b.html], (with permission).

In general, the molecular electronic cloud will not exhibit spherical symmetry with respect to any particular nucleus in the molecule. As a result $\boldsymbol{B_{induced}}$ at any particular nucleus will depend on the orientation of the molecule with respect to $\boldsymbol{B_0}$, as well as on the position of the nucleus in the molecular structure. Therefore, in general the chemical shielding will be anisotropic, given by a second rank tensor, which for a given orientation of the molecule in the laboratory frame (*xyz)*, can be written

$$\sigma = \begin{bmatrix} \sigma_{xx} & \sigma_{xy} & \sigma_{xz} \\ \sigma_{yx} & \sigma_{yy} & \sigma_{yz} \\ \sigma_{zx} & \sigma_{zy} & \sigma_{zz} \end{bmatrix} . \tag{2.21}$$

Considering that $\mathcal{H}_{cs} = \boldsymbol{\mu} \cdot \boldsymbol{B_{induced}}$ we have

$$\mathcal{H}_{cs} = \gamma \hbar \boldsymbol{B_o} \cdot \boldsymbol{\sigma} \cdot \boldsymbol{I} \ , \tag{2.22}$$

where γ is the gyromagnetic ratio, $\hbar$ is Plank's constant and *I* is the spin operator.

$\mathcal{H}_{cs}$ can produce shifts in resonance frequencies, which may lead to a spectrum that provides information about the chemical shift tensor. This in turn may lead to information about the structure of the molecule on which the spins reside.

It is possible to define a Principal Axis System (PAS), fixed in the molecule, such that the shielding tensor becomes diagonal. Let the PAS be defined by X, Y and Z and the corresponding shielding tensor components be σ_{XX}, σ_{YY} and σ_{ZZ}. The geometry involved is shown in Fig. 2.3.

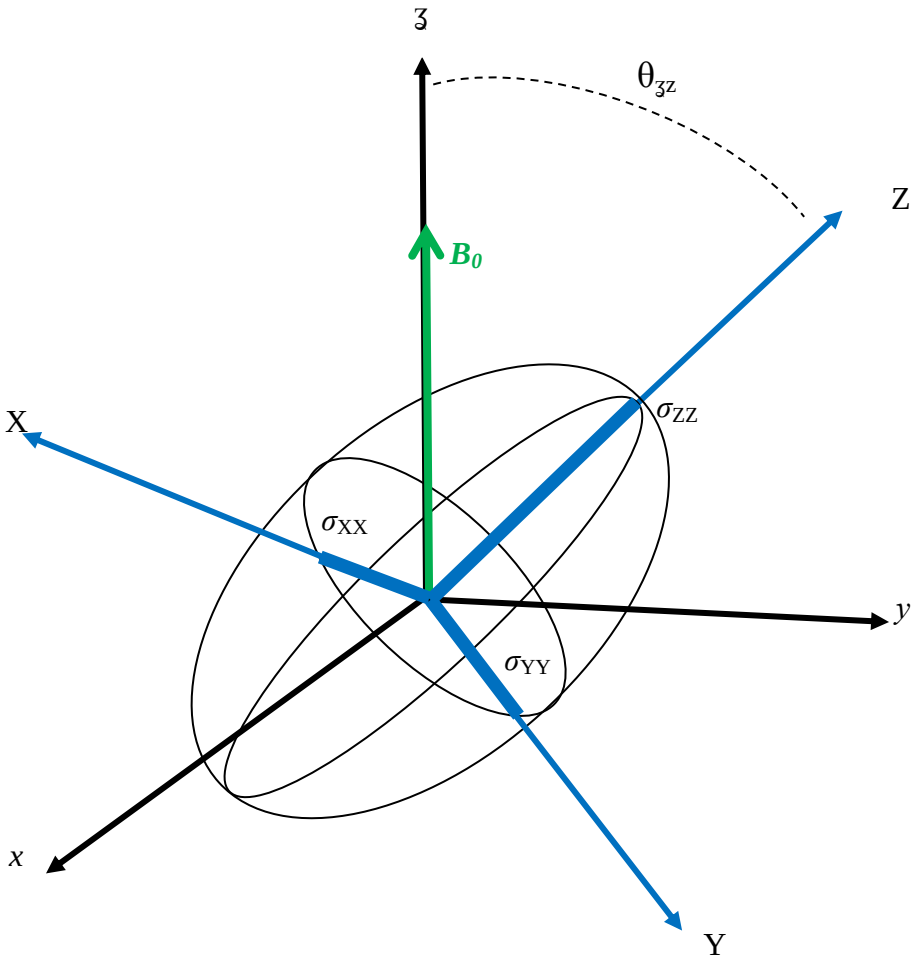

Figure 2.3 Diagram showing axes defining the laboratory (*x*, *y*, *z*) and the PAS (X, Y, Z), frames as well the principal components of the chemical shielding tensor.
Adapted from Chemwiki.

In the principal axes system

$$\sigma^{PAS} = \begin{bmatrix} \sigma_{XX} & 0 & 0 \\ 0 & \sigma_{YY} & 0 \\ 0 & 0 & \sigma_{ZZ} \end{bmatrix}. \tag{2.23}$$

In high field NMR experiments one typically measures only the secular part of the chemical shift interaction (excluding terms containing I_x and I_y); *i.e.*, effectively σ_{zz}, in the laboratory frame. The components of the shielding tensor in the laboratory frame can be obtained from those in the PAS frame using rotation matrices where the transformation involves rotations about each coordinate axis in turn. A convenient development is presented by Stejskal and Memory [11]. Letting the angles between the principal axes of the shielding tensor and $\boldsymbol{B_0}$ be $\theta_{\mathfrak{Z}X}$, $\theta_{\mathfrak{Z}Y}$, $\theta_{\mathfrak{Z}Z}$ they give

$$\sigma_{\mathfrak{Z}\mathfrak{Z}} = \sigma_{XX} cos^2\theta_{\mathfrak{Z}X} + \sigma_{YY} cos^2\theta_{\mathfrak{Z}Y} + \sigma_{ZZ} cos^2\theta_{\mathfrak{Z}Z} \ . \tag{2.24}$$

For fast, random motion, this becomes [11]

$$\sigma_{\mathfrak{Z}\mathfrak{Z}} = \sigma_{iso} = \frac{1}{3}(\sigma_{XX} + \sigma_{YY} + \sigma_{ZZ}) = \frac{1}{3} Tr\{\boldsymbol{\sigma}\} \ . \tag{2.25}$$

This is also referred to as the isotropic chemical shift, which is typically measured in liquids [11].

2.2 Magnetization Exchange in Biological Material

A “spin group” is a group of spins which exhibit the same relaxation characteristics, the spins involved experiencing a similar structural and dynamic environment. The sum of the proton signals from all spin groups in the sample will make up the observed proton NMR signal. Under ideal conditions the NMR signal can be decomposed into components representing the individual spin groups. Then, the intrinsic NMR characteristics of individual spin groups, in the different environments can be studied to deduce information about molecular structure and dynamics.

In the presence of magnetization exchange, the observed relaxation rates and sizes of different spin groups may deviate from the intrinsic values. Instead, the evolution of the magnetizations involved is modified by exchange, so that only the apparent relaxation parameters are observed. The distinction between intrinsic and apparent parameters is described schematically in Figure 2.4 for a 2-site case consisting of a site "a" with intrinsic, equilibrium magnetization M_a and intrinsic spin-lattice relaxation rate R_a, and a site "b" with corresponding parameters M_b and R_b. With exchange, the observed rates and fractions are determined by the M’s and R’s, as well as, the exchange rates (k’s), and are called the apparent relaxation rates (λ’s) and apparent magnetization fractions (C’s), respectively. Then, information about the molecular dynamics and structure of the spin groups cannot be obtained directly from the observed relaxation rates and magnetization fractions. Under favorable conditions intrinsic relaxation parameters, or relaxation information, can be extracted from the observed, or apparent, parameters through exchange analysis [12, 13].

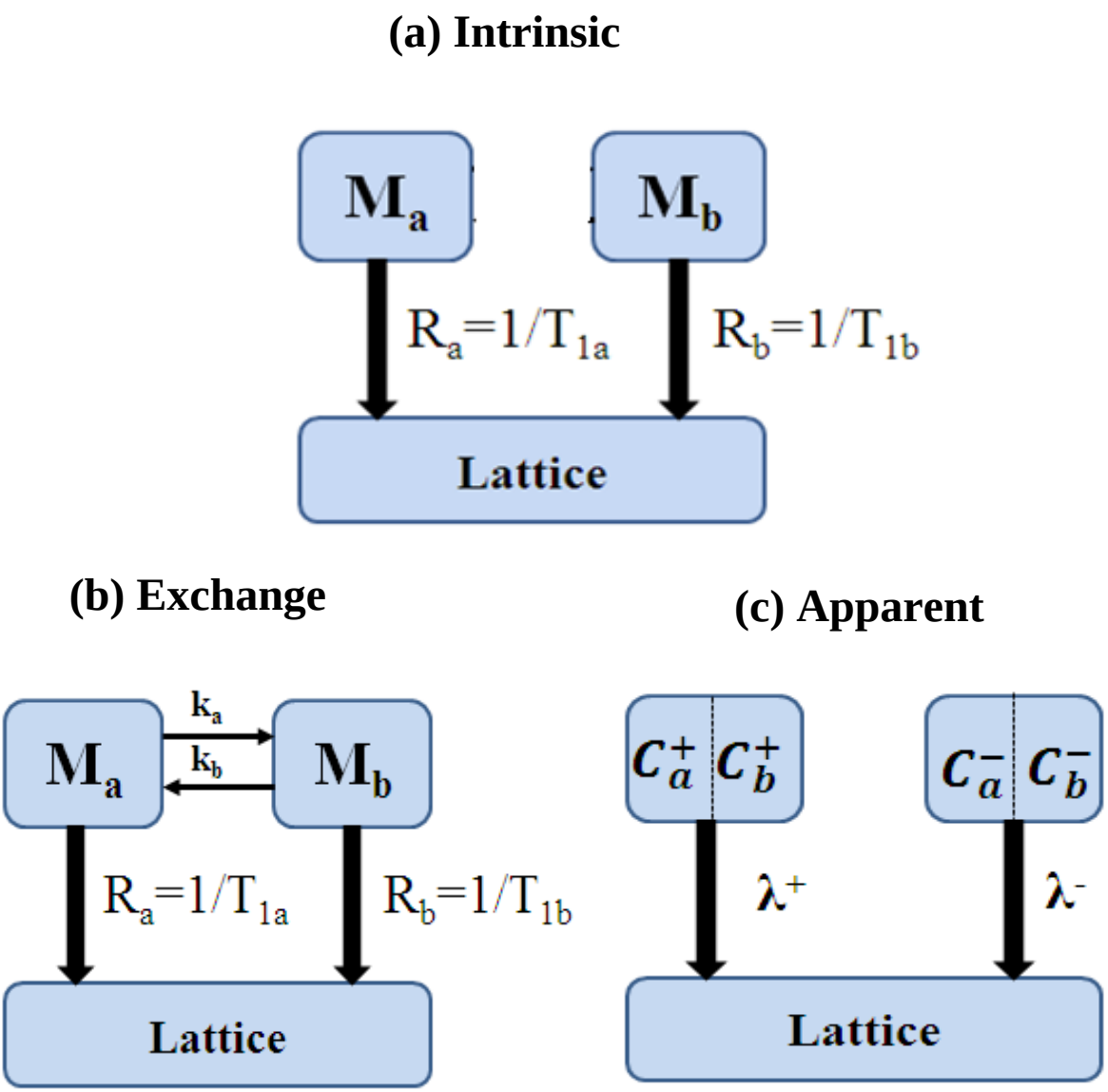

Figure 2.4 Schematic representation of the intrinsic and apparent relaxation scenario for 2-site exchange. (a) No exchange: The intrinsic rates and magnetization fractions are shown, which in this case are also the corresponding observed rates and fractions. (b) With exchange: The intrinsic parameters and the exchange rates are shown. (c) With exchange: Only the apparent relaxation rates (λ's) and apparent magnetization fractions (C's) are observed.

In a biological structure such as cartilage, spin groups can experience three different types of magnetization exchange: chemical, physical and magnetic exchange. Chemical exchange involves exchange of hydrogen atoms between molecules or between atomic groups on molecules, effecting proton magnetization exchange between water molecules, between water molecules and macromolecules, between different macromolecules and between intra macromolecular atomic groups. Physical exchange involves the exchange of molecules themselves between sites, carrying the molecules' proton magnetizations with them. The term "magnetic exchange" is commonly used to refer to magnetization exchange effects produced by magnetic coupling of dipoles across the interface between two spin groups. Commonly it is assumed that magnetization exchange due to physical and chemical exchange between bound water and bulk water is in the fast exchange regime [14, 15]. The magnetization exchange due to magnetic coupling between the nuclei of two or more different spin groups on macromolecule is called spin diffusion if the motions of the internuclear vectors involved satisfy $\omega_D \tau >> 1$ [16], or cross-relaxation if the motions (or some motional modes) do not satisfy this condition.

A multisite magnetization exchange scenario is used to model cartilage. Each site or spin group or spin reservoir "*i*" has a unique spin temperature, distinguishable from the other sites through a unique set of NMR spin relaxation parameters: M_{oi}, T_{1i}, T_{2i}, *and* $T_{1\rho i}$, as well as rates of magnetization exchange with other sites. It is assumed that spin groups are coupled, so that magnetization exchange between reservoirs is possible. In addition, this coupling mechanism is assumed to effect magnetization exchange only and does not act as a relaxation mechanism. The reduced magnetization of the i^{th} site for the T_2 experiment can be

define as $m_i\ (\tau) = M_{yi}\ (\tau)/M_{0i}$. For the inversion recovery (T_1) experiment the reduced magnetization is expressed by $m_i\ (\tau) = (M_{0i} - M_{zi}\ (\tau))/\ 2M_{0i}$, and for the spin lattice relaxation time in the rotating frame ($T_{1\rho}$) experiment, the reduced magnetization is given by $m_i\ (\tau) = M_{xi}\ (\tau)/M_{0i}$. The reduced magnetization as function of time, and exchange between spin reservoirs, can be described by modified Bloch equations as given by Zimmerman and Brittin, [13],

$$\frac{dm_i(\tau)}{d\tau} = -\left(R_i + k_{ij} + \cdots + k_{il} + \cdots\right)m_i(\tau) + k_{ij}m_j(\tau) + \cdots + k_{il}m_l(\tau) + \cdots \qquad (2.26)$$

where *R's* is the intrinsic relaxation rate of the i^{th} spin group or site, and k_{ij} is the rate of the magnetization exchange from site *i* to site *j*, and k_{ji} is the rate of exchange in the reverse direction.

In this work exchange between up to four sites is considered. For four site exchange, the solutions to (2.26)

$$m_i(\tau) = C_i^{--}e^{-\lambda^{--}\tau} + C_i^{-+}e^{-\lambda^{-+}\tau} + C_i^{+-}e^{-\lambda^{+-}\tau} + C_i^{++}e^{-\lambda^{++}\tau}\ , \qquad (2.27)$$

where *i* = 1, 2, 3, 4 and the *C's* are the apparent magnetization fractions, which are functions of the intrinsic parameters (*R's*, *k's*, and M_o*'s*).

The *λ's* are the apparent relaxation rates which can be expressed in terms of the intrinsic relaxation rates and exchange rates. The superscripts (++, +-, -+, --) express the fastest, fast, slow, and slowest relaxation rates, respectively.

Numerous multi-site exchange discussions have been presented by NMR spectroscopists; for example see Ernst [17]. Specifically, four- site exchange modified Bloch equations and their solutions have been discussed in detail in J. Hinke's thesis (2D Time Domain NMR Study of Wood, 1997) [18]. By solving the coupled differential equations 2.26, the apparent parameters, C's and λ's, can be expressed in terms of the intrinsic parameters R_i, k_{ij} and M_{0i}, and vice versa.

W. P. Weglarz (see ref. 18), developed an exchange analysis procedure which is based on the minimization of the difference between the experimental apparent parameters and the apparent parameters calculated from equations relating the apparent to the intrinsic parameters, according to the particular exchange model being considered (Oleskevich *et al.* [19]). The procedure involves the minimization of the following function

$$F\left[k_{ij}, C_i, T_i, m_i(0)\right] = \sum_n \sum_l \frac{\left\{P\left[k_{ij}, C_i, T_i, m_{in}(0)\right] - P_{ln}\right\}^2}{\sigma_{ln}^2} \quad . \qquad (2.28)$$

The subscripts *i, j* represent a pair of sites from sites 1, 2, 3 and 4 of the four-site exchange system. The spins in the i^{th} site are presented by the reduced magnetization $m_i(0)$. The *k's, C's* and *T's* are the intrinsic relaxation parameters. The function of these intrinsic parameters is represented by $P\,[k_{ij}, C_i, T_i, m_i(0)]$. The function of the apparent parameters is represented by P_{ln} where the apparent parameters are taken from the corresponding experimental values. The σ_{ln} are the standard deviations from the analysis of relaxation curves [19]. The sums in Eq. 2.28 run over all *l* apparent parameters obtained from the results of one experiment and over *n* experiments, such as T_{1HH} and T_{1SH}. The SIMPLEX minimization routine is used to minimize this function, which provides estimates of the intrinsic parameters[20].

2.3 NMR Techniques

2.3.1 Magic Angle Spinning (MAS)

In a dipolar coupled solid significant line broadening results from dipole-dipole interactions and chemical shift anisotropy. Such line broadening severely limits spectral resolution. In solution, the anisotropic parts of these interactions are averaged out by the fast isotropic tumbling of molecules, resulting in narrow lines and high resolution spectra. It is possible to undo the line broadening resulting from anisotropic interactions in solids by imposing the appropriate time dependence on such interactions by means of mechanical rotation of the sample. In MAS NMR, rotating the sample at the magic angle $\theta_m = 54.74°$ with respect to the static field (see Fig. 2.5) and at a spinning frequency higher than the coupling (in frequency units) of the spin species, will average all anisotropic interactions expressed by symmetric second rank tensors [21, 22].

The coupling due to the terms A and B of $\mathcal{H}_D$

$$\alpha\ (3cos^2(\theta) - 1)\ , \tag{2.30}$$

where θ is the angle between the interaction vector and the external magnetic field. Now consider rotation or spinning of a solid sample with the rotation axis making an angle θ_r with $\boldsymbol{B_o}$. Define an angle β between the interaction vector and rotation axis. Here θ_r and β are assumed fixed. If the spinning frequency is much greater than the interaction (in frequency units) being considered, the time average of $((3cos^2(\theta) - 1)$ becomes:

$$\overline{3cos^2\theta - 1} = (3cos^2\theta_r - 1)(3cos^2\beta - 1)\ , \tag{2.31}$$

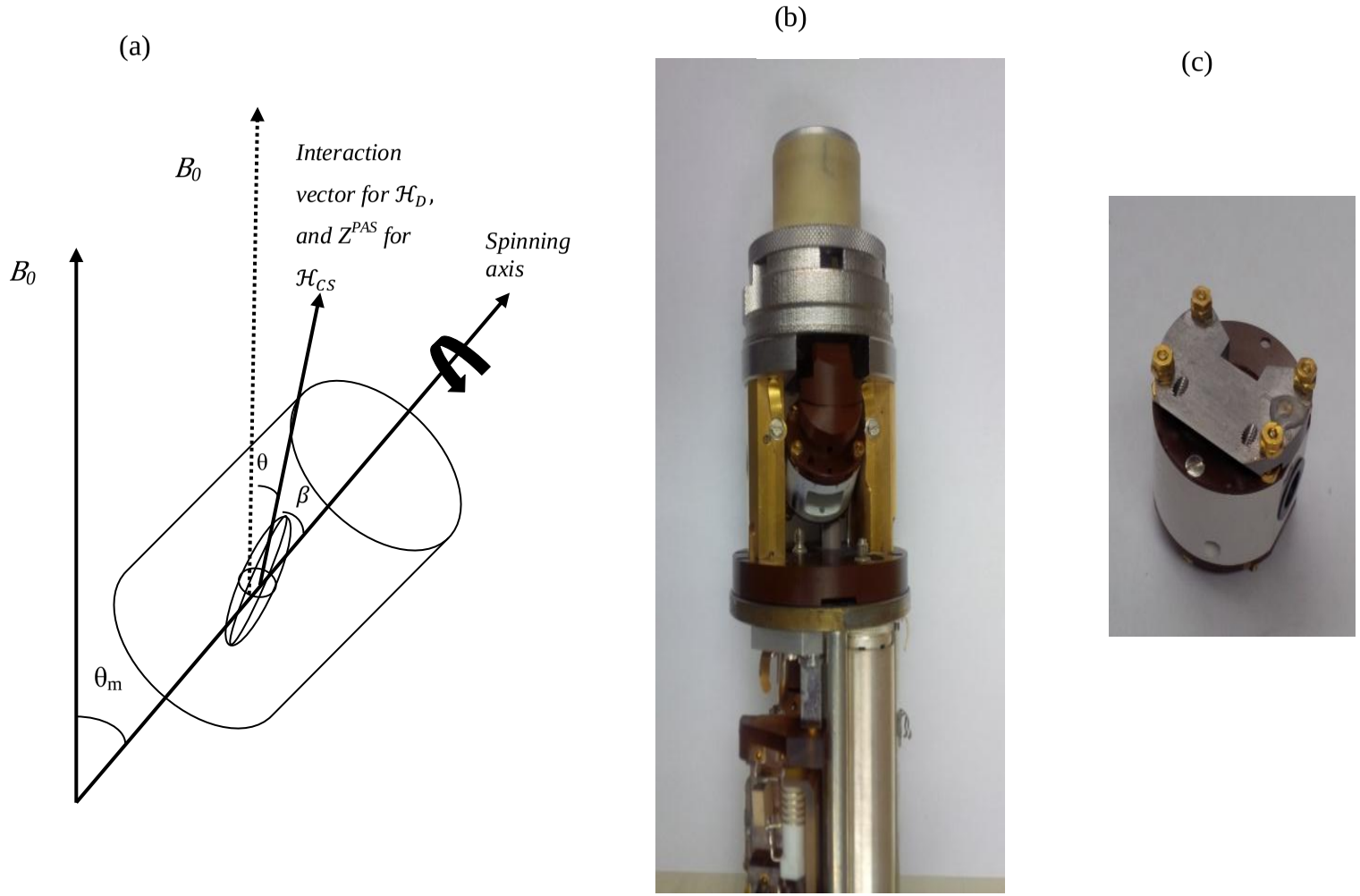

Figure 2.5 a) Diagram showing the vectors and angles associated with MAS. b) MAS probe. c) MAS stator.

where the overbar indicates time average with respect to sample rotation. The angle θ_r, can be adjusted and is normally set to $\theta_r = \theta_m \approx 54.7^o$, with the result that the secular contribution to dipolar line broadening vanishes.

Consider the chemical shielding tensor given in equation 2.24. If the sample is rotating about an axis, making an angle θ_r with respect to $\boldsymbol{B}_o$, and χ_x, χ_y and χ_z are the angles between the principal axes and the rotation axis, Stejskal and Memory [11] give

$$\overline{\sigma_{zz}} = \left(\frac{1}{2}\right)(sin^2\theta_r)(\sigma_{XX} + \sigma_{YY} + \sigma_{ZZ}) + \left(\frac{1}{2}\right)(3cos^2\theta_r - 1)(\sigma_{XX}cos^2\chi_X + \sigma_{YY}cos^2\chi_Y + \sigma_{zz}cos^2\chi_Z) \ . \tag{2.32}$$

For $\theta_r = \theta_m$ only the first term survives and the chemical shift reduces to σ_{iso}.

Thus, fast rotation ($\omega_{rotation}$ > interaction being addressed) of the sample about an axis oriented at 54.7° (magic-angle) with respect to the static magnetic field, removes broadening effects due to chemical shift anisotropy and dipolar interactions [11]. In addition, MAS can average out first-order quadrupole interactions, and decrease effects due to inhomogeneity of the magnetic susceptibility. MAS results in an enhancement of spectral resolution by line narrowing also in articular cartilage tissue and is used in the present study.

2.3.2 Chemical Shift Imaging (CSI)

Chemical shift imaging (CSI) combines MRI with magnetic resonance spectroscopy in a 2D or 3D setting. In effect a chemical shift spectrum is obtained for each pixel or voxel in the MRI experiment; each pixel or voxel can be represented by a spectrum. CSI can be

combined with other NMR experimental protocols such as inversion recovery experiments, for example. With the development of CSI various chemical shift selective imaging schemes, involving chemical shift encoded excitation, saturation and chemical shift insensitive slice selective RF pulses, were developed. This technique was initially presented in 1982 by T. R. Brown *et al.* [23] and has now become a powerful tool in biomedical research and clinical diagnostics.

A simple sequence for 1D CSI, using the spin echo, is given in Figure 2.6. The sequence contains a 90^o RF pulse to start excitation, followed by a 180^o pulse to refocus the spins at time t_E. A pulsed magnetic field gradient (G_x) of duration δ, applied after the refocusing pulse, encodes spatial information into the phases of the free induction decay signal. At time t_E the magnetic field gradient is switched off and the ensuing FID signal (second half of the echo) evolves under the influence of only T_2 and the distribution of frequencies associated with the chemical shift distribution.

The FID is recorded along the t axis for times $t_E + t$, for several values of G_x. A 2D Fourier transform with respect to $k_x = \frac{\gamma G_x \delta}{2\pi}$, the *k*-space variable, and *t* yields the spatial distribution (here along *x*) of frequencies (chemical shifts).

While MAS can remove dipolar coupling and chemical shift anisotropy, resulting in sharper spectra, CSI does not. Nevertheless, CSI has been successfully applied in the observation of high resolution spectra of small metabolites in tissue. PG undergoing motion in cartilage is not a small structure, but owing to large and fast segmental motions, relatively

sharp spectra of PG can be obtained under stationary conditions. A circumstance, which combined with CSI, could provide a practical method of observation *in vivo* [24-26].

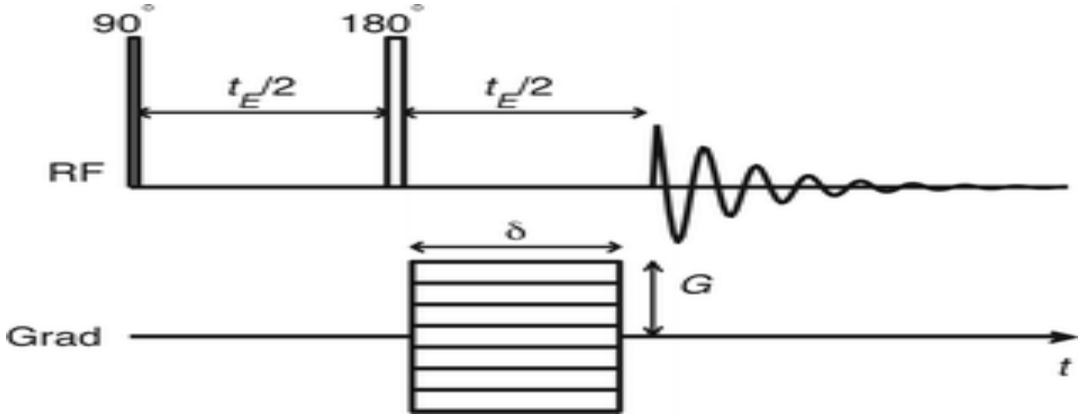

Figure 2.6 Simple 1D chemical shift imaging (CSI) pulse sequence starting with the excitation pulse = 90°, followed by a refocusing pulse = 180°. The magnetic field gradient pulse is placed after the refocusing pulse and before the data aquisition. t_E is the echo time, G is the magnetic field gradiant pulse amplitude and δ is the pulse duration.
Reproduced from RCS with permission [26].

Chapter 3
Articular Cartilage

3.1 Bovine Articular Cartilage

Articular cartilage (AC) is a smooth, connective tissue made up of 10-20% collagen, 5-10% proteoglycan (PG) and 70-85% water [27, 28]. It is designed to smooth the movement of joints and to act as a shock absorber. It helps to distribute the pressure and weight over the joint and helps to minimize friction between bones. The extracellular matrix (ECM) of the cartilage, comprised mostly of collagen, proteoglycan and water, maintains tissue integrity. AC is a heterogeneous material and is a relatively complex system. This tissue does not have a direct blood supply, lymphatic vessels or nerves, and it contains only a small percentage (< 1% of dry tissue weight) of chondrocyte cells [2, 29], which leads to difficulties in the tissue repairing itself. With the onset of osteoarthritis (OA), tissue repair is unable to keep up with breakdown of cartilage, resulting in a net loss of PG in the early stages, as well as collagen as the disease progresses. Cartilage loss causes joint stiffness and pain, leading to difficulties in movement. A representative sketch of cartilage on one articulating bone, showing the different cartilage zones and main cartilage constituents, is given in Figure 3.1. A more detailed sketch of the extracellular matrix is given in Figure 3.2.

Articular cartilage has been studied intensively in the literature to understand this unique tissue's morphology and physiology. Within the present context, of particular interest are details about the structure and dynamics of the main extracellular matrix-components with a view towards their detection in early OA. With the aim of providing a basis for

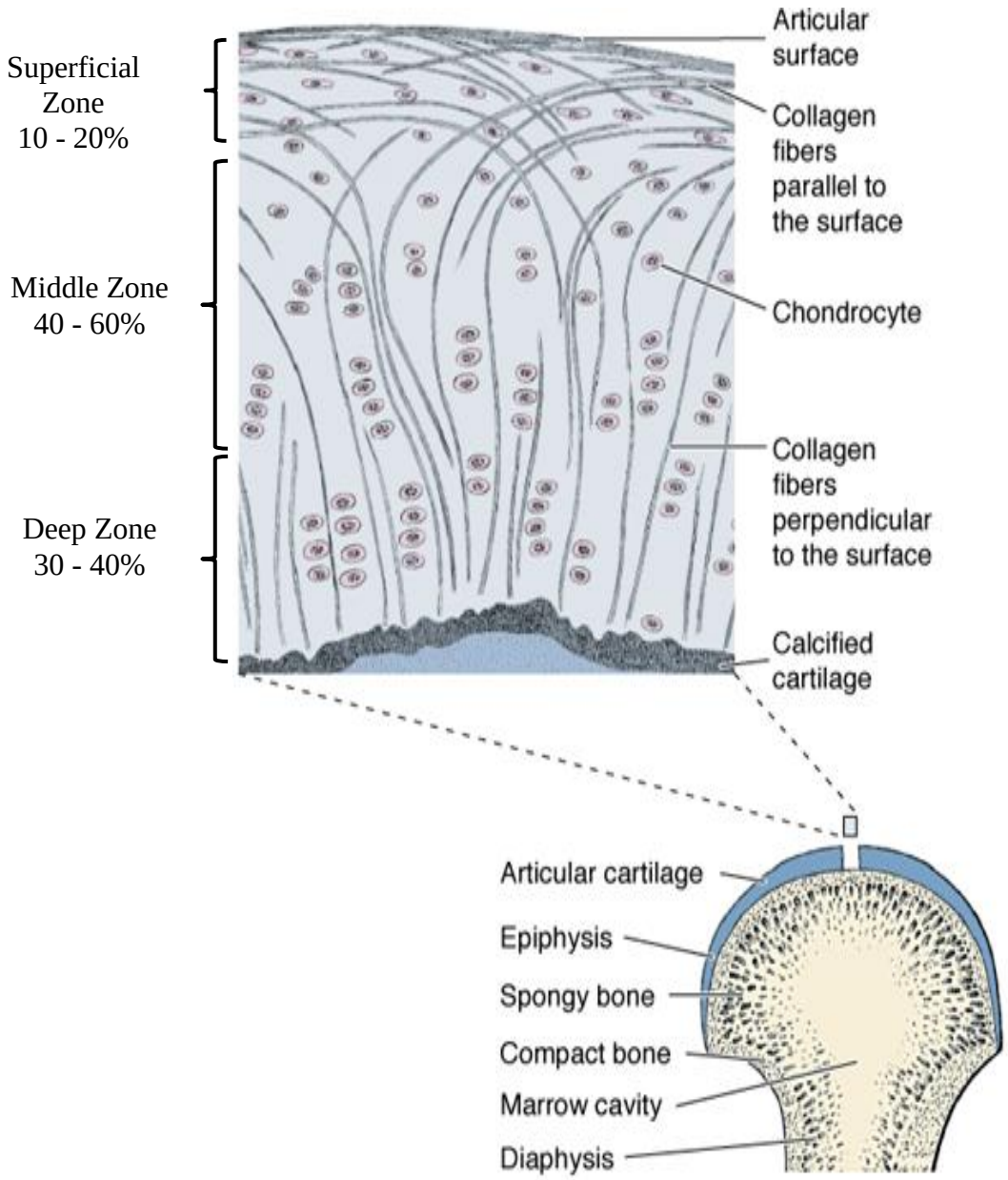

Figure 3.1 Cartilage on an articulating bone showing the collagen distribution through different zones. Reproduced with permission, from Mescher Anthony, Edition 12, Junqueira's Basic Histology: Text and Atlas [29].

interpreting results obtained in NMR experiments, the structure and composition of collagen and PG of bovine articular cartilage are considered below.

The extracellular matrix comprises two main structures, collagen and proteoglycan [28].

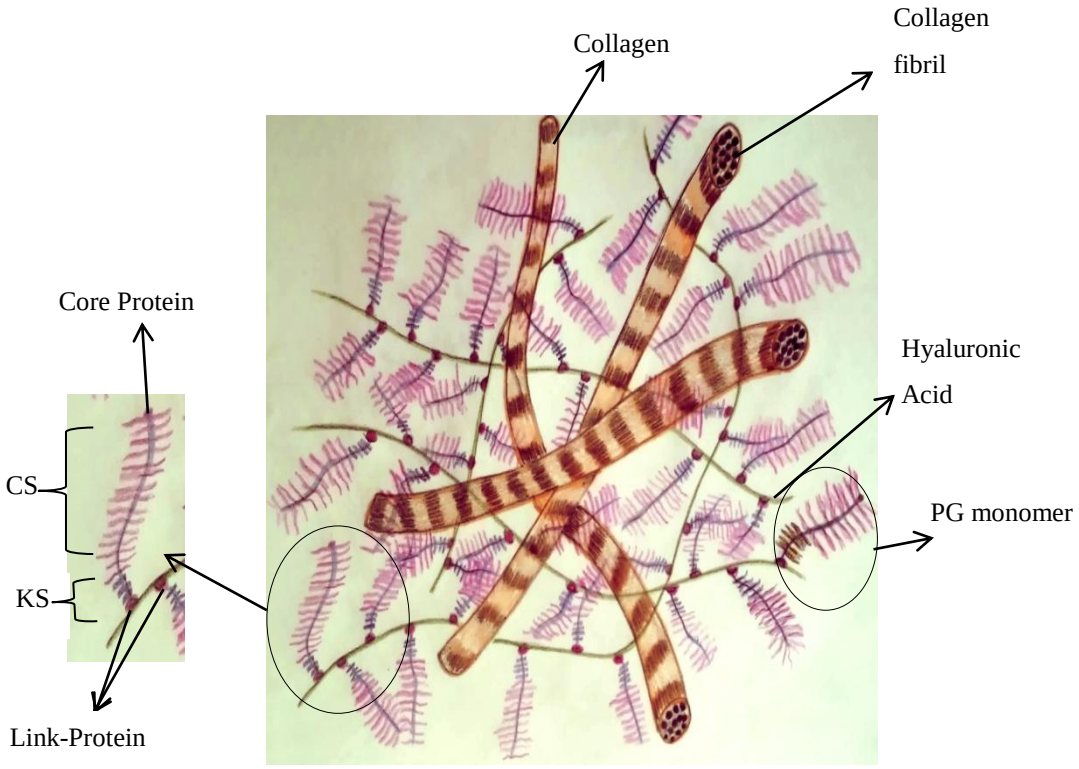

Figure 3.2 Extracellular matrix composition. Adopted from " Functional anatomy of the musculoskeletal system/ Clinical gate".

3.1.1 Chondrocytes

Chondrocytes are highly specialized cells. They vary in size and morphology and their arrangement changes with depth in the tissue (Fig. 3.1) [30]. They are found in a scattered flat shape in the superficial zone, while they are organized into columns in a rounded shape in the middle zone, and grouped in clusters in the deep zone. The cell density decreases from superficial to deep zone [31]. Chondrocytes produce collagen, proteoglycans, etc. as needed. They are ~ 5 % of the cartilage wet weight and about < 1 % of the dry tissue weight [2, 29].

3.1.2 Collagen

Collagen found in articular cartilage is mainly collagen II. Collagen exists as a long-fiber protein. Its tensile strength is ~ 300 MPa, comparable to steel. Collagen type II fibers are made of three α-helices as presented by Ramachandran [32]. These characteristics of collagen explain the strength and characteristics of the cartilage tissue under pressure and deformation. Collagen creates a framework that houses the other components of cartilage. Collagen fibers are arranged in the cartilage tissue with different orientations, depending on the zone in which they appear in the cartilage (Fig. 3.1) [30]. In the surface zone, collagen fibers are parallel to the surface, while in the middle zone, they are more randomly distributed, with some fibers partially perpendicular and others partially horizontal to the articular surface, but in the deep zone, collagen fibers are arranged perpendicular to the articular surface which holds the tissue to the bone surface. Collagen II is rich with hydroxyl-lysine, which makes those fibrils thinner than other collagen types. Each fibril is made up of a triple helix of collagen whereby the left-handed polypeptide helices are grouped together to

form a right-handed super-helical structure. Each chain is made up of 1000 amino acids with a repetition of Gly-Pro-Hyp. This kind of packing holds the fibrils together to form the collagen fiber and gives the collagen its rigidity. This triple helical structure is responsible for its strength. Each tropocollagen is about 300 nm long with a diameter of 1.5 nm and a molecular weight of 2.85 x 10^5 g/mol.

3.1.3 Proteoglycan

Proteoglycan has a high molecular-weight aggregating structure in articular cartilage. It has been extensively studied over the last decades; e.g., Hascall, [33], Paulsson *et al.* [34], Evered and Whelan [35], Hassell *et al*. [36], Kuettner *et al*, [37] Heineggrd and Sommarin [38]. Hyaluronic acid (HA) is the backbone for the PG structure and it is made up of a linear, unsulphated polysaccharide high in molecular weight (0.25-1 million in cartilage) with interspersed glucuronic acid and N-acetyl glucosamine residues [39]. The aggrecan is made up of the globular N-terminal G1 domain which contains a lectin-like binding site to bond with Hyaluronan acid (Figure 3.3). Hyaluronan acids are very long chains, and each chain can bind a large number of aggrecan which are made of core proteins and disaccharides that resemble bottle brushes of keratin sulfate (KS) and chondroitin sulfate (CS), (Figure 3.3). Link protein is a small glycoprotein (45 kDa) that works to stabilize the aggrecan binding to Hyaluronan. The G1 domain of aggrecan is called the proteoglycan tandem repeat (PTR) which works as the link module protein. The G2 domain of aggrecan is structurally similar to G1 and link protein. HA interacts with link protein and core protein within the amino-terminal domain of the core proteins to aggregate together and form large

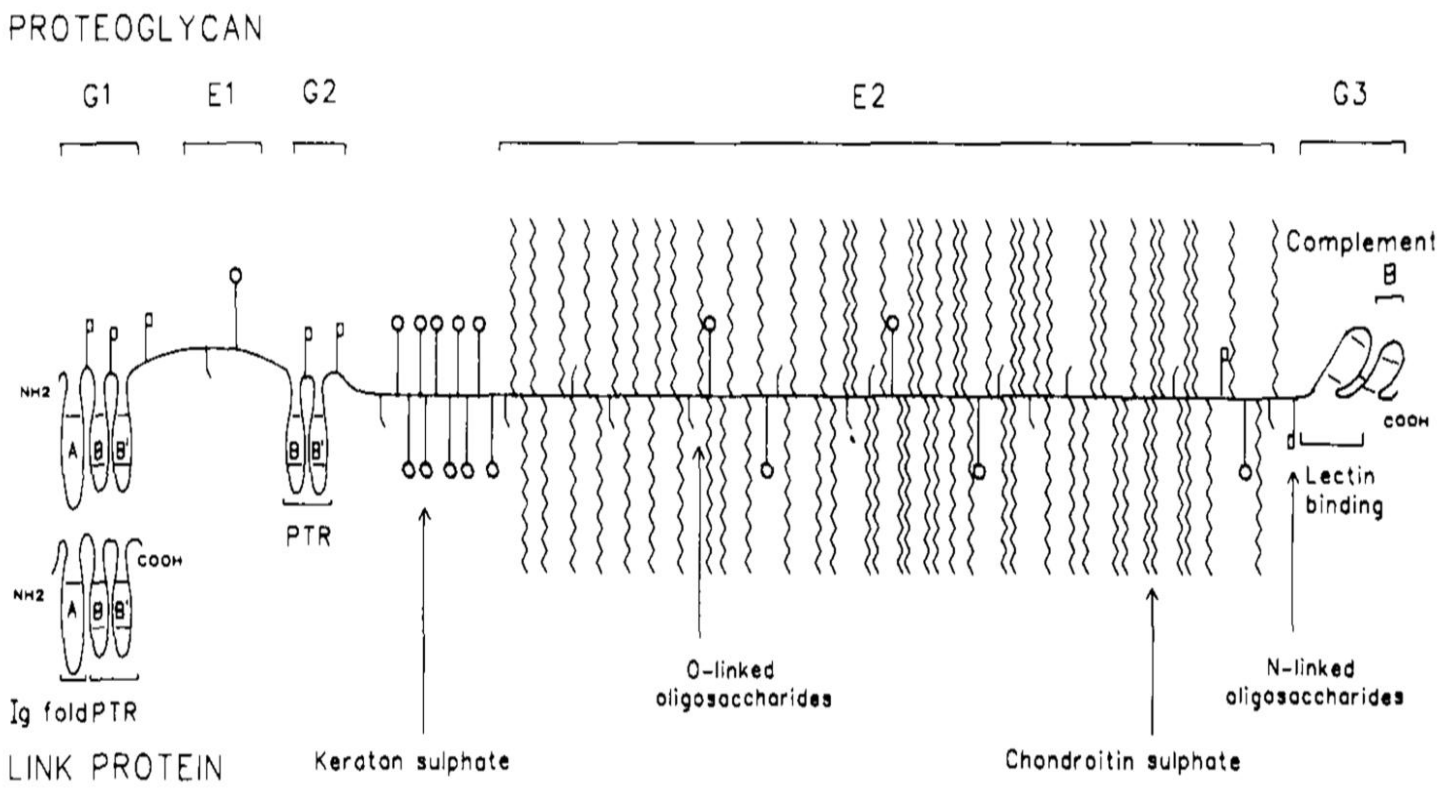

Figure 3.3 Schematic representation of the carbohydrate and protein structural features of aggregating proteoglycan and link protein of cartilage. Reproduced with permission, from Timothy E. *et al.*, 1990, Biochemical Society Transactions, 18,794

proteoglycan units. One Proteoglycan monomer contains core protein connected with hyaluronic acid to create a bottlebrush tree-like structure [33]. The glycosaminoglycan (GAG) is made up of three main sugar rings (disaccharides), composed of chondroitin 4-sulfate, chondroitin 6-sulfate, and keratin sulfate. GAG is full of carboxyl residues (-COO-) and sulfate ester groups (O-SO3-) that bind to the disaccharide sequences which gives a high electrostatic feature of a fixed charge density to the PG [40-42]. The fixed charge density plays a major role in maintaining AC integrity when it is under pressure and controls the amount of water getting into the tissue due to osmotic pressure [43-45]. Table 3.1 shows the decomposition of a PG monomer into different parts, with each part characterized by its molecular weight, in kDa and its proton spin density in spins/kDa [46, 47]. The number of spins has been calculated from the molecular mass of each part multiplied by its spin density. In addition, the percentage of proton spins for each subunit has been calculated, Table 3.1.

Table 3.1 Proteoglycan components and number of ^{1}H nuclei in the PG monomer subunits.

Domain as defined in Fig. (3-2)	Mol. mass (kDa)	Proton Spin Density (spins/kDa)	Number of Spins	^{1}H content (%)	Liquid (L)	Solid (S)
LP	39	45	1755	5.2	-	S
G1	38	65	2470	7.3	-	S
E1 (IGD)	12	30	360	1	L	-
G2	25	65	1625	4.8	-	S
E2 KS	5-10 (KS)	52 (8.8: N-Ac)	364 (62)	1	L	-
E2 CS	125 (CS)	46 (8.7: N-Ac)	5750 (1088)	16.9 (3.2)	L	-
E2 CS	~110 (KS)	52 (8.8: N-Ac)	5720 (968)	16.8 (2.8)	L	-
G3	25	65	1625	4.8	-	S
Core Protein	200	65	13000	38.2	-	S
HA	25	55	1375	4	-	S
Sum	606	475	34044	100	35.7	64.3

By combining information about the structural morphology of each subunit within the large PG monomer with our experience about the liquid-like (L) and solid-like (S) NMR characteristics of polymeric systems, the various subunits have been assigned as S or L character (Table 3.1). The Link-Protein (LP) (Figure 3.3) has been assigned as solid (S). The G1 and G2 regions are globular proteins, which form the N-link and O-linked oligosaccharide, have been assigned as solid. E1 region contains a small percent of Keratin-Sulfate (KS) and has been assigned as liquid (L), Figure 3.3. The E2 region is the most mobile region of the PG monomer as it contains the chondroitin-sulfate (CS) and keratin-sulfate (KS) chains and has been assigned as liquid (L). The G3 globular protein from N-link has been assigned as solid, similar to G1 and G2. The core protein and the hyaluronic acid are the backbone of the structure and have been assigned as solid. The N-acetyl group is found everywhere in the structure, but we assumed that the groups from CS and KS are the most mobile ones. Information about these N-acetyl groups is presented in Table 3.1 in brackets.

The S and L characterization will help to explain the relaxation results and interpretation in Chapter 5.

3.2 NMR of Cartilage Tissue

Nuclear Magnetic Resonance (NMR) has proven to be a sensitive method for studying structural details and molecular dynamics in articular cartilage [48-54]. Much work has been done using Magnetic Resonance Imaging (MRI). T_2 relaxation time experiment is an important starting point when characterizing the biological tissue (solid and liquid components) and studying the macromolecule and water molecule dynamics [55-61]. Crema *et al.* [62] concluded that MRI has been proven to be a non-invasive for cartilage diagnosis. NMR has been used extensively to study/detect changes in articular cartilage tissue with the progression of osteoarthritis (OA) [63]. Dardzinski *et al.* [64] observed that T_2 relaxation time increases from the subchondral bone to the cartilage superficial surface, which is related to collagen orientation. Xia *et al.* and Lammentausta *et al.* [65, 66] reported dependence of T_2 on collagen orientation, within the same slice and at the same locations. Wang and Xia [63, 67] pursued an NMR and MRI investigation on multi-component relaxation in nasal cartilage, and found that the tissue orientation, relative to the main magnetic field B_o**,** influences the number of observed components in the T_2 and $T_{1\rho}$ experiments.

Various NMR relaxation time studies in articular cartilage have been used to accompany the MRI research [54]. The various MRI and NMR approaches are used; the most promising techniques for the detection of OA are magnetization transfer experiments and low-field $T_{1\rho}$ spin-lattice relaxation experiments [68-71]. Previous studies have shown that osteoarthritis could be monitored by water proton NMR as the water behavior in the tissue changes with OA [54, 72, 73]. Therefore, it is important to understand the physics of the water in cartilage; specifically, the dynamics of water interacting with macromolecules of

cartilage tissue, and magnetization exchange between various water pools and macromolecules [54, 74-77].

A major challenge facing researchers investigating the details of macromolecule-water interactions in cartilage is the high moisture content (*MC* ~350 - 400%) of natural tissue [53]. As a result of the large *MC*, only a small fraction of the proton NMR signal is from macromolecules and bound water. In this study, the effect of the bulk water in the tissue was diminished through freezing and deuterating the tissue. Temperature dependence of phase transitions in cartilage tissue has been studied by Tzou *et al.* [78]. They reported that cross-relaxation spectroscopy rates can estimates the NMR parameters of the cartilage tissue and the temperature dependence technique can provide molecular dynamics information of bulk and bound water in cartilage. Understanding the molecular dynamic of the water in the tissue can be used to clarify the tissue characterization [78]. Fullerton *et al.* [75, 79] reported multiple non-bulk water regions in hydrate collagen and lysozyme systems and they concluded that in three water regions the water could be characterized as interfacial monolayer water. Haskin *et al.* [80] used three different methods (flow rate, dehydration monitored by proton NMR, and freezing point characteristics) on temporomandibular joint (TMJ) disc to study the different water compartments in it. They concluded that all of the water in the intact TMJ disc is bound water. They identify two major non-bulk water components and gave their sizes as 1.13-1.30 g water/g DM in the least tightly bound water region, and 0.90-0.99 g water/ g DM in the tightly bound water region. Haskin *et al.* [80] performed proton NMR spectral measurements in TMJ discs over the temperature range of 4^{o}C to -98^{o}C to check where water phase transitions occur. As the temperature was lowered

from 20^{o}C, a clear freezing phase tradition was observed at -12^{o}C at which point about 60% of the signal was lost due to freezing of the least tightly bound water. Another distinct decrease in water proton signal, signifying additional freezing of water, occurred at -72^{o}C, but a signal was still detectable at the lowest temperature. In the present work, the idea behind freezing the tissue is to allow tissue characterization in the presence and absence of bulk liquid water.

The dynamics and mobility of collagen in cartilage have been extensively studied by Huster *et al.* [81, 82] , and the assignment of the collagen spectra have been presented by Saito *et al.* (1992) [83]. NMR was shown to be a promising technique for the detection of small fragments by Huster *et al.* [29]. In the same study, the Huster group described different NMR techniques to study the macromolecular dynamics, water diffusion, and enzymatic degradation of the tissue in vitro [29]. In order to study and investigate macromolecule and water proton magnetization exchange, Ghiassi-Nejad *et al.* [53] and Lattanzio *et al.* [54] used a D_2O buffer solution to deuterate the tissue. Deuterating the cartilage tissue helps to reduce the water proton magnetization signal and to minimize complications resulting from the coupling between water and the macromolecule spins. It is also used to characterize the motions and interactions of collagen and PG in the tissue matrix. Schiller *et al.* [84] and Huster *et al.* [82] showed that HR-NMR spectroscopy can differentiate between the effects of different proteases, such as Trypsin, Papain, and Collagenase on cartilage. Lattanzio *et al.* [54, 85] investigated the effect of PG-depletion on NMR relaxation parameters by using trypsin enzyme to achieve three depletion levels (20, 30, and 40%) and monitoring the changes on NMR relaxation times. Using optical techniques Moody *et al.* [86]

demonstrated that the rate of progression of trypsin into cartilage is affected by the distribution of matrix molecules in the tissue as well as trypsin concentration. The authors suggest that in view of the details of the 3D PG distribution, different from sample to sample, the methodology for characterizing the tissue degradation for any particular sample needs to be standardized.

A $T_{1\rho}$-weighted MRI technique that allows for the determination of the spatial distribution of absolute PG content, was demonstrated by Regatte *et al*. [71] . In this approach a spatial map of % GAG content is arrived at utilizing the ratio of two $T_{1\rho}$-weighted images taken at two different spin-lock fields.

Magnetization exchange between cartilage tissue constituents is a complicating factor when attempting to deduce intrinsic relaxation information about the tissue, which is needed if details about molecular dynamics are being sought after. At the same time, details about magnetization exchange can change as the tissue becomes osteoarthritic, so that this complicating factor has potential application in the detection of OA. Considerable literature exists on magnetization exchange in articular cartilage tissue (see [54, 77, 87-90]). A key aspect of any magnetization exchange analysis, within the present context, is the definition of the correct exchange model, involving an appropriate number of spin reservoirs or sites. In 1992, Morris *et al.* [91] used an inversion transfer approach, involving selective magnetization inversion with high and low power pulses, to study magnetization exchange in cartilage tissue. They concluded that about half of the macromolecule spins are found in a liquid-like state and have similar T_2 as the "free" water in the tissue so that these two signal components become indistinguishable in the experiment. The liquid-like macromolecular T_2

component was assigned to very mobile proton groups on PG. A similar conclusion was reached by Ghiassi-Nejad *et al.*[53], Nightingale *et al.* [92], and Lattanzio *et al.* [54] in NMR relaxation studies of cartilage.

Using magnetization transfer experiments Kim *et al.* [77] investigated magnetization exchange between water and a) collagen in solution, b) PG in solution and c) macromolecules in articular cartilage. These authors observed significant magnetization transfer effects between water and collagen protons, but not between water and PG protons; in effect a 2 - site exchange model was considered.

Tessier *et al.* [88] applied a magnetization transfer approach to study magnetization exchange in a number of macromolecule – water system, including bovine nasal cartilage. A 2 – site exchange model, consisting of water and collagen, was found inconsistent with the experimental results. By including a third site, assigned to protons of mobile PG, these authors found that the χ^2 values associated with the fitting of the exchange model to the data, decreased significantly relative to that found for the 2-site case.

Adler *et al.* [89] used a projection operator approach to model cartilage as a 3-component system (solid, bound water, free water), rather than the usual approach based on the Bloch equations modified for exchange. The rate equations, derived using the projection operator approach, allow for non-exponential solutions, including Gaussian functions for the solid-like magnetizations.

Nieminen *et al.* [93] studied the collagen arrangement in articular cartilage using polarized light microscopy and found a strong correlation between the collagen arrangement

and the spatial distribution of T_2, as determined using MRI. With the aim of resolving multiple T_2 components in articular cartilage, Reiter *et al.* [94] first simulated the multi-exponential evolution of the magnetization to optimize the acquisition parameters needed, and then performed the T_2 experiments.

Different techniques have been used to investigate early detection of osteoarthritis. Broche *et al.* [95] found that fast field-cycling (FFC) NMR can detect changes in the ^{14}N quadrupolar peaks of cartilage as it changes from a normal state to an osteoarthritic state. $T_{1\rho}$ imaging has been shown to be sensitive to PG changes in cartilage [70, 71, 96]

Ficat and Maroudas [97] discovered a correlation between the different ions distributed in articular cartilage and the fixed negative charge density for proteoglycan. Kusaka *et al.* [98] used manganese ions (Mn^{2+}) in saline solutions with different concentrations as contrast agents for articular cartilage in MRI experiments. They found that MRI of articular cartilage was enhanced by using Mn^{2+}, which allows researchers to visualize the internal structure of PG distribution in the cartilage tissue. McKeag *et al.* [99] combined MR spectroscopy and tissue pathology results to estimate the severity of osteoarthritis. They found a correlation between severity of osteoarthritis, percent water and T_1.

Werner *et al.* [100] studied calcium induced structural changes of cartilage proteoglycans using proton NMR relaxation and diffusion measurements. They showed that increased osmotic pressure of proteoglycan can be caused by osteoarthritis, or ageing and will induce these changes in the cartilage.

Magic Angle Spinning (MAS) NMR technique has been used to resolve spectra of articular cartilage, which are strongly dominated by broad resonances [101-103]. Naji *et al.* [104] was the first to investigate cartilage by applying high resolution magic angle spinning (HRMAS). These authors studied ^{13}C NMR because the broad range of ^{13}C chemical shifts is helping in resonance assignment. Schiller *et al.* [84, 105, 106] concluded that HR-MAS experiments are the most suitable techniques for differentiating between the different cartilage components, which is needed to study the effect of enzymatic treatments. Ling *et al.* [107] presented ^{1}H and ^{13}C spectroscopic results for bovine patellar cartilage and chondroitin sulfate (CS) solutions, which will serve as a guide for the spectral assignments in cartilage tissue. Borel *et al.* [102] reported ^{1}H HRMAS characterization of osteoarthritic articular cartilage. They found close relation between the degradation of macromolecules (PG, collagen) and chondrocyte death. Scheidt *et al.* [103] applied ^{13}C MAS NMR spectroscopy to investigate and characterize the mobility of chondroitin sulfate in articular cartilage.

Magnetic Resonance Imaging has been one of the most popular techniques to investigate cartilage and to find markers toward early OA detection [108, 109]. Proton MRI signals in cartilage are dominated by water proton signals because water makes up about 85% of the tissue by weight. The larger fraction of the water is free water, which is in fast exchange with water bound to macromolecules. Thus, in MRI of cartilage changes in the macromolecules is observed indirectly from proton MRI [110].

The Chemical Shift Imaging (CSI) NMR technique was introduced in 1982 by Brown *et al.* [23]. The CSI technique showed promise for obtaining high resolution with a high signal to noise ratio and chemical shift distribution range. This technique has been used mostly to study small metabolites, such as phosphorylated metabolites, in the brain [25, 26, 111]. In this project, CSI is used for the first time to investigate large macromolecules in cartilage to find a sensitivity marker that could have application in clinical detection of OA.

Chapter 4
Experimental and Analysis Methods

4.1 30 MHz Experiments

4.1.1 Sample Preparation

Femoral articular cartilage tissue samples were harvested from freshly-slaughtered bovine animals, between twelve and twenty four months in age. Each sample plug was 6 mm in diameter and approximately 1 mm in thickness in order to fit into a thin-walled NMR tube with an outer diameter of 7.5 mm. Each tube contained ten plugs of cartilage so that the sample length measured ~ 1 cm. All plugs were stored in a phosphate buffer saline solution (PBS) at 4^{o}C until use.

Some of the samples were deuterated in order to achieve a better resolution of the macromolecule signal by decreasing the contribution to the signal from water protons. Cartilage plugs were deuterated by treating them with a deuterated balanced solution (D_2OPBS), changing the bath three times under nitrogen gas flow in a glove box to completely replace H_2O with D_2O. The first bath was changed after four hours, the second was changed after twelve hours, and the last left for forty-eight hours to give enough time for slow exchange to occur. The plugs were then removed from the bath, blotted gently using Kim wipes to remove excess PBS and introduced into the NMR tube and quickly flame sealed to avoid any moisture (H_2O) contaminating the sample. Both deuterated and non-deuterated samples were measured at 3^{o}C and -10^{o}C. After completion of NMR experiments each sample was dried fully by opening a small hole in the glass tube and placing it in ~ 10^{-4}

Torr vacuum for 48 hours. Each sample was weighted before and after drying to calculate the moisture content.

4.1.2 Apparatus

A low-field home built NMR spectrometer system operating at 30 MHz was used to perform all relaxation time measurements using broad band RF electronics combined with a PC-operated data collection and analysis program. The sample temperature was controlled at a given temperature, between 16^{o}C and -30^{o}C using a nitrogen gas flow system to maintain the temperatures within ± 0.5^{o}C.

4.1.3 NMR Relaxation Experiments

4.1.3.1 Free Induction Decay (FID) Experiment

When a 90^{o} RF pulse is applied at resonance, to the spin system at thermal equilibrium, with macroscopic magnetization M_0 along the z-axis, it will flip the magnetization into the xy plane. Due to a distribution of local fields the frequencies of spins will be randomly distributed over a small range of frequencies centered at $\omega_0 = \gamma B_0$, where B_0 is the applied static field. As a consequence of the resulting spin dephasing in the xy plane the macroscopic magnetization will decay. The y-component of the magnetization can be expressed as

$$M_y(t) = M_0 \exp\left(\frac{t}{T_2}\right) \qquad (4.1)$$

where T_2 equals the spin-spin relaxation time and is the time it takes for the magnetization to reduce to 1/e of its quantity at t = 0. Therefore, T_2 can be measured from the free induction decay (FID) following a single RF 90^o pulse (length 1.75 μs). In the present FID experiments the signal was averaged using up to 200 accumulations, depending on the signal-to-noise ratio (S/N); i.e., natural or deuterated sample and above or below freezing. Due to inhomogeneities in the magnetic field produced by the magnet used in this study, T_2 values of about a millisecond or longer, obtained from the FID measurements are artificially shortened. Therefore, in cases where T_2 ~ ms, or larger, the transverse decay was also taken using the Carr-Purcell-Meiboom-Gill (CPMG) pulse sequence (Meiboom *et al.* 1958, Carr *et al.* 1954) [112, 113].

4.1.3.2 Carr-Purcell-Meiboom-Gill (CPMG) Experiment

Inhomogeneities in the static magnetic field will result in different spins precessing at different rates within the sample, resulting in the dephasing of spin isochromats, which in turn contributes to the rate of the transverse decay. While the loss in coherence due to spin-spin interaction is irreversible. Reversing the inhomogeneous dephasing can be done by using a 180^o pulse at a time t, which will invert the magnetization vectors and lead to refocusing of the magnetization vectors, forming an echo at time *2t*. In uncomplicated cases, the echo intensity, relative to the initial signal, is given by e^{-2t/T_2} where T_2 is the time constant for spin-spin relaxation. Instead of utilizing a single Hahn echo, the CPMG pulse sequence consists of a 90_x^o pulse applied along the *x*-axis followed by a train of 180_y^o pulses resulting in an echo train. In the present experiments an inter-pulse spacing CPMG pulse

(also inter-echo spacing) of 200 μs was used. To improve S/N ratio, 20 echo trains were averaged. To determine the baseline typically a hundred echoes were collected at $t \geq 10\ T_2$ for each accumulated echo train, and averaged.

4.1.3.3 Spin-Lattice Relaxation Time ($T_{1\rho}$) Experiment in the Rotating Frame

$T_{1\rho}$ was measured using the spin-locking technique. After rotating the magnetization into the *xy* plane, say along x-axis, a low-power RF pulse B_1 -a spin locking pulse- is applied along the *x*-axis, exactly at resonance. During the spin-locking pulse the spin system will see $B_0 + B_1$. In effect this adds another spin-lattice relaxation mechanism that involves transitions between energy levels separated by $\hbar\omega_1 = \gamma\hbar B_1$. In the spin-locking experiment the magnetization is allowed to relax along the B_1 field for a time τ. The RF field is turned off and the FID is recorded. The experiment is repeated for various τ values. The magnetization decay in the rotating frame, in the presence of the spin-locking field, can be written as

$$M_z(\tau) = M_0 exp\left(-\frac{\tau}{T_{1\rho}}\right) \tag{4.3}$$

where $T_{1\rho}$ is the characteristic time for the magnetization to decay 1/e of its initial value. $T_{1\rho}$ is very sensitive to motions occurring at a Larmor frequency $\omega_1 = \gamma B_1$. As molecular dynamics in polymeric systems, such as tissues, typically also include slow motional modes, the relaxation rate $1/T_{1\rho}$ can be dominated by such slow modes. As a consequence, in tissues, the spin-lattice relaxation time in the rotating frame is often considerably shorter than T_1. Therefore, $T_{1\rho}$ measurements may provide relaxation parameter values that are less influenced by exchange and are closer to intrinsic values. $T_{1\rho}$ measurements were performed

with a B_1 spin-locking field set to 10 G. The relaxation in the rotating frame may have a contribution from relaxation of the dipolar reservoir when the value of the spin-locking field approaches the local field or has a value less than the local field. Slichter (1996) shows that for protons in the presence of a static field and a spin-locking field B_1, for $B'_L \leq B_1 \leq 3B'_L$ the spin-lattice relaxation rate in the rotating frame becomes

$$\frac{1}{T_{1\rho}} = \frac{1}{B_1^2 + B_L'^2}\left(\frac{B_1^2}{T_{1x}} + \frac{B_L'^2}{T_{1D}}\right), \tag{4.2}$$

where T_{1x} is the Zeeman spin-lattice relaxation time in the rotating frame, T_{1D} is the dipolar spin-lattice relaxation time and B_L' is the dipolar local field in the rotating frame. For the solid polymeric component the local field ~ 2 G. So that at B_1 = 10 G coupling between dipolar and Zeeman reservoirs is negligible.

4.1.3.4 Spin- Lattice Relaxation Time (T_1) Experiments in the Laboratory Frame

Spin- Lattice relaxation time, T_1, was measured with inversion recovery pulse sequences which involve non-selective and selective excitation. The T_{1HH} sequence uses a hard, non-selective 180^o preparation (inversion) pulse (3.45 μs in length) followed by a hard 90^o monitor pulse (1.75 μs in length), separated by a time τ (i.e., hard 180^o- τ - 90^o). The T_{1SH} sequence uses a soft, selective 180^o preparation (inversion) pulse (100 μs), followed by a hard 90^o monitor pulse (1.75 μs), and separated by a time τ (i.e., soft 180^o- τ - 90^o). The dependence of the magnetization M_z on τ is characterized by decay time T_1 and can be written as

$$M_z(\tau) = M_0\left(1 - 2e^{\frac{\tau}{T_1}}\right) \quad (4.3)$$

The soft 180^o pulse is a low-amplitude pulse, with a sharp spectral width in the frequency domain, which is much less than that of the spectral width for the signal of macromolecules in the cartilage and much larger than the spectral width of the water signal. Therefore, the water-component magnetization will be inverted completely while leaving the solid magnetization largely untouched. The hard 90^o pulse affects all magnetizations equally and allows the monitoring of all magnetization components. Edzes and Samulski [16] were the first to introduce the use of this selective inversion-recovery pulse sequence to study magnetization exchange between solid-like macromolecules and water. This approach has proven to be particularly effective in studying exchange in solid-liquid systems. Specifically, by differentially inverting the liquid component, it is possible to directly observe the effects of exchange as the liquid and solid magnetization evolves towards a semi-equilibrium following selective excitation. 40 τ values were utilized in for all longitudinal relaxation experiments, with 120-200 signal accumulations.

4.1.4 Analysis Aspects of Multicomponent Relaxation Decay and Recovery Curves

To determine the number of magnetization components relevant for a specific multicomponent analysis, such as for the CPMG curves, analysis was performed using one to five component fittings. To this end a Marquardt nonlinear least-squares minimization algorithm[114], within the ORIGIN 7.0 software package (Origin lab, Northampton, USA), was used. In the analysis, the changes in minimum of $\chi 2$, and the correspondence between

the fitted curve and data, were monitored with increasing number of components (see Fig. 4.1).

In this study, χ^2 decreased approximately by a factor of two or more as the number of components was increased up to a number N of components. For the N+1 component analysis, χ^2 decreased only by about 20% or less. Then, the number of components deemed most appropriate was N.

The T_1 relaxation curves were similarly fitted with exponential functions using the same χ^2 criteria. For the free induction decays the fits involved a mixture of Gaussian and exponential functions.

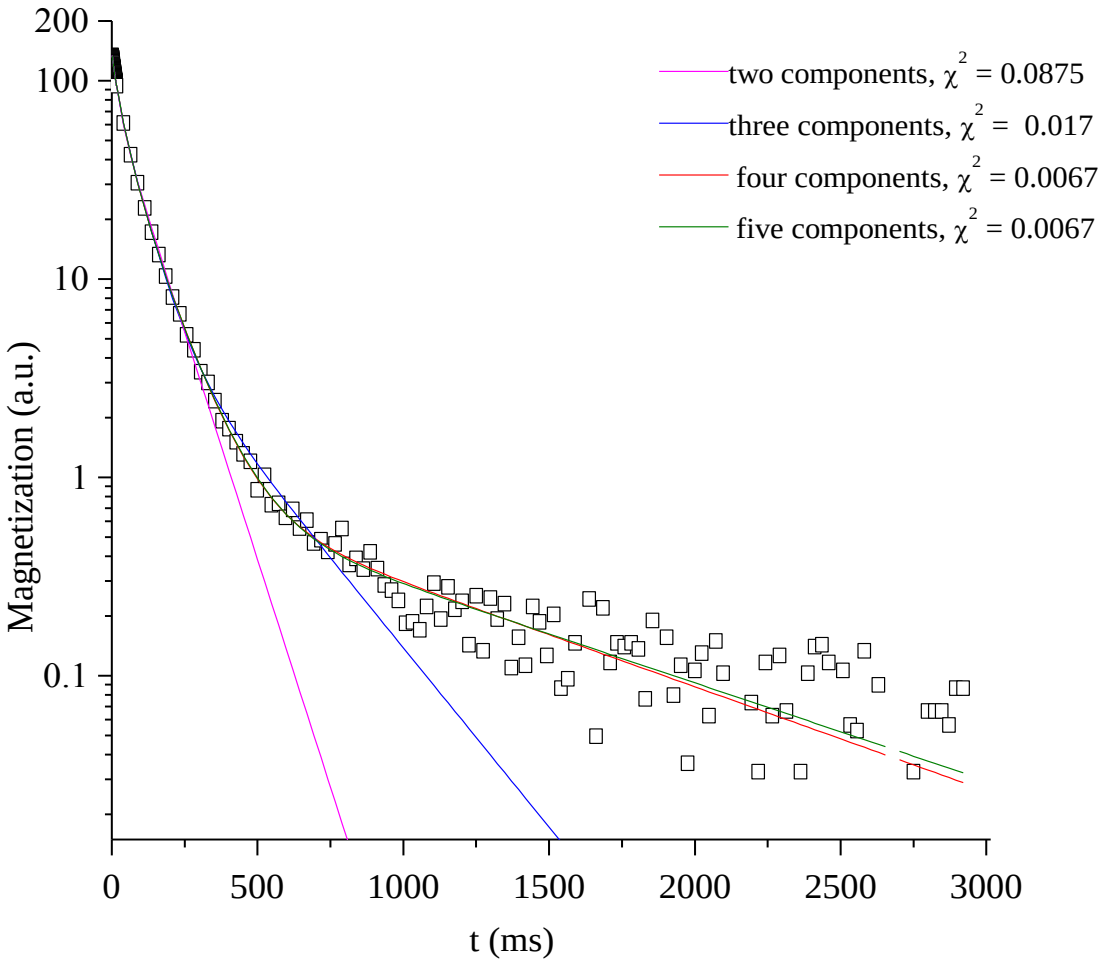

Figure 4.1 CPMG echo train for the natural cartilage sample at 3°C , shwing the variation of the minimum χ^2 value and the best-fit lines for two to five component multi-exponential analyses. The χ^2 values are given in the figure legend and adjustabale parameters providing the best fit for each case are presented in Table 4.1.

Table 4.1 CPMG of natural cartilage at 3°C with different decompositions and χ^2 values for best fitting

Components of natural CPMG at (3°C)	T_2 (ms)	Magnetization (%)	χ^2
Two component	22.0 ± 0.5	63 ± 1	0.0875
	95 ± 1	76 ± 1	
Three components	16.5 ± 0.5	41 ± 1	0.017
	69 ± 1	89 ± 1	
	240 ± 13	9 ± 1	
Four components	12 ± 1	23 ± 2	0.0067
	41 ± 2	64 ± 2	
	105 ± 3	52 ± 3	
	827 ± 78	1.0 ± 0.1	
Five Components	11 ± 3	17 ± 15	0.0067
	24 ± 29	21 ± 35	
	49 ± 22	56 ± 36	
	111 ± 11	44 ± 15	
	881 ± 107	1.0 ± 0.5	

4.1.5 2D-TD NMR

A crucial element of a meaningful exchange analysis is the availability of a relaxation parameter data set (apparent relaxation times and spin group sizes) that is as complete as possible. Drawing upon results from different spin relaxation experiments (T_1, T_2, $T_{1\rho}$) is important in this regard. In addition, it has been shown that 2D-TD NMR relaxation parameters can be particularly effective in characterizing different spin groups or reservoirs such as those of macromolecules and water, as well as to detect and define inter-spin group magnetization exchange [19, 54, 115-118].

In 2D-TD NMR, the evolution of the magnetization along the τ-axis (time for recovery of magnetization along the z-axis in T_1 experiment; time for decay of magnetization along the y-axis in $T_{1\rho}$ experiment) and the t-axis (time defining evolution of the FID) are monitored in a single spin-lattice relaxation time experiment. The magnetization recovery (T_1 experiment) or decay ($T_{1\rho}$ experiment) for each time point t_i (sampling point) along the FID can then be analyzed, and if applicable, decomposed into magnetization components. For each t_i, this analysis yields the T_1 (or $T_{1\rho}$) values and $\tau = 0$ intercepts of each magnetization component obtained from the decomposition.

The resulting T_1 (or $T_{1\rho}$) values are averaged over all sampling points for each resolved component, yielding a more reliable component magnetization T_1 ($T_{1\rho}$) compared to that determined in a single sampling point experiment/analysis. For each resolved component, the $\tau = 0$ intercepts, viewed as a function of t, define the component's "reconstructed FID." Fitting these reconstructed decay curves to either a Gaussian (for solid-

like components) or exponential (for liquid-like components) function, we determine the T_2 values of the magnetization components obtained from the 2D spin-lattice relaxation experiment.

In this work, the analysis of the 2D spin-lattice relaxation data was performed using the program CracSpin [119]. This program utilizes 2D data as input, and uses a Marquardt nonlinear least-squares minimization algorithm [114]. This provides the best-fit reconstructed FID data, as well as the t_i- averaged values of the T_1 of each resolved magnetization component.

4.1.6 Magnetization Exchange Analysis

To analyse the relaxation results for exchange, the approach outlined in Oleskevich *et al.* [19], was used. In this approach, the apparent relaxation parameters *(λ's* (T_1^{-1}'s) and C's (*t* = 0 intercept from reconstructed FIDs) are expressed in terms of the intrinsic relaxation parameters (R's (relaxation rates), k's (exchange rates) and spin reservoir sizes) [19]. Then, using an iterative, minimization algorithm, based on SIMPLEX (Vetterling *et al.*) [20], with the experimental, apparent parameters as input, and the intrinsic parameters as adjustable parameters, the apparent relaxation parameters are calculated. These are then compared to the corresponding experimental values. The intrinsic parameters providing the best-match values for the apparent parameters are used to define the articular cartilage intrinsic relaxation parameters and exchange rates. Typically, the number of apparent parameters needed to define all intrinsic parameters properly, exceed the number of apparent parameters available in any given experiment. In part, this shortcoming can be overcome by combining results

from different experiments. For example, a certain apparent T_1 not available from the T_{1HH} experiment may be defined in the T_{1SH} experiment. In certain cases, some of the intrinsic parameters may be known from other sources and can be fixed in the minimization procedure. For example, intrinsic magnetization fractions may be available from T_2 experiments, or defined from the sample stoichiometry. Figure 4.2 shows a summary of the steps for magnetization exchange.

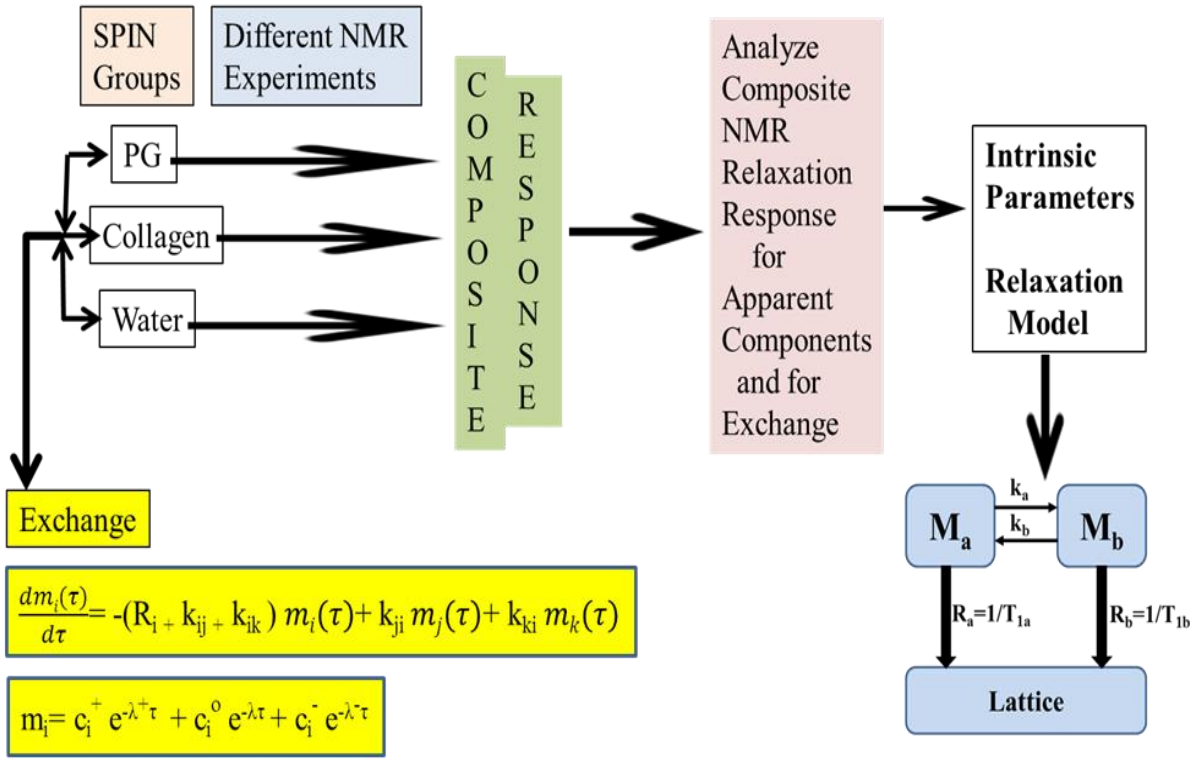

Figure 4.2 Summary of steps for magnetization exchange analysis and modeling.

4.2 500 MHz Experiments

4.2.1 Sample preparation

Femoral articular cartilage tissues were harvested from freshly slaughtered bovine animals, between twelve and twenty four months of age. In anticipation of the NMR scans, the tissue was cut in cylindrical plugs of 3 mm diameter and 1 mm thickness. Typically, 100 plugs were stored in a standard phosphate buffer solution (PBS) with pH 7.4 at 4^{o}C until use.

Deuterated and non-deuterated samples were prepared. For the deuterated samples, the tissue was treated with a deuterated PBS (D_2OPBS), changing the bath three times to completely replace the H_2O with D_2O. The first bath was changed after four hours, the second was changed after twelve hours, and the last after forty eight hours; at this point, and the samples were ready for measurements. The D_2OPBS mixture was made of 100g D_2O; 722.4 mg NaCl; 18.06 mg KCl; 130.03 mg Na_2HPO_4; and 21.67 mg KH_2PO_4. All chemicals and deuterated water, with an isotopic purity of 99.9%, were purchased from Sigma-Aldrich Co, St. Louis, MO, USA.

In order to model diseased cartilage, half of the plugs were treated with trypsin enzyme to deplete proteoglycan (PG). Trypsin is known as a selective enzyme and works mainly by cleaving PG at the C-terminus of a lysine or arginine residue [84]. It works without touching the collagen. To achieve different PG depletion levels, the tissue samples were placed in a trypsin buffer solution bath for different time durations, and for different bath concentration levels. In order to stop the trypsin enzyme activity and to stabilize the samples were then rinsed and placed in a trypsin-inhibitor buffer solution bath for two hours

[85]. The samples were ready for NMR measurements. After the measurements, all samples were weighted then placed in centrifuged vials with small hole openings under ~10^{-4} Torre vacuum for four hours to achieve fully dehydrated samples. Depending on the sample dried weight a specific papain volume (1mg/ml) was added. Papain is a non-selective enzyme, was used to complete the digestion of the cartilage. The tissue was left in a papain bath at 65^{o} C for 12 hours. Afterward, the samples were centrifuged, the supernatant liquid extracted and stored at 4^{o} C. For further analysis of the proteoglycan content and the calculation of the percentage of depletion, supernatant liquid obtained from the trypsin and trypsin-inhibitor treatments were also stored. All enzymes were purchased from Sigma-Aldrich Co., St. Louis, MO, USA.

4.2.1.1 Standard curve preparation

In order to prepare a standard curve for media, papain was incubated in a digestive buffer at 65^{o}C for twelve hours. A stock solution of Chondroitin Sulphate (CSC) was prepared by dissolving 50 mg of CSC in 1% Bovine Serum Albumin (BSA) in PBS. The working solution of CSC was prepared by diluting 30 µl stock CSC in 1470 µl of incubated papain in digest buffer , while for media 1,9-dimethylmethylene blue (DMMB) it was the same dilutant ½ media: ½ papain in a digestive buffer. The standard curve was constructed according to a set of different dilutions. The standard curve was tested to determine accuracy and slope before plating the actual samples. If the standard was good, the standard and samples (3x50 µl) were pipetted into a 96 well plate. The standard curve showed a specific color range when the 200 µl dye was added. It was important to make sure that the samples

fell into that color range, while some samples were diluted far more than others to fall into the standard curve.

For all the supernatant solutions, a DMMB assay from Sigma was prepared [120]. The proteoglycan content of each solution was measured by absorbance spectroscopy at 525 nm using a Thermo Lab System Multiskan. The absorbance results were compared with the calibration curve relating the absorbance to the concentration. The concentrations thus determined were used to calculate the percentages of depletions.

4.2.2 Apparatus

The NMR scans were performed on a Bruker AVANCE 500 WB working at 500MHz for proton. The MAS experiment used a triple tuned MAS probe with a 4 mm zirconia rotor sealed with an O-ring gear cap. The CSI experiment used a micro-imaging probe with a 5 mm coil insert.

4.2.3 NMR Data Acquisition

Two complementary NMR experiments were performed on two series of depleted cartilage. These experiments were designed to single out PG and collagen with distinct scanning protocols. In one series, the tissue was scanned with a magic angle spinning (MAS) technique and in the other, a chemical shift imaging (CSI) technique.

For the MAS experiment, the cartilage plugs were packed into a KEL-F form inserted in the zirconia rotor, typically 6 plugs at a time; this configuration insured a better localization of the sample inside the coil, and a better DC and RF field homogeneity. Furthermore, the plugs were submerged in liquid medium D_2OPBS, added to minimize

magnetic field susceptibility distortions from air-cartilage interfaces. This configuration was centrifuged to remove air bubble formation. The MAS rate was 5 kHz. The pulse sequence was a standard spin echo sequence with a repetition rate (TR) of 5 s, an echo time delay (TE) of 1 ms, and a number of scans, (NS) equal to 32. The acquisition dwell time (DW) was 2 μs. The width of the 180^{o}-pulse was 8 μs.

The collagen signal was obtained at MAS rate equal to zero, with a one pulse sequence modified to alternatively invert the z-magnetisation prior to the 90 degree excitation pulse: a technique used to subtract interfering non-inverting spurious probe signals from the observed signal, so as to obtain the collagen signal. For this scan: TR = 5 s; NS = 32; DW = 2 μs. As above the 180^{o}-pulse length was 8 μs.

The CSI experiments (see section 2.4.2 and T. R. Browne *et al.*) [23] were performed on cartilage samples made of 4 plugs, packed in a static KEL-F sample holder filled with D_2OPBS, and closed with a KEL-F adjustable plunger. This package was put into a 5 mm NMR tube and installed in the imaging coil. For the PG scan, the pulse sequence was a 1D CSI spin echo sequence with water suppression. The three suppression pulses were 6 ms in duration and centered on the residual water peak. Each of these pulses was followed by dephasing gradients in the X and Y directions. The spin echo segment of the sequence used non-selective RF pulses with TR = 5 s, TE = 7 ms, NS = 64, and a width of 10 μs for the 180^{o}-pulse; the acquisition dwell time was 2.4 μs. The 1D CSI phase encoding direction was along the z-axis parallel to the magnet's main field. As the sample was typically 4 mm long and centered in the coil, the field of view (FOV) was set at 6 mm. Prior to the actual CSI scan, a standard 2D spin echo image was taken with a 6 X 6 mm FOV , a 1 mm slice

thickness, and TR = 5 s, TE = 7 ms, NS = 4. This scan was used to assert the position of the sample in the coil, and to observe morphological details in the content of the plugs. The collagen signal was obtained as for the MAS experiment, but with a 180^{o}-pulse length of 10 μs.

Chapter 5
Results and Discussion

5.1 Transverse Decay Curves at 30 MHz

Transverse decay experiments were performed in natural and deuterated articular cartilage, at above and below freezing temperatures. Although the macromolecule component contributes only about 15 % of the sample signal it plays a key role in defining the tissue in both healthy and diseased states, and is an important focus here. Cartilage tissue is made of ~80% water with a dominant proton NMR signal. Deuteration of cartilage serves to eliminate the water signal and the complications produced by its coupling to the macromolecules. Because this component is expected to be more readily resolvable in the deuterated tissue, in which the dominant water proton NMR signal seen in the natural sample is absent (or at least substantially reduced), the results from the transverse decay experiments in the deuterated tissue are considered first.

5.1.1 Proton T_2 in Deuterated Cartilage at 3°C

Figure 5.1a shows a typical proton FID of deuterated bovine articular cartilage sample at 3°C. The following transverse decay model, consisting of a sum of Gaussians and exponentials, has been successfully applied to various hydrated biopolymer systems

$$M_y(t) = \sum_{i=1}^{N_G} M_{0Gi} e^{-ln2(t/T_{2Gi})^2} + \sum_{i=1}^{N_E} M_{0Ei} e^{-t/T_{2Ei}} \quad (5.1)$$

where N_G and N_E are the respective number of Gaussian (G) and exponential (E) components, T_{2Gi} and T_{2Ei} are the T_2 values of component magnetizations M_{0Gi} and M_{0Ei}, respectively.

A good fit to the data was obtained using Eq. 5.1 with the sum of two Gaussian decays, with T_2 = 17 μs (S_{1D}) and 79 μs (S_{2D}), and one exponential decay with T_2 ~ 4 ms. This 4 ms component amounts to ~ 36 % of the signal. The magnitudes of the Gaussian and exponential components, together with the corresponding T_2 values, are given in Table 5.1. The FID data for longer times (t > ~ ms; not shown) start to curve downward with increasing t. This is attributed to diffusion of spins in an inhomogeneous magnetic field. A pure water sample has a T_2 of a few ms in the magnet used in this work. Therefore, in keeping with the literature, the T_2 derived from the short-time (~ 400-1400 μs), exponential (linear on semi-log plot) portion of the FID is labeled T_2^* (Table 5.1).

The true T_2 of this more liquid–like magnetization can be obtained from a CPMG experiment, Fig. 5.1b. The echo train amplitude is well described by the sum of three exponentials with T_2 ~ 1 ms (L_{1D}), 17 ms (L_{2D}) and 370 ms (L_{3D}). These T_2 values and associated magnetization fraction are given in Table 5.1. These fractions have been normalized so that their sum equals 36.1 %, the fraction of the magnetization with $T_2 \sim T_2^*$ ms found in the FID experiment.

(a)

(b)

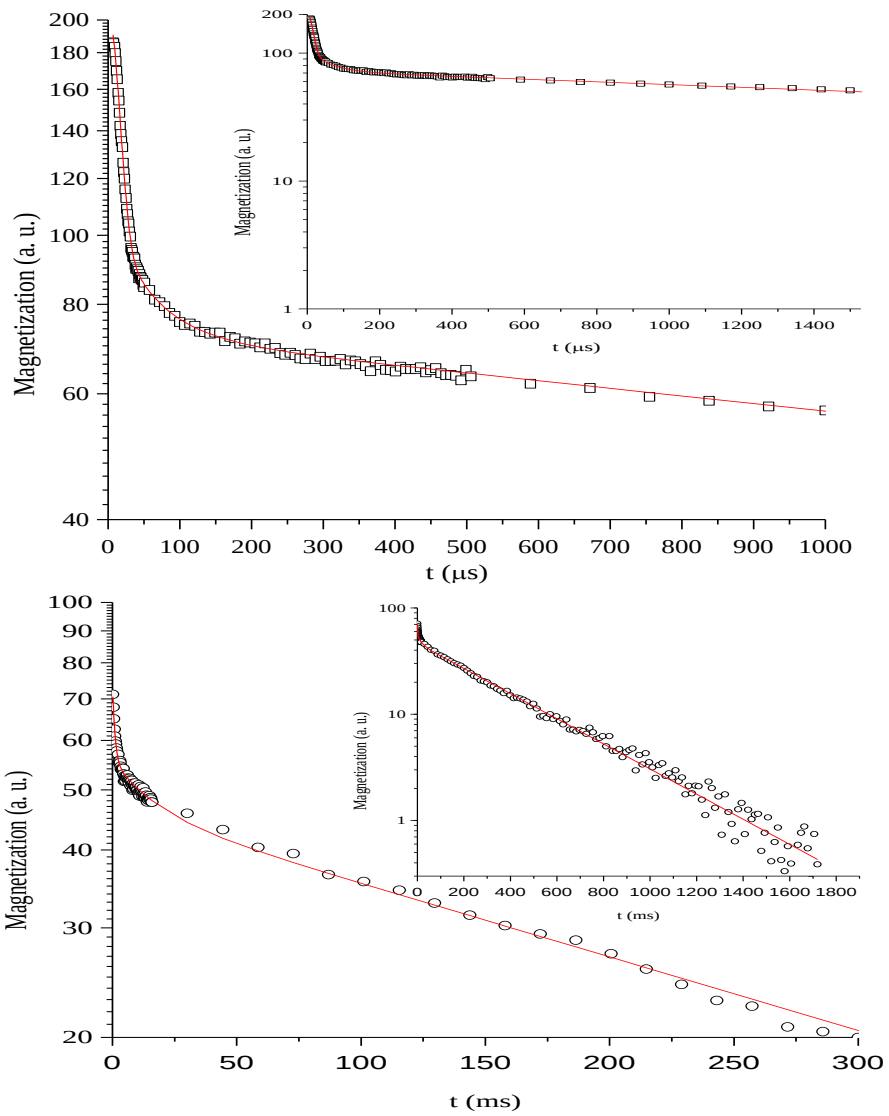

Figure 5.1 a) FID signal of deuterated articular cartilage sample , measured at 3°C and Larmor frequency of 30 MHz (a. u. ≡ arbitrary units). The inset shows the FID data, vertically rescaled in order to offer a better perspective of the relative amplitudes of solid-like and liquid-like signals. The solid line was calculated using equation 5.1 with the best-fit parameters given in Table 5.1. b) The first 300 ms of the CPMG echo train (2 τ = 200 μs) for the same sample with data points representing the peaks of the echoes. The inset shows the echo train data down to about ½ percent of the amplitude at t = 0. The solid line represents a 3-exponential fit, with the best-fit parameters given in Table 5.1.

Table 5.1 Best-fit parameters describing the transverse decay in deuterated articular cartilage at 3°C, Fig. 5.1 and at -10°C, Fig. 5.4. Repetition time was 60 s for the FID and CPMG at 3°C and at -10°C.

	Experiment	T_2	Assignment	Magnetization (%)
3°C	FID	16.5 ± 0.5 µs	Collagen (S_{1D})	55 ± 1
	FID	79 ± 3 µs	CH_3 (S_{2D})	9.0 ± 0.5
	FID	T_2^*	-	(36.0 ± 0.5)
	CPMG	1.0 ± 0.5 ms	PG (L_{1D})	9.0 ± 0.5
	CPMG	17 ± 2 ms	L_{2D}	4.0 ± 0.5
	CPMG	370 ± 10 ms	HDO (L_{3D})	23.0 ± 0.5
-10°C	FID	15.0 ± 0.5 µs	Collagen (S_{1D})	82.0 ± 0.5
	FID	69 ± 2 µs	CH_3 + HDO ice(S_{2D})	9.0 ± 0.5
	FID	T_2^*	-	(9.0 ± 0.5)
	CPMG	2.0 ± 0.5 ms	PG (L_{1D})	6.0 ± 0.5
	CPMG	11± 1 ms	L_{2D}	3.0 ± 0.4

In a fully deuterated sample the proton signal is expected to originate from macromolecule protons only, with T_2 values ranging from ~ 20 μs for solid-like proton groups, to milliseconds for more mobile groups. About 20-22 % of the protons of macromolecular components of cartilage are expected to be exchangeable with D_2O aqueous medium. These are expected to have been removed in the deuteration procedure described in chapter 4. Liquid-like T_2 would only be expected for protons on very small/short non-aggregated PG fragments. To estimate the size of fragments corresponding to T_2 ~ 0.4 s, we use the Stokes- Einstein- Debye relation:

$$\tau_c = \frac{4\pi\eta a^3}{3kT} \ , \tag{5.2}$$

where τ_c is the correlation time for rotational motion, η is the viscosity, a is the radius of the macromolecule, k is Boltzmann constant and T is the temperature.

Taking the radius of a water molecule equal to its van der Waals radius of 3^oA, water proton T_2 = 3 s and considering T_2 α $\frac{1}{\tau_c}$ in the extreme motional narrowing regime, we have

$$\frac{a^3_{fragment}}{a^3_{H_2O}} = \frac{T_2(H_2O)}{T_{2\ fragment}} = \frac{3\ s}{0.4\ s} \sim 7 \ . \tag{5.3}$$

Since the volume, and approximately the mass, of the molecule can be considered to scale as a^3, the weight of the fragments should not be much more than ~ 10 times the water molecule weight (~ 10 MW_{H_2O} ~ 200 g/mol). This represents extremely small fragments, and if

fragments are not be expected to contribute significantly to the mass of the cartilage. Based on the above we conclude that the L_{3D} component is due to protons in the water pool.

As will be considered later, in section 5.3, this conclusion is consistent with the observation of a significant water proton peak, at ~ 4.7 ppm in the proton spectrum taken in the deuterated cartilage at 500 MHz.

In order to gain insight into the source of the significant water proton content in the deuterated tissue the proton signal was measured in the following samples of known volume: H_2O, D_2OPBS, as well as the first and last D_2OPBS bath used in the tissue deuteration, immediately following the extraction of the tissue from the bath (Table 5.2). The sample sizes are shown, as well as the proton signals, expressed in arbitrary units, and adjusted so that the same gain condition applies.

The magnitude of the proton signal in the H_2O sample of known volume was measured as reference for the ^1H signals in the other samples and was used to normalize the signals in Table 5.2, such that its magnitude equals 100 %. In the process of normalizing the signals from the samples, other than for the H_2O sample, each signal was first adjusted to take into account the different sample volumes. Although, D_2O of 99.9 % purity was used for D_2OPBS preparation, a 0.2 % ^1H signal (relative to equivalent volume of H_2O) was detected. This means that instead of 100 % deuterons in the D_2OPBS sample, there are 99.8 % deuterons and 0.2 % protons. A clear reduction in ^1H content is observed from the first bath to the final solution used. Also given in Table 5.2 is the water proton signal (normalized as above) in the cartilage tissue used in the experiments.

Table 5.2 ^{1}H content in the deuterated solutions and deuterated cartilage sample under same-gain conditions. The NMR signal for each sample was normalized with respect to an equivalent volume of H_2O.

Sample	Deuteration Time	Sample size	Proton signal (arbitrary units)	^{1}H content (%)
H_2O	N/A	100 µl	448	100
D_2OPBS	N/A	400 µl	3.3	0.2
First Bath	4 hours	400 µl	122	8.2
Last Bath	48 hours	400 µl	9.5	0.5
D_2O Cartilage	-	277 µl	72	5.8

If we expect about the same percentage of ^{1}H in the aqueous medium of the deuterated articular cartilage sample, as in the final solution (0.5 %), then we can estimate the size of the expected liquid-like water proton signal in the deuterated tissue as follows.

Considering that the moisture content of the present sample is

$M.C. = \frac{mass\ D_2O}{mass\ dry\ tissue} \times 100 = 470\ \%$, that the relative spin densities relative to spin density of water of PG and collagen are ρ_{PG} = 0.56 and ρ_{coll} = 0.58, respectively, and using an estimated collagen to PG mass ratio of $\frac{74}{26}$, we find that in the present sample the ratio of water protons to macromolecule protons is expected to be about:

$$\frac{0.5\ \%\ of\ 470}{(0.58 \times 74) + (0.56 \times 26)} = \frac{2.35}{57.5} \quad .$$

This would mean that about 3.9 % of the signal in the deuterated cartilage is due to the ^{1}H content of the last exchange bath.

In order to ascertain the actual ^{1}H content in the water in the D_2O cartilage sample, the observation that the transverse decay curve in this tissue consists of several components (see Table 5.1) needs to be considered; i.e., which component(s) are associated with protons in the tissue water rather than with macromolecular components. As found by others (Ghiassi-Nejad *et al.* and Lattanzio *et al.*) [53, 54], liquid-like T_2 values in natural cartilage are in the range from tens of milliseconds to hundreds of milliseconds. In the deuterated tissue most of the water protons are residing on HDO molecules. Letting *I* and *S* be the ^{1}H and ^{2}H spins, respectively: then the ^{1}H-^{2}H dipole-dipole interaction is only

$\left[\left[\frac{1}{3}\gamma^2 \pm \gamma_s^2 S(S+1)\right] / \left[\frac{3}{4}\gamma_I^4 I(I+1)\right]\right]^{1/2} = 1/35.8$ of the ^{1}H-^{1}H dipole-dipole interaction in natural tissue, so that it is reasonable to assign only the L_{3D} (370 ms) T_2 component to tissue water protons in the deuterated tissue. This component has a magnitude of 72 signal units (Table 5.2) for the same gain conditions as used for the other data given in Table 5.2 (column "proton signal"). This result indicates that in terms of the percent ^{1}H content in the tissue water, this 22.7% cartilage magnetization component amounts to 5.8 %, i.e., an increase of about a factor 11 relative to such content in the last deuteration bath. We can also estimate the proportion of D_2O, H_2O and HDO in the tissue water for a deuterated sample with *x*% protons in the water component of the tissue, the proportions of D_2O, H_2O and HDO for a 5.8% proton content the proportions of D_2O, H_2O and HDO become 88.7%:0.3%:10.9%.

The observation that only about (1/5) of the L_{3D} component can be accounted for by the H- content in the D_2OPBS bath used in the last deuteration step, taken together with the absence of a significant contribution from macromolecules or macromolecular fragments with molecular weights of the order of a few hundred g/mol, could be taken to suggests that a part of the L_{3D} component may be due to protons of H_2O molecules trapped in isolated regions in the tissue (e.g., intrafibrillar spaces), which are not water accessible for D → H exchange to occurs on the time scale of the present experiments.

An alternate explanation for the unexpectedly large proton signal with L_{3D} (T_2 = 370 ms) in this sample is that following the last deuteration step (48 hours in duration) additional exchangeable macromolecule hydrogens exchange with deuterons in the water, to add to the water proton signal. However, this possibility can be discarded because the H → D exchange already had been allowed to proceed for a period of 4 + 12 + 48 = 64 hours; an additional 1 to 2 hour period, between removal of the tissue from the last D_2OPBS bath and the FID/ CPMG measurement (see Fig. 5.1, Table 5.1, 5.2), cannot be expected to release/ exchange any appreciable, additional amount of water ^{1}H content.

Based on the above discussion we associate the S_{1D}, S_{2D}, L_{1D}, L_{2D} and L_{3D} components (Table 5.1) with cartilage macromolecular constituents. For the main part, the collagen proton spin groups are expected to be solid-like, with T_2 in the rigid-lattice regime. Therefore, the S_{1D} component, with T_2 = 17 μs, is assigned to collagen protons. The T_2 ~ 80 μs of the S_{2D} component, amounting to 9 % of the cartilage magnetization, is too long to be assigned to a typical, solid-like polypeptide, and may be associated with collagen or PG

protons, which are either somewhat more mobile than those of the S_{1D} component or experience a smaller dipole – dipole interaction with neighboring protons.

5.1.2 Proton T_2 in Natural Cartilage at 3^oC

Figure 5.2a shows a typical FID of a natural bovine articular cartilage sample at 3^oC and Larmor frequency of 30 MHz. The solid line was calculated using equation 5.1 with the best-fit parameters given in Table 5.3. Figure 5.2b shows the CPMG echo train ($2\tau = 200$ μs) for the same sample with data points representing the peaks of the echoes. The solid line represents a 2-exponential fit, with the best-fit parameters given in Table 5.3. The inset shows the echo train data down to about ½ percent of the amplitude at t = 0 and shows the first 300 ms of the echo train, more clearly showing the fit and behavior of the decay at earlier times.

An excellent fit of eq. (5.1) to the data (Fig. 5.2, a) was obtained for the sum of two Gaussian decays, with $T_2 \sim 18$ μs (S_{1N}) and 64 μs (S_{2N}), and one exponential decay with $T_2 \sim$ 22 ms. The magnitudes of the Gaussian and exponential components are 7.4%, 1%, and 92%, respectively, and are shown, with the corresponding T_2 values in Table (5.3).

(a)

(b)

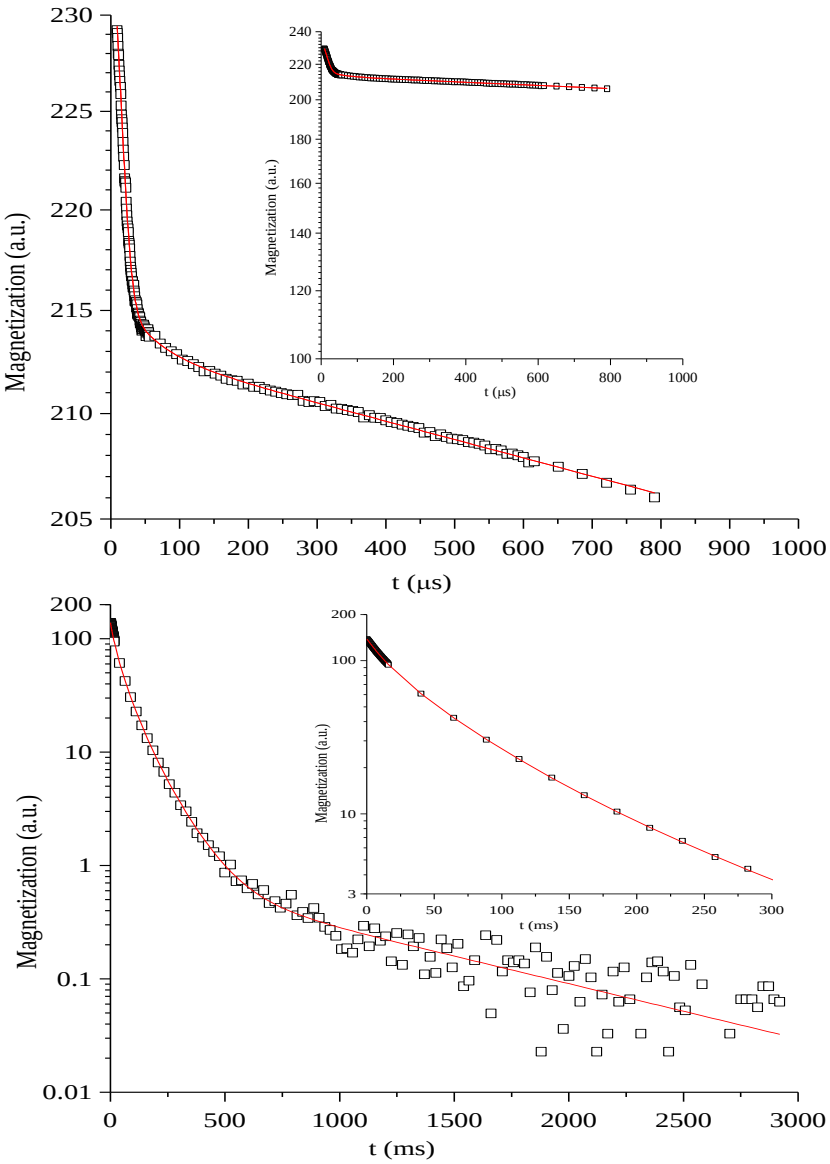

Figure 5.2 a) FID signal of natural articular cartilage sample, taken at 3^{o} C and Larmor frequency of 30 MHz. The inset shows the FID data vertically rescale in order to offer a better prespective of the relative amplitudes of solid-like and liquid-like signals. The solid line was calculated using equation 5.1 with the best-fit parameters given in Table 5.3. b) CPMG echo train for the same sample. The solid line represents a 2-exponential fit, with the best-fit parameters given in Table 5.3.The inset shows the first 300 ms of the echo train, more clearly showing the fit and behavior of the decay at earlier times.

Table 5.3 Best-fit parameters describing the transverse decay in natural articular cartilage at 3°C, (Fig. 5.2) and at -10°C, (Fig. 5.4). Repetition time was 6 s for the FID at 3°C and 60 s for the CPMG experiment at 3°C, while it was 60 s for both FID and CPMG at -10°C.

	Experiment	T_2	Assignment	Magnetization (%)
3°C	FID	18.0 ± 0.5 μs	Collagen (S_{1N})	7.5 ± 0.5
	FID	64 ± 4 μs	CH_3 (S_{2N})	1.0 ± 0.5
	FID	T_2^*	-	(91.5 ± 0.5)
	CPMG	12.0 ± 0.5 ms	H_2O + PG (L_{1N})	15 ± 1
	CPMG	41 ± 2 ms	H_2O (L_{2N})	42 ± 2
	CPMG	105 ± 3 ms	H_2O (L_{3N})	34 ± 2
	CPMG	900 ± 100 ms	L_{4N}	0.5 ± 0.5
-10°C	FID	9.5 ± 0.5 μs	Ice (S_{1N})	48 ± 3
	FID	16.5 ± 0.5 μs	Collagen (S_{2N})	36 ± 3
	FID	T_2^*	-	(16.0 ± 0.5)
	CPMG	1.0 ± 0.5 ms	PG + H_2O (L_{1N})	15.5 ± 0.5
	CPMG	6 ± 1 ms	Bound H_2O (L_{2N})	1.0 ± 0.5

The FID data for longer times (t > ~ ms; not shown) starts to curve downward with increasing t. This is attributed to diffusion of spins in an inhomogeneous magnetic field. The T_2 derived from the short-time (300- 1000μs), exponential (linear on semi-log plot) portion of the FID is labeled T_2^* (Table 5.3). The true T_2 of this more liquid-like magnetization can be obtained from a CPMG experiment, Fig. 5.2b. From the echo train three exponential magnetization components were resolved; components labeled L_{1N}, L_{2N} and L_{3N}, with T_2 = 14 ms, T_2 = 48 ms and T_2 = 113 ms, respectively.

A very small component (L_{4N}), amounting to ½ %, and with long T_2 ~ 900 ms, was assumed to be due to a small amount of water (mostly H_2O) on the surface of the tissue. Protons of such water are expected to have relatively long T_2, since the macromolecular surface proton - water molecule proton interaction is expected to be relatively unimportant for these water molecules. These T_2 and the associated magnetization fractions are given in Table 5.3. These fractions have been normalized so that their sum equals the amplitude (92 %) of the long, 20 ms exponential component found in the FID experiment. From results in the literature (Lattanzio *et al.* [54] and Ghiassi-Nejad *et al.* [53]) indications are that a significant fraction of the PG proton pool in fully hydrated cartilage tissue is relatively mobile with T_2 in the 1 - 2 ms range. This component was not resolved in the present FID experiment in the natural cartilage, likely because its T_2 is too similar to the "magnet T_2". In addition, it is expected that in the presence of the large water proton signal, the PG signal amounts to only a few percent of the total natural cartilage signal and therefore is difficult to resolve in either the FID experiment or the CPMG experiment. Although the FID (Fig. 5.2a) clearly shows a small (< 1%) S_{2N} component with T_2 = 64 μs, which may be attributed to protons on somewhat mobile collagen components (perhaps on CH_3 groups) or relatively immobile protons on PG (perhaps on parts of core proteins), a definitive assignment is not possible from this T_2 data alone.

A fundamental aspect in the identification and characterization of the intrinsic relaxation parameters in the tissue involves the identification of water and polymer signal components. In this connection the water content or moisture content (*MC*) is an important

parameter. Neglecting the tissue's cell content and inorganic component of the matrix, which combined only amount to ~ 1 % of the dry mass [53], the moisture content can be written as

$$MC\ (\%) = \frac{water\ mass}{sum\ of\ PG\ and\ coll\ masses} \times 100 \quad . \tag{5.4}$$

Considering that the spin densities of collagen and PG, relative to that of water, are 0.58 and 0.56, respectively, we can rewrite the *MC* in terms of the component magnetizations (see Ghiassi-Nejad *et al.* [53]):

$$MC\ (\%) = \frac{M_{H_2O}}{\left(\frac{M_{PG}}{0.56}\right) + \left(\frac{M_{coll}}{0.58}\right)} \times 100 \quad . \tag{5.5}$$

Since PG is not separately resolved in this T_2 experiment (Fig. 5.2, Table 5.3), we use the result from the literature [53], that within about one percent, the non-water part of the cartilage is made up of 74 % collagen and 26% PG by mass, to write

$$MC\ (\%) = \frac{M_{liquid-like} - \frac{26}{74}\left(\frac{M_{coll}}{0.58}\right)}{\left(\frac{26}{74} + 1\right)\left(\frac{M_{coll}}{0.58}\right)} \times 100 \tag{5.6}$$

Here it has been assumed that the PG magnetization + water magnetization make up the $M_{liquid\text{-}like}$ component in Fig. 5.2a. Then using the data from Table 5.3 the *MC* becomes 508%.

Therefore, in this tissue the water, collagen and PG masses are related as *H_2O: Coll: PG* = 87.5:12.7:4.5.

The 14 ms T_2 component (L_{1N}, Table 5.3) may have contributions from water and macromolecular protons and cannot be clearly identified based on the present data. The 48 ms component (L_{2N}) and the 113 ms components (L_{3N}) are likely associated with water reservoirs in the tissue. The origin of the components L_{2N} and L_{3N} will be considered further below.

5.1.3 Transverse decay in frozen cartilage

5.1.3.1 Frozen natural cartilage

The macromolecular content in natural fully hydrated cartilage amounts only to relatively small fraction, which makes the investigation of these macromolecular components challenging. Besides deuterating the tissue, the resolution of the macromolecular component of the tissue can be increased in an NMR experiment by freezing the bulk water in the tissue. An increase in resolution is realized as a result of a) the T_2 of the bulk water assuming the value of ice (T_2 ~ 10 μs), so that this signal is typically partially hidden in the dead time of the receiver, and b) the T_1 of the protons involved (of the ice) becoming relatively long so that this signal can be substantially decreased due to saturation effects.

With the aim of obtaining a better resolution for the macromolecular component the same transverse decay measurements described in the previous section were repeated at -10^{o}C.

A first step is to define / characterize the freezing phase transition in our cartilage tissue. Considering results in the literature it is expected that the major part of the bulk water in the tissue is frozen at -10°C. In this work, the freezing phase transition temperature was determined by monitoring the change in the transverse relaxation times of magnetization components, and their fractions, in natural cartilage with decreasing temperature, from 14°C to -30°C (Fig. 5.3 and 5.4, respectively).

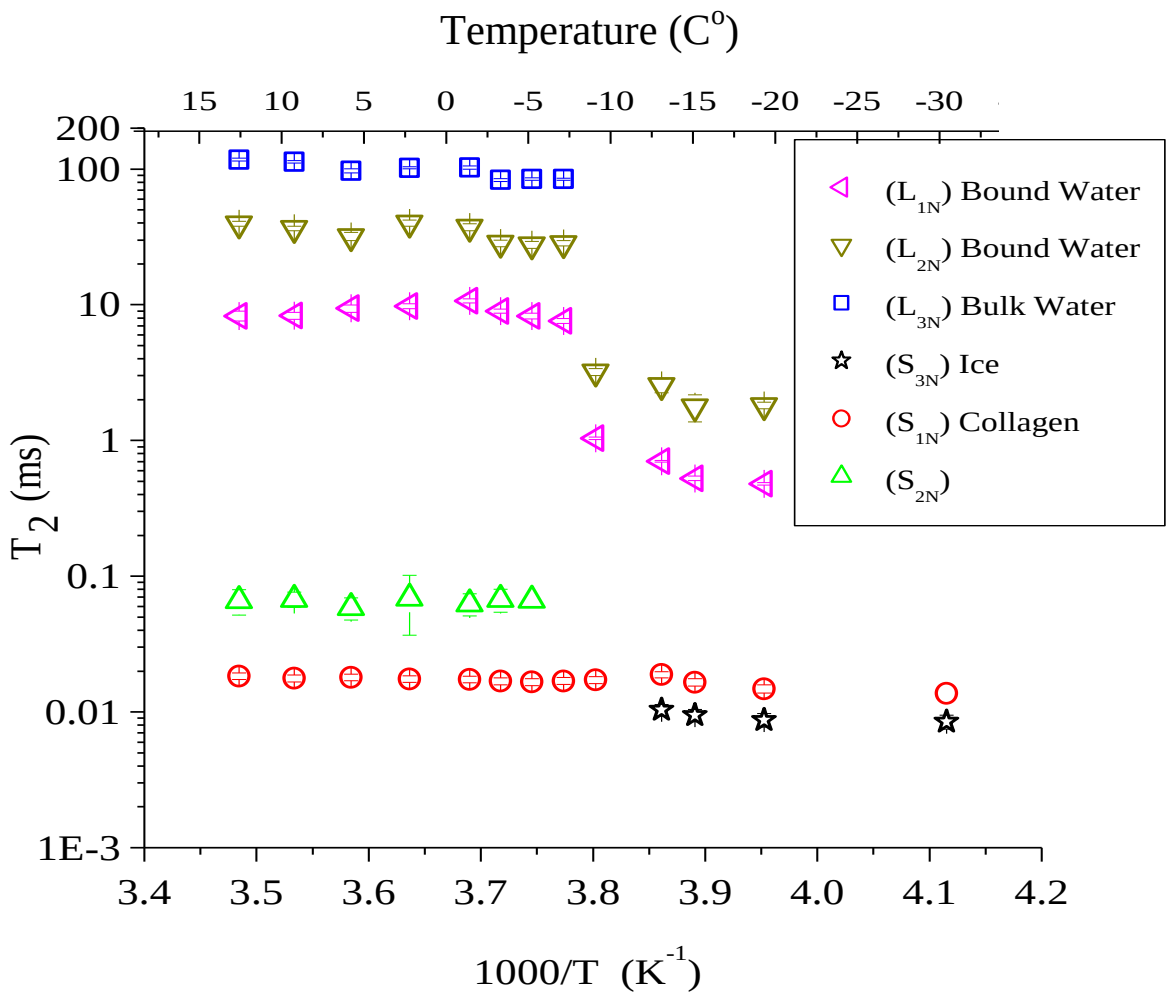

Figure 5.3 T_2 of solid-like and liquid-like components of the FID and CPMG signals versus 1000/T. The freezing of the bulk water can be seen to occure between -5°C and -8°C.

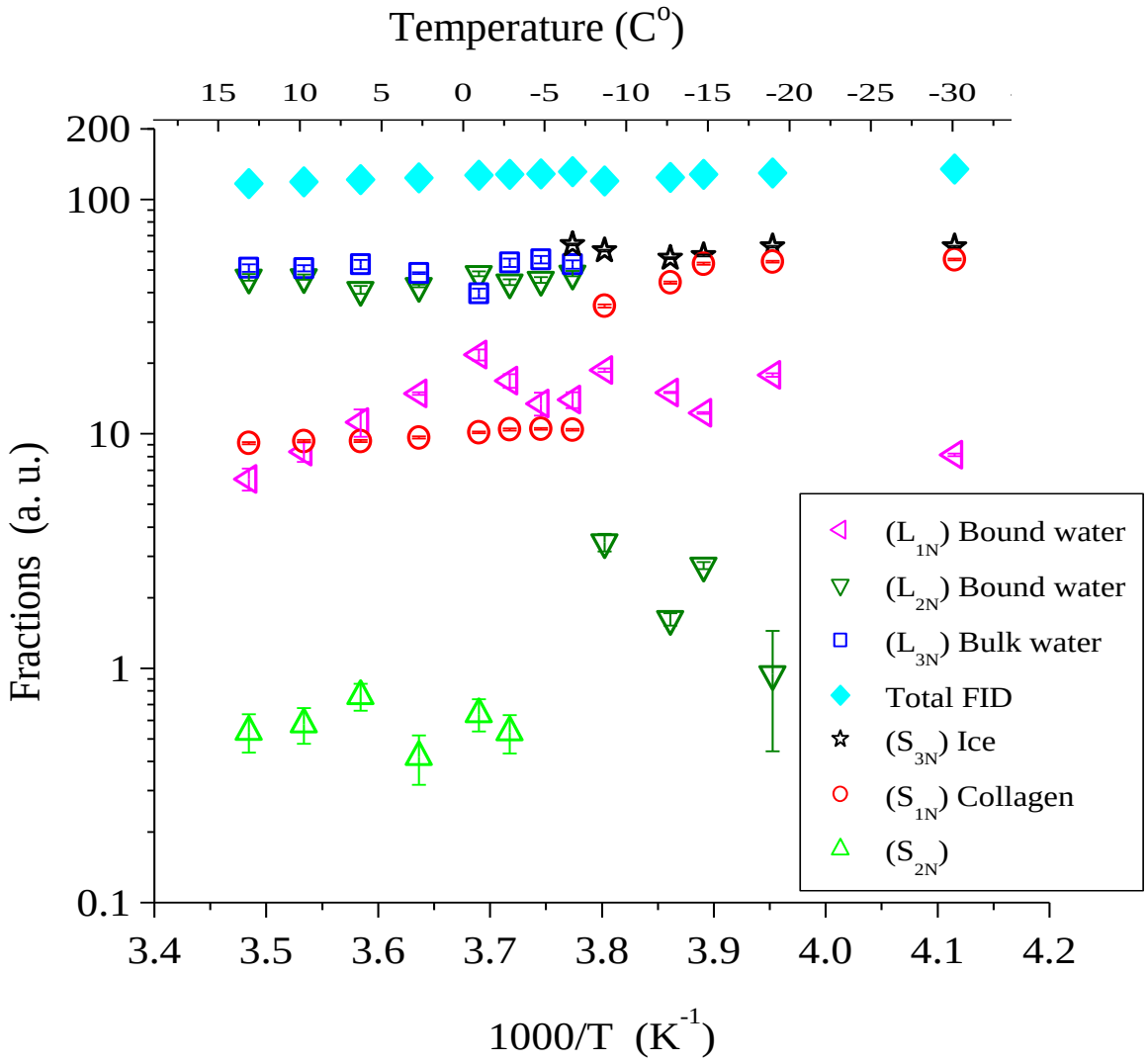

Figure 5.4 Fractions of solid-like and liquid-like components of the FID and CPMG signals versus 1000/T. The freezing of the bulk water can be seen to occure between -5°C and -8°C.

The 5-component structure of the transverse decay curves in the natural cartilage, seen at 3^{o}C (Table 5.3), also is observed at other temperatures in the 14^{o}C to -8^{o}C temperature range (Fig. 5.3). Between -8^{o}C and -10^{o}C a clear transition is observed in which the liquid-like magnetization components L_{1N}, L_{2N} and L_{3N} disappear.

Figure 5.5 shows FID and CPMG decay curves in natural cartilage at -10^{o}C. As for the FID at 3^{o}C, the FID curve on a semi-log plot at -10^{o}C also curves downward for long times, (see Fig. 5.5a). Therefore only the first 800 μs of the FID data was used in the analysis of the FID curve (see Fig. 5.5a). A good fit to the FID data (0 – 800 μs) is obtained using Eq. 5.1, with two Gaussian components and one exponential component. The solid line in Fig. 5.5a was calculated with Eq. 5.1 using the best-fit T_2 values and magnetizations given in Table 5.3. As the long tail of the FID is clearly influenced by field inhomogeneity, the T_2 of the long, exponential component is labeled T_2^*. The T_2 ~ 65 μs of the S_{2N} component, attributed to protons of solid biopolymers (mostly collagen) above -10^{o}C, appears unaltered by the transition. This would be expected as the T_2 of protons contributing to this component is in the rigid lattice regime at temperatures above this transition and would remain in this regime as the temperature is lowered further.

(a)

(b)

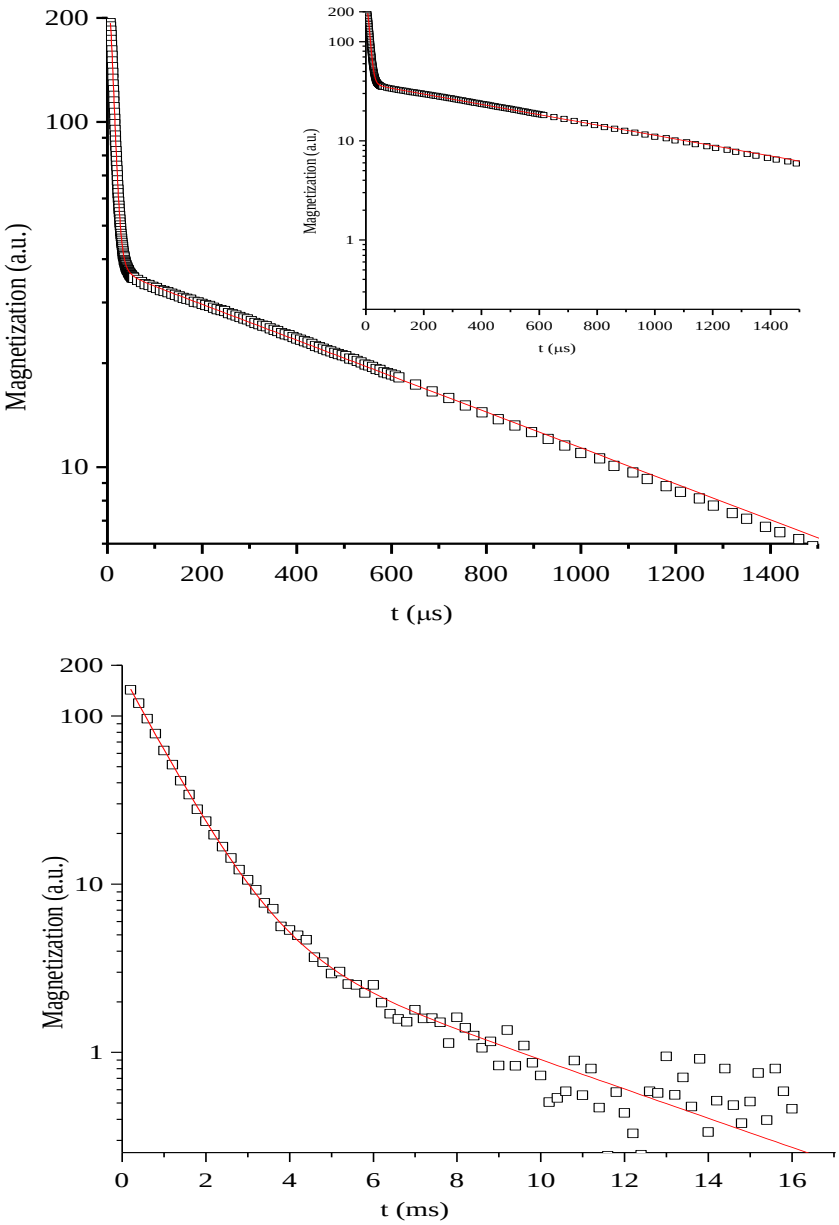

Figure 5.5 a) FID signal of natural articular cartilage sample, taken at -10^{o}C and Larmor frequency of 30 MHz. The solid line was calculated using eq. 5.1 with the best-fit parameters given in Table 5.3. b) CPMG echo train for the same sample. The data points represent the peaks of the echoes and the solid line represents a 2-exponential fit, with the best-fit parameters given in Table 5.3.

However, the assignment of this component magnetization (with T_2 ~ 65 μs) to polymer protons cannot be entirely correct. The signal magnitude of this component amounts to about 9 % of the signal above this freezing transition, but increases to about 30 % just below this transition. An increase would be expected if we assume that macromolecule proton groups, which are very mobile above the transition so as to exhibit a more liquid-like transverse decay, are immobilized by the freezing event. The only macromolecular proton groups which may be in this category, to make more than a negligible contribution, are on mobile parts of PG. Considering that the PG/Collagen mass ratio $\sim\frac{4.5}{12.7}$, and that we expect only about $\frac{1}{2}$ of PG to be relatively mobile above the freezing event, means that there may be a liquid-like polymer component above the transition, amounting to $\frac{\frac{1}{2}(4.5)}{12.7+\frac{1}{2}(4.5)}\times 100\ \% =$ 15 % of the solid-like component seen above the transition. This amounts to 1.5 signal units in Fig. 5.4. As the sample passes through the transition the corresponding magnetization likely takes on rigid- lattice character and adds to the 9 unit solid-like component, to become a 10 – 11 unit component at -10^{o}C. However, this signal component becomes about 30 units at -10^{o}C, which can only mean that a significant contribution to this signal component comes from water protons. This water is expected to be associated with the macromolecules in the cartilage in a way that prevents formation a) of ice structure (ice water $T_2 \leq 10$ μs, discussed below), and b) of a liquid-like bound water pool. To our knowledge this represents the first time that such a "solid-water" component has been observed in cartilage.

This result/interpretation is corroborated by results from T_2 experiments in deuterated cartilage, as well as results from the 2D spin-lattice relaxation experiments at -10^{o}C.

In section 5.1.2 the L_{3N} component was assigned to protons of bulk water. It is expected that the bulk water (navy squares), observed above -8^{o}C, freezes as the temperature is lowered to -10^{o}C and appears as ice at temperatures ≤ -10^{o}C; i.e., the S_{3N} component with $T_2 \leq 10$ μs (black stars data points in Fig. 5.3).

The T_2 components assigned to bound water (pink left tip triangles and olive green upside down triangles in Fig. 5.3).

The data from the frozen cartilage clearly shows a 1-2 ms component from natural and deuterated cartilage sample respectively, which was been assigned by Lattanzio et al. 2000, as PG. The 5-11 ms from both natural and deuterated cartilage sample respectively can be assigned as bound water (see Fig. 5.2, and Fig 5.6).

Freezing the cartilage tissue at (-10^{o}C) was one of the special approaches have been used to investigate on the changes of all relaxation times and compare them with the above freezing data at (3^{o}C).

5.1.3.2 Frozen deuterated cartilage

The macromolecular content in deuterated, fully hydrated cartilage was better resolved and less challenging relatively to the natural cartilage because of the elimination of the proton signal in the deuterated case. In order to increase the resolution of the macromolecular component of the tissue, we followed the same technique of freezing the bulk water in the natural tissue. As the FID at 3^{o}C and the FID at -10^{o}C curves downward for long times, inset of Fig. 5.5a. Therefore only the first 1000 μs of the FID was used in the analysis of the FID curve (see Fig. 5.5a). A good fit the FID data (0 – 1000 μs) is obtained using Eq. 5.1, with two Gaussian components and one exponential component. The solid line in Fig. 5.5a was calculated with Eq. 5.1 using the best-fit T_2 values and magnetizations given in Table 5.1. As the long tail of the FID is clearly influenced by field inhomogeneity, the T_2 of the long, exponential component is labeled T_2^*. A good fit to the data was obtained using Eq. 5.1 with the sum of two Gaussian decays, with T_2 = 15 μs (S_{1D}) and 69 μs (S_{2D}), and one exponential decay with T_2 ~ 1 ms. This 1 ms component amounts to 9.2 % of the signal. The magnitudes of the Gaussian and exponential components, together with the corresponding T_2 values, are given in Table 5.1. The FID data for longer times (t > ~ ms; not shown) start to curve downward with increasing t. This is attributed to diffusion of spins in an inhomogeneous magnetic field. A pure water sample has a T_2 of a few ms in the magnet used in this work. Therefore, in keeping with the literature, the T_2 derived from the short-time (0-1000 μs), exponential (linear on semi-log plot) portion of the FID is labeled T_2^* (Table 5.1). The true T_2 of this more liquid–like magnetization can be obtained from a CPMG experiment, Fig. 5.4b. The echo train amplitude is well described by the sum of three

exponentially with T_2 ~ 2 ms (L_{1D}) and 11 ms (L_{2D}). These T_2 values and associated magnetization fraction are given in Table 5.1. These fractions have been normalized so that their sum equals 9.2%, the fraction of the magnetization with T_2 ~ 1 ms found in the FID experiment.

The T_2 ~ 69 μs of the S_{2N} component, attributed to protons of semisolid biopolymers (mostly CH_3) above -10^{o}C, appears unaltered by the transition. This would be expected T_2 of protons contributing to this component is in the rigid lattice regime at temperatures above this transition and would remain in this regime as the temperature is lowered further. However, the assignment of this component magnetization (with T_2 ~ 69 μs) to polymer protons cannot be entirely correct. The signal magnitude of this component amounts to about 9 % of the signal above this freezing transition, and it stays the same below this transition in the deuterated sample.

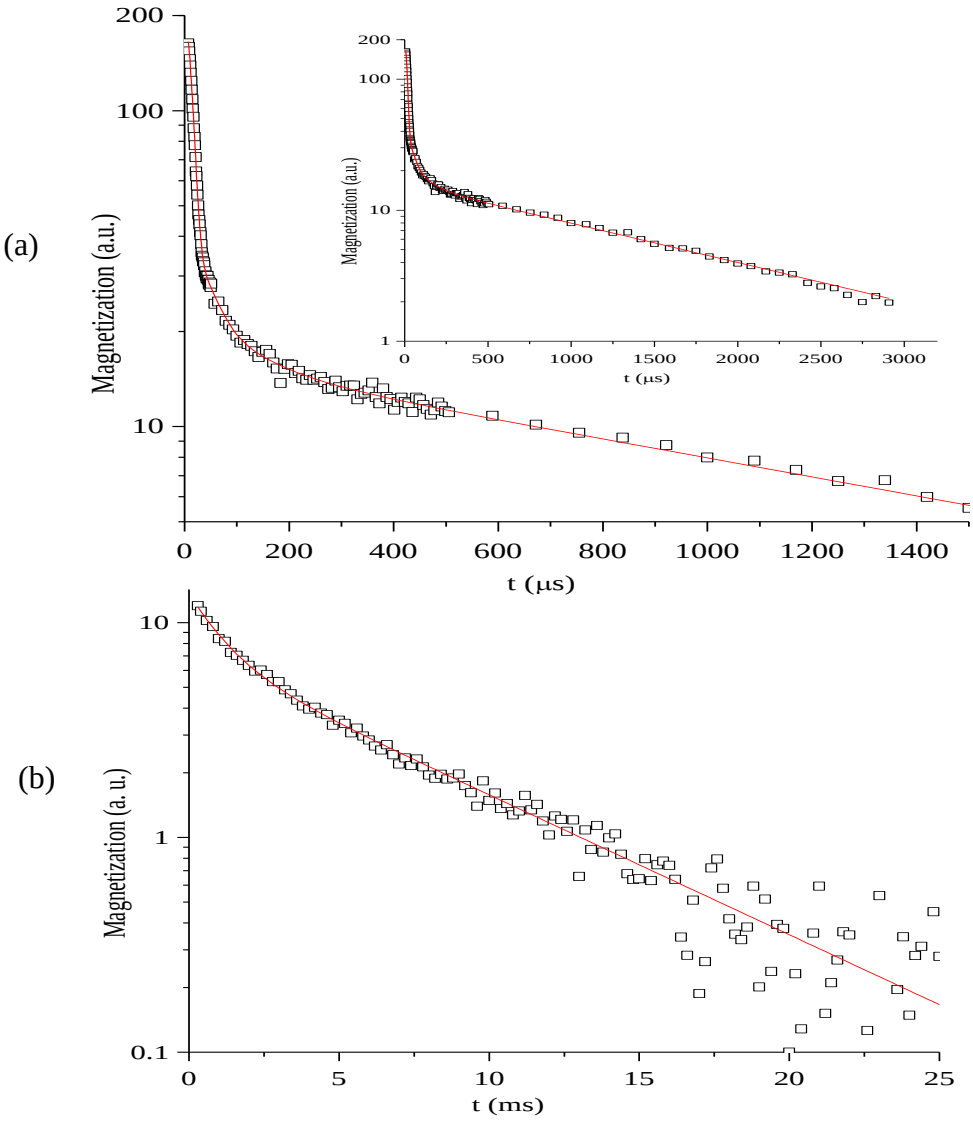

Figure 5.6 a) FID signal of deuterated articular cartilage sample, taken at -10°C and Larmor frequency of 30 MHz (a. u. ≡ arbitrary units). The inset shows the FID data, vertically rescaled in order to offer a better perspective of the relative amplitudes of solid-like and liquid-like signals. The solid line was calculated using equation 5.1 with the best-fit parameters given in Table 5.1. b) The first 12 ms of the CPMG echo train (2 τ = 200 μs) for the same sample with data points representing the peaks of the echoes. The inset shows the echo train data down to about ½ percent of the amplitude at t = 0. The solid line represents a 2-exponential fit, with the best-fit parameters given in Table 5.1.

5.2 2D Time Domain NMR Relaxation Results and Exchange Modeling at 30 MHz

One of the major goals of the 30 MHz relaxation experiments is to develop a comprehensive magnetization exchange model for cartilage tissue. The transverse decay experiments described in the previous section have provided information about different macromolecular and water phases, as observed and characterized through NMR spin-spin relaxation parameters, T_2 and magnitudes of magnetization components (or spin reservoir sizes). Some evidence for exchange between the L_{1N} and L_{2N} spins reservoirs is indicated (see Fig. 5.4). A very effective method for studying exchange, in particular also involving solid-like spin groups, is via 2D-TD NMR, combined with magnetization exchange analysis. As different spin-lattice relaxation experiments (e.g., T_1 and $T_{1\rho}$) typically yield different values of relaxation times- often differing by orders of magnitude- these experiments allow us to explore exchange on different time scales, which in turn allow us to access different system exchange regimes.

Here we report on 2D-TD T_1 and $T_{1\rho}$ results in natural and deuterated cartilage tissue at 3^oC and -10^oC.

5.2.1 2D Relaxation in Deuterated Cartilage

$T_{1\rho}$ values are typically much shorter than T_1 values and provide results closer to the intrinsic relaxation parameters. Figure B.1 in Appendix B shows a typical $T_{1\rho}$ τ-plot in deuterated cartilage at 3^oC using a spin-locking field strength of 10 G. As shown in Appendix B, the decay was well described by the sum of three exponential decays with $T_{1\rho}$ = 1.6 ms, 7.6 ms and 662 ms. By analyzing such $T_{1\rho}$ τ-plots at 40 time points on the FID, sometimes

also referred to as time windows, we effectively are generating a 2D data set of signal magnitude versus t (time along FID) and τ (length of spin-locking pulse). This 2D data set is analysed as described in section 4.1.5 to produce a reconstructed FID for each $T_{1\rho}$ component. In this case, with three $T_{1\rho}$ components, three reconstructed FIDs are obtained as shown in Fig. 5.7a.

(a)

(b)

(c)

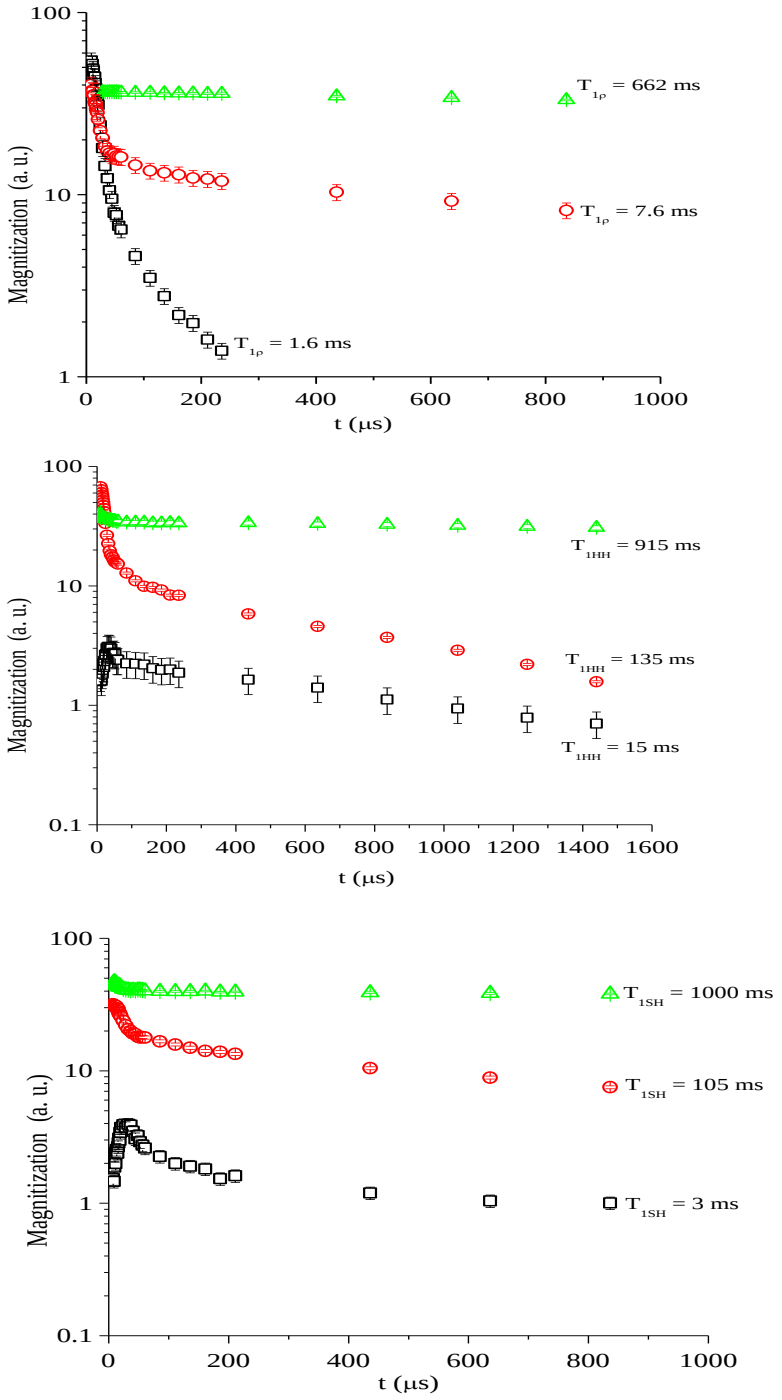

Figure 5.7 Reconstructive FID's of deuterated articular cartilage at 3°C. Data up to t = 1800 μs was used in the analysis, and shown in this figure up to 1000 μs in order to show the short T_2 component clearer. a) $T_{1\rho}$, b) T_{1HH}, and c) T_{1SH}.

As discussed in section 4.1.5, this analysis also yields a $T_{1\rho}$ value for each resolved $T_{1\rho}$ component, which represents the $T_{1\rho}$ averaged over all sampling points along the FID, as obtained from the 2D analysis. In this case the three component $T_{1\rho}$ values are 1.6 ms, 7.6 ms, and 662 ms. Each reconstructed FID was analysed using a sum of Gaussian and exponential decays as dictated by the decay behavior, and making use of the approach for analysing multicomponent decay curves discussed in section 4.1.4. The detailed decomposition analysis for each of the three reconstructed FIDs is given in Appendix C.7. The magnetization fractions and associated T_2 values obtained from such analysis are given in Table 5.4.

Although an equivalent number of accumulations may be used in the 2DTD experiment and the FID T_2 experiment, the S/N of the reconstructed FID's is lower than that of the FID's obtained in the T_2 experiments. This is because reconstructed FID's are arrived at through a two-step process, rather than directly from the data. In the 2D experiments a number of 1D spin-lattice relaxation experiments (40 in this thesis) are performed at various time windows on the FID, which are then analysed for multi-component behavior. The $\tau = 0$ intercepts, as a function of t, for each resolved component define the reconstructed FID's. An explicit weakness in this approach is that these intercepts are based on the multi-exponential decomposition of relaxation curves defined by a maximum of only 40 points (rather than 200 points, as used in the FID T_2 experiments). Experience in our laboratory has shown that in 2DTD experiments of the type described in this work the definition of the reconstructed FID's at low amplitudes (about 2% of M_0 and below) decreases relatively rapidly, which can introduce artifacts into the low-amplitude tails of the reconstructed decay curves. To prevent

such artifacts from influencing the analysis of the reconstructed FID's, the reconstructed points below about 2% of M_0 were not utilized in the analysis.

The magnetization with the long $T_{1\rho}$ = 662 ms makes up 25.2 % of the sample total magnetization. The associated FID exhibits the curving down at the longer times, on a semi-log plot, characteristic of a sample with $T_2 \geq T_2^*$. In this case only the initial flat portion (on semi-log plot) was fitted to a single exponential to determine the size of this magnetization. The data over the first 1000 μs was used for this purpose (see Fig. 5.7a) and the associated T_2 is labeled T_2^*, Table 5.4. The magnetization with the intermediate $T_{1\rho}$ = 7.6 ms makes up 30.9% of the sample magnetization, and the associated three component reconstructed FID consists of two Gaussians with T_2 ~ 16 μs and T_2 ~ 80 μs, and one exponential with T_2 ~ 1.7 ms. The observation that these components, with very different T_2 values, have the same $T_{1\rho}$ = 7.6 ms means that either the three spin reservoirs accidentally have the same $T_{1\rho}$, or these magnetizations are sufficiently strongly coupled to exhibit a common $T_{1\rho}$. The fact that the T_2 values of the three spin groups involved differ considerably suggests that the latter is the case. The magnetization with the short $T_{1\rho}$ = 1.6 ms makes up 43.9 % of the sample magnetization, and the associated, reconstructed FID is well described by the sum of two Gaussian (33.4 % of signal with T_2 = 17.1 μs, 4.9 % of signal with T_2 = 40 μs) and are exponential (5.6 % of signal with T_2 = 129 μs) as shown in Figure 5.7a and C.7, and Table 5.4. Considering the different T_2 values associated with these three components, it is expected that exchange plays a role in a single $T_{1\rho}$ = 1.6 ms being observed.

Table 5.4 Observed 2D Relaxation Parameters of the deuterated articular cartilage at 3°C.The repetition time for all experiments is 10 seconds. The component labeled "?" will be discussed in connection with exchange, in section 5.2.1 (subsection Exchange Analysis in deuterated Cartilage). The symbols (G) and (E) indicate Gaussian and exponential FID shapes.

Deuterated 3°C	**T_1, $T_{1\rho}$ (ms)**	**T_2 (μs)**	**Assignment**	**Magnetization %**
$T_{1\rho}$				
long	662 ± 20	T_2^*	HDO (L_{2D})	25 ± 1
medium	7.6 ± 0.5	16 ± 0.5 (G)	Collagen a (S^a_{1D})	19 ± 1
		79 ± 10 (G)	CH_3 (S_{2D})	3 ± 0.5
		1668 ± 74 (E)	PG (L_{1D})	9 ± 0.5
short	1.6 ± 0.5	17.0 ± 0.5 (G)	Collagen b (S^b_{1D})	33 ± 2
		40 ± 9 (G)	CH_3 (S_{2D})	5 ± 2
		129 ± 32 (E)	"?"	6 ± 2
T_{1HH}				
long	915 ± 14	15 ± 1 (G)	Collagen b (S^b_{1D})	6.0 ± 0.5
		T_2^*	HDO (L_{2D})	28 ± 2
medium	135 ± 7	17.0 ± 0.5 (G)	Collagen a (S^a_{1D})	50 ± 3
		78 ± 5 (E)	CH_3 (S_{2D})	6 ± 1
		700 ± 37 (G)	PG (L_{1D})	9 ± 1
Short- T_{1HH}	15 ± 5	24 ± 14 (E)	Collagen a (S^a_{1D})	(-2) ± 5
		38 ± 34 (G)	CH_3 (S_{2D})	1 ± 5
		1118 ± 191 (E)	"?"	2.0 ± 0.5
T_{1SH}				
long	1000 ± 15	16 ± 1 (G)	Collagen a (S^a_{1D})	9 ± 0.5
		T_2^*	HDO (L_{2D})	49 ± 1
medium	105 ± 4	21.0 ± 0.5 (G)	Collagen b (S^b_{1D})	18 ± 0.5
		119 ± 14 (E)	CH3 (S_{2D})	5.0 ± 0.5
		1200 ± 53 (E)	PG (L_{1D})	18 ± 1
Short- T_{1SH}	3.0 ± 1	15 ± 1 (G)	Collagen a (S^b_{1D})	(-5.0) ± 0.5
		42 ± 6 (G)	CH3 (S_{2D})	3.0 ± 0.5
		600 ± 200 (E)	PG (L_{1D})	3.0 ± 0.5

Guided by the T_2 results in section 5.1.1, the assignments of T_2 components, resolved in the present 2D experiment, to specific cartilage constituent components, is given in Table 5.4, under the heading Assignments. In summary, the assignments are listed below.

S_1: T_2 = 15-18 μs, solid-like magnetization; assigned to collagen.

S_2: T_2 = 40-120 μs, solid-like magnetization associated with proton spin reservoir where i) on average the distance between protons is greater than for S_1, and/or ii) the motion of the spin group involved has a component with $\omega_D \tau_c \leq 1$; assigned to CH_3 groups and/or solid-like hyaluronic acid and core protein components of PG.

L_1: T_2 = 0.7- 2 ms, liquid-like magnetization, relatively mobile polymers; assigned to mobile PG (CS and KS chains).

L_2: $T_2 \geq 10$ ms, T_2^*, liquid-like magnetization; assigned to liquid water- here mostly HDO.

Figure B.2 shows a typical recovery curve in T_{1HH} experiment in deuterated cartilage at 3^{o}C for a time window 7.5 μs. The recovery curve is well described by sum of three exponential components with the T_1 values and component spins given in Table B.2. The reconstructed FID's from the 2D T_{1HH} experiment are given in Figure 5.7b. The component T_1 values along with the parameters (T_2 and FID component amplitudes) defining the reconstructed FID's are given in Table 5.4. The component magnetization with short T_1 = 135 ms has associated with it a three-component reconstructed FID; two Gaussian components with T_2 ~18 μs and ~ 80 μs and a single exponential component with T_2 = 0.7 ms, which, as in the T_2 and $T_{1\rho}$ experiments, is assigned to the mobile PG component. The component magnetization with short T_1 = 15 ms has associated with it a three-component

reconstructed FID; two Gaussian components with T_2 = 24 μs and 38 μs and a single exponential component with T_2 ~ 1 ms.

The T_1 values in the deuterated tissue are longer than the $T_{1\rho}$ values so that it is expected that inter-spin group magnetization exchange will be more apparent in the T_1 experiments. That this is the case here is clearly seen in Figure 5.7, (and Table 5.4). The reconstructed FID, associated the long $T_{1\rho}$ = 662 ms, which was a single exponential with T_2 = T_2^* in the $T_{1\rho}$ experiment, exhibits two-component behavior in the T_{1HH} experiment, second component being a 15 μs Gaussian. This is strong evidence that the collagen is coupled to the water (largely HDO) reservoir on the T_1 time scale. The T_{1SH} experiments in the deuterated cartilage at 3^{o}C also resolved three T_1 components, Figure B.3. The reconstructed FIDs are shown in Figure 5.7b. The results of the analysis of the reconstructed FIDs are shown in Figure C.8, and are summarized in Table 5.4. The long T_1 and medium T_1 relaxation components, (1000 ms and 105 ms, Table 5.4), had associated with them similar reconstructed FIDs as in the T_{1HH} results. The short T_{1SH} = 3 ms is faster than that observed for short T_{1HH} = 15 ms. To avoid confusion the short T_1 in the T_{1HH} and T_{1SH} experiments are labeled short-T_{1HH} and short-T_{1SH}, respectively. The reconstructed FID for the magnetization with short-T_{1SH} was reasonably well described by the sum of a "negative" Gaussian component with T_2 = 16 μs (collagen), another Gaussian component with T_2 = 42 μs, and an exponential component with T_2 = 0.6 ms. The observation of a negative solid FID (T_2 = 16 μs) and positive, liquid FID (T_2 = 0.6 ms) with a common fast T_1, constitutes strong support for the above conclusion of strong coupling between collagen and PG spin reservoirs.

An identical set of 2D spin-lattice relaxation time measurements were performed on the deuterated cartilage sample at -10°C. All analyses of the 2D relaxation results at -10°C parallel those performed in this tissue at 3°C, and are summarized in Figure 5.8, Figure C.10-C.12 and Table 5.5.

The most obvious change seen in the 2D relaxation results, as the tissue is frozen, is the disappearance of the L_2 component, and the appearance of a relatively substantive component (S_{3D}) which has T_2 = 113 μs and T_2 = 166 μs in the T_{1HH} and T_{1SH} experiments, respectively. The S_{D3} component is clearly distinguishable from the other components because of the relatively long T_1 ~ 3 seconds. This component is assigned to HDO ice in the tissue.

It will be shown below, in discussion of the 2D results for the natural tissue at -10°C, that T_2 (H_2O ice) ~ 13 μs, (Table 5.7). Since the gyromagnetic ratio of deuterons is smaller than that of protons ($\frac{\gamma_H}{\gamma_D} \sim 6.5$), the T_2 (HDO ice) is expected to be longer than T_2 (H_2O ice); 113 μs – 166 μs in the T_1 experiments. In addition, the $T_{1\rho}$ results for the natural tissue at -10°C indicate that $T_{1\rho}$ (H2O ice) ~ 100 μs. This, taken together with the observed ratio $T_2(HDO\ ice) \Big/ T_2(H_2O\ ice) \sim \frac{\sim 140\ \mu s}{12\ \mu s} \sim 12$, prompts the assignment of the $T_{1\rho}$ component in the frozen, deuterated tissue, with $T_{1\rho}$ = 1.1 ms and T_2 = 67 μs, to HDO ice.

(a)

(b)

(c)

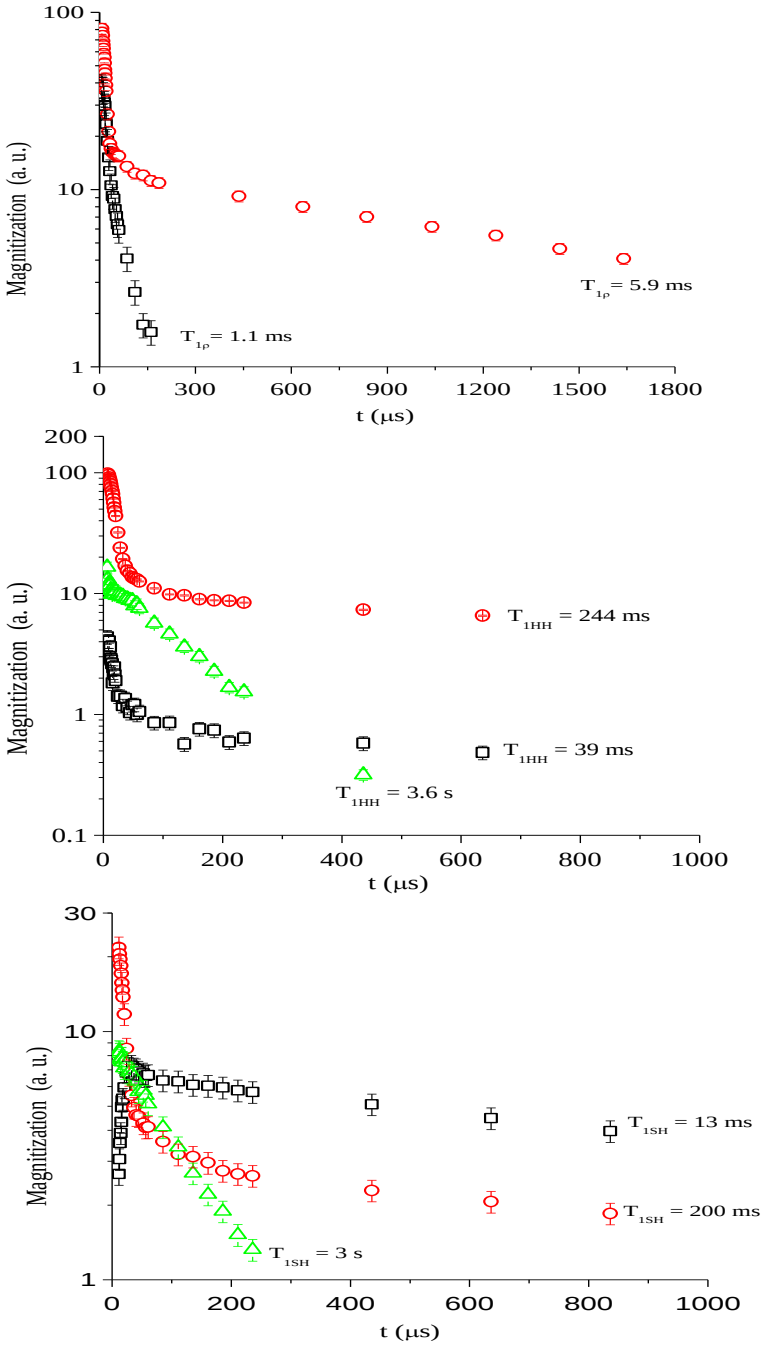

Figure 5.8 Reconstructed FID's of frozen deuterated cartilage at -10°C. Data up to t = 1800 μs was used in the analysis, and shown in this figure up to 1000 μs in order to show the short T_2 component clearer. a) $T_{1\rho}$, b) T_{1HH} and c) T_{1SH}

Table 5.5 Observed 2D Relaxation Parameters of the deuterated articular cartilage at -10^{o}C. The repetition time for all experiments is 10 seconds. The symbols (G) and (E) indicate Gaussian and exponential FID shapes.

Deuterated -10^{o}C	**T_1, $T_{1\rho}$ (ms)**	**T_2 (µs)**	**Assignment**	**Magnetization (%)**
$T_{1\rho}$				
long	6 ± 1	15.0 ± 0.5 (G)	Collagen a (S^{a}_{1D})	55 ± 1
		86.0 ± 15.5 (G)	CH_3 (S_{2D})	4.0 ± 0.5
		1500 ± 142(E)	PG (L_{1D})	9.0 ± 0.5
short	1.1 ± 0.5	19.0 ± 0.5 (G)	Collagen b (S^{b}_{1D})	21 ± 1
		69 ± 11(G)	HDO_{Ice} (S_{3D})	11 ± 1
T_{1HH}				
long	3600 ± 1	113 ± 1 (E)	HDO_{Ice} (S_{3D})	9.5 ± 0.5
medium	244 ± 17	16.0 ± 0.5 (G)	Collagen a (S^{a}_{1D})	75 ± 3
		68 ± 33 (G)	CH_3 (S_{2D})	4 ± 1
		1548 ± 610 (E)	PG (L_{1D})	7.5 ± 1
Short-T_{1HH}	39± 12	12 ± 1 (G)	Collagen b (S^{b}_{1D})	3.0 ± 0.5
		56 ± 23 (G)	CH_3 (S_{2D})	0.5 ± 0.5
		1363 ± 1527 (E)	PG (L_{1D})	0.5 ± 0.5
T_{1SH}				
long	3000 ± 1	166 ± 8 (E)	HDO_{Ice} (S_{3D})	23.0 ± 0.5
medium	200 ± 24	15.5 ± 0.5 (G)	Collagen a (S^{a}_{1D})	67 ± 3
		80 ± 7 (G)	CH_3 (S_{2D})	4.5 ± 0.5
		1631 ± 104 (E)	PG (L_{1D})	8.0 ± 0.5
Short-T_{1SH}	13 ± 1	15 ± 1 (G)	Collagen b (S^{b}_{1D})	(-24.5) ± 1
		31 ± 4 (G)	CH_3 (S_{2D})	4.5 ± 1
		1500 ± 25 (E)	PG (L_{1D})	17.5 ± 1

Exchange Analysis in Deuterated Articular Cartilage

The exchange models in this work were explored using a computer modeling program (EXFIT). This program was developed in our laboratory, and was first used by Oleskevich *et al.* and Weglarz *et al.* [19, 116] to inspect macromolecular and water molecule proton magnetization exchange and dynamics. As discussed in section 2.3, the intrinsic relaxation parameters can be expressed in terms of the apparent parameters and vice versa. In the present approach the apparent parameters are calculated from a set of intrinsic parameters which are adjustable parameters within an iterative minimization algorithm that compares the calculated apparent parameters to the experimental parameters. The adjustable, intrinsic parameters which provide the closest match between the experimental apparent values and the calculated apparent values are taken as the intrinsic parameters for the articular cartilage. In this analysis the exchange rates also are adjustable parameters.

A complication that enters into the present exchange analysis is that typically an insufficient number of experimental relaxation parameters are available from any given experiment. For example, consider a 4-site exchange scenario; this would involve four apparent relaxation time values, and sixteen apparent spin group sizes, and six exchange rates. At best we may obtain 10-12 parameters from the experiment. Therefore one must fix some of the apparent and/or intrinsic parameters at values that may be deemed reasonable and then fit the rest. A next step involves adjusting some of the parameters manually, in a methodical fashion, with the aim of improving the overall match between experimentally observed, apparent parameters and modeled apparent parameters. In view of the combination of fitting and manual adjustment of parameters this approach cannot be considered as a least-

squares fitting procedure. Perhaps it is more appropriate to think of this approach as a simulation procedure.

As has been addressed in section 5.2.1, it is expected that inter-spin group magnetization exchange will be more apparent in the T_1 experiments, because typically $T_1 > T_{1\rho}$ in the deuterated cartilage tissue (see Tables 5.4 and 5.5). In order to explore the needed number of spin reservoirs and their intrinsic sizes, the exchange analysis was started with the 2D $T_{1\rho}$ results in deuterated cartilage at -10^{o}C.

From Figure 5.8a (and Table 5.5) it is seen that the 67 μs T_2 component (S_{3D}) that has been assigned to HDO ice protons does not appear to have associated with it any other T_2 component. However, it is understood that a part of this component is very likely attributable to S_{2D} magnetization that was observed to be linked to the collagen b spin group in the T_{1HH} experiment at -10^{o}C and also in all 2D experiments at 3^{o}C. This contribution is only a few percent of the total signal and, to simplify exchange analysis, is added to collagen b signal component in the exchange analysis for the deuterated cartilage tissue. Similarly the S_{2D} signal component, seen to be associated with the collagen a signal in all the reconstructed FID's for the deuterated tissue, is added to collagen a signal component for simplicity. The fact that a significant fraction of the collagen a signal is associated with PG (L_{1D}) and a significant fraction is not, suggests that on the $T_{1\rho}$ time scale either *i*) collagen acts as one spin reservoir [S_{1D} (a) + S_{1D} (b)] which is relatively strongly coupled to PG, but such coupling is not strong enough to yield single $T_{1\rho}$ behavior for (PG + Collagen), *ii*) collagen is very strongly coupled to a part of collagen (Collagen a) and essentially uncoupled from another part of collagen (Collagen b). Which particular scenario applies can be tested by

performing the exchange analysis and determining which scenario satisfies the observed 2D results. Here we start with scenario (*i*). The apparent and intrinsic parameters obtained from the exchange analysis are given in Table 5.6. Within the present context, where the best match between experimental and calculated parameter is searched for, by utilizing a combination of fitting and manual adjustment of parameters, a perfect match is not generally expected. Although various mismatches are clearly recognized, the most glaring mismatch pertains to $C_b^+ = -9.8$. Using various combinations of k_a , T_a and T_b, while maintaining a rough correspondence between experimental and calculated parameters, it was not possible to significantly affect the negative character of C_b^+. Experimentally there was no indication of a significant negative C_b^+. Therefore scenario (*i*) was deemed to be inapplicable.

Table 5.6 Simple two sites exchange analysis results for the $T_{1\rho}$ experiment in deuterated cartilage at -10°C. The left table shows the experimental and calculated values for each parameter. The right table shows the exchange rate (k_a), intrinsic times (T_a , T_b) and intrinsic reservoir sizes (P_a , P_b).

Parameter	Calculated	Experimental
T^+	1.2 ms	1.1 ms
T^-	2.6 ms	5.9 ms
C_a^+	23.6 %	27.1 %
C_b^+	-9.8 %	0
C_a^-	63.8 %	63.3 %
C_b^-	22.2 %	9.6 %

Rates	Values
k_a	80 s^{-1}
T_a	2 ms
T_b	20 ms
P_a	87.5 %
P_b	12.5 %

This result prompted the modeling of scenario (*ii*), which involves two collagen groups a and b; *i.e*, three site exchange model: Collagen a, Collagen b, PG (L_{2D}).

Results of the 3-site exchange model simulation for the deuterated cartilage at -10^{o}C is given for $T_{1\rho}$, T_{1HH} and T_{1SH} experiments in tables D.10 - D.12. For the above freezing case, at 3^{o}C, four sites exchange modeling is indicated and exchange simulation for all 2D experiments for the deuterated cartilage at 3^{o}C are presented in Tables D.7 – D.9.

In the T_{1SH} experiments selective inversion of the magnetization is involved. Therefore, for the T_{1SH} exchange modeling we need to find the inversion factors. These can be calculated for a particular magnetization component by taking the ratio of the FID amplitude representing M_0 (amplitude following a 90^{o} pulse) of the component to the FID amplitude representing M (τ = 0) in the soft 180^{o} – 90^{o} pulse sequence. The latter FID amplitude is approximated by using τ = 100 μs.

An example of the FIDs for the τ = 0 and τ = 100 μs cases, for the deuterated cartilage at 3^{o}C, are shown in Figure 5.9a and 5.9b, respectively.

Initial simulations of exchange for $T_{1\rho}$ results for the deuterated cartilage tissue at 3^{o}C indicated a small negative value for the PG (L_{1D}) component with $T_{1\rho}$ = 1.6 ms. In the position, in Table 5.4, where this negative component would be located, a 129 μs component is shown. The reconstructed FID was reanalyzed without the signal below ~2 % being cut off. The result shown in Figure 5.10 suggests that a negative PG (L_{1D}) component may be a part of this FID. The "fit" shown in the figure was arrived at by fixing the T_2 = 800 μs and amplitude = -1 of such PG (L_{1D}) signal component. The simulated 3-site exchange scenario for the -10^{o}C case (deuterated cartilage) is shown in Figure 5.11b.

(a)

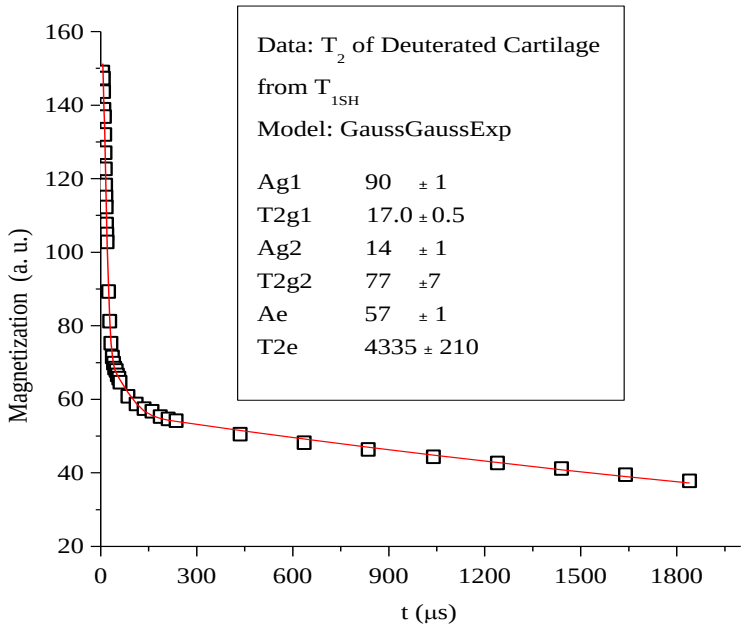

(b)

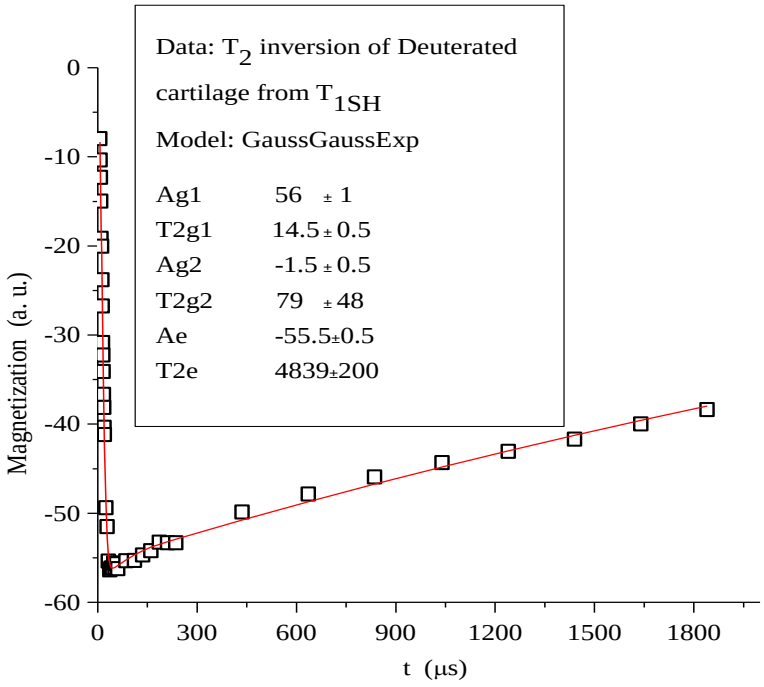

Figure 5.9 Reconstructed FIDs from selective inversion experiment a) at $\tau = 0$ μs, b) at $\tau =$ 100 μs.Both FIDs were analysed for two Gaussians (Ag1 and Ag2) and one exponential (Ae)

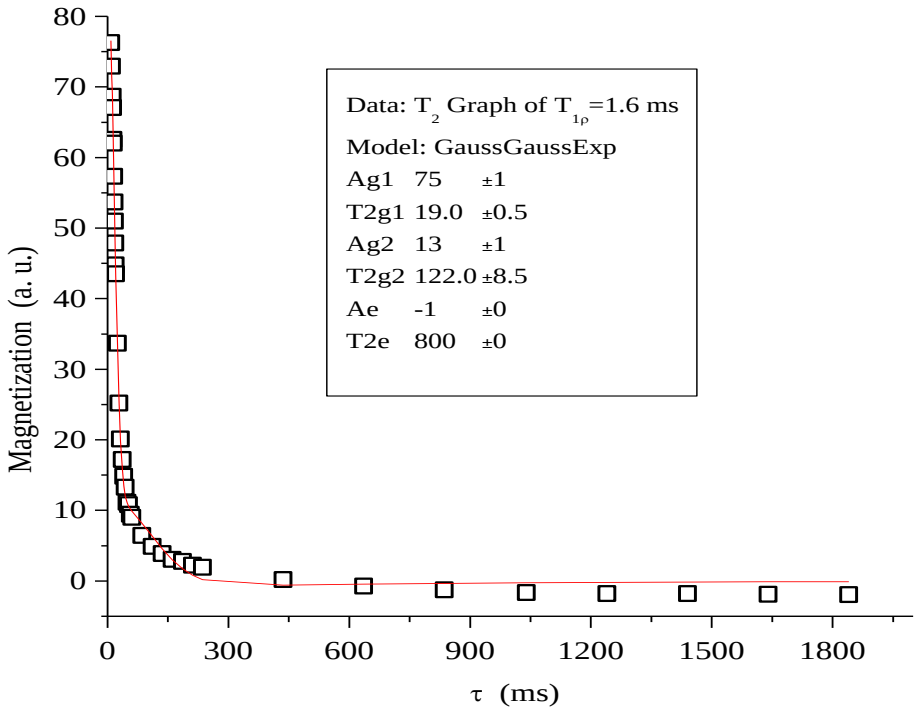

Figure 5.10 Reconstructed FID for magnetization with $T_{1\rho}$ = 1.6, showing the possibility of a small negative component.

Table 5.7 Renormalization for the reconstructed FID associated with the short-$T_{1\rho}$ component of the deuterated articular cartilage at 3°C from Fig. 5.10 analysis.

Deuterated 3°C	**T_1, $T_{1\rho}$ (ms)**	**T_2 (μs)**	**Assignment**	**Magnetization %**
$T_{1\rho}$				
long	662 ± 20	T_2^*	HDO (L_{2D})	25 ± 1
medium	7.6 ± 0.5	16.5 ± 0.5 (G)	Collagen a (S^a_{1D})	19 ± 1
		79 ± 10 (G)	CH_3 (S_{2D})	3.0 ± 0.5
		1668 ± 74 (E)	PG (L_{1D})	9.5 ± 0.5
short	1.6 ± 0.5	18.5 ± 0.5 (G)	Collagen b (S^b_{1D})	38 ± 1
		122.0 ± 8.5 (G)	CH_3 (S_{2D})	7 ± 1
		800 ± 0 (E)	PG (L_{1D})	-0.6 ± 0

(a)

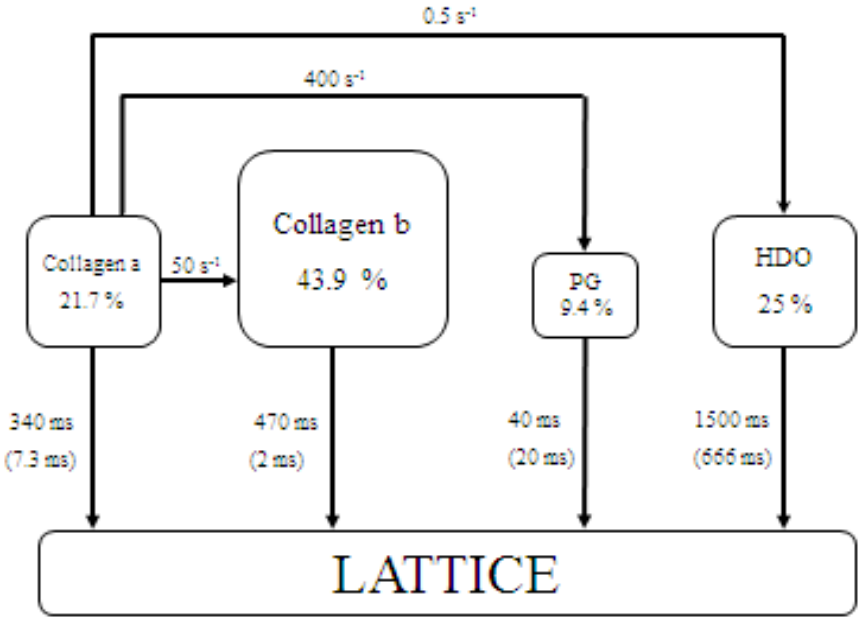

(b)

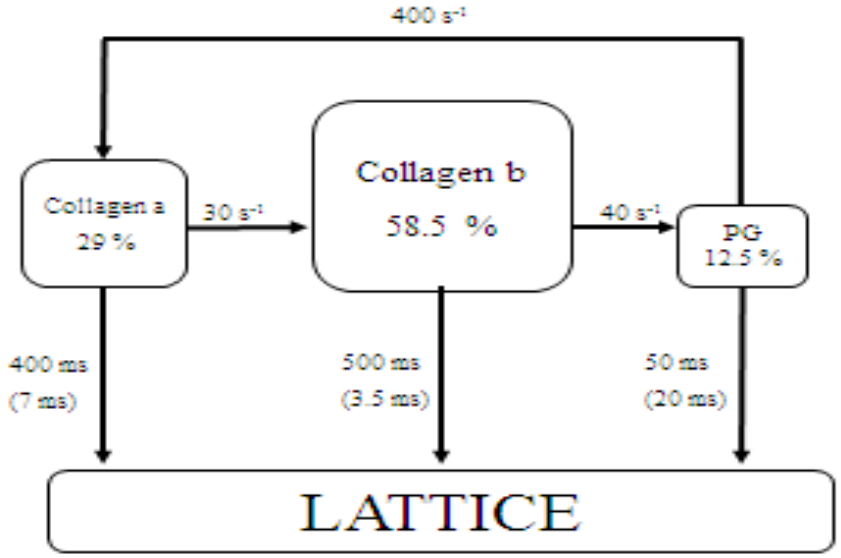

Figure 5.11 Exchange model for deuterated cartilage, a) at 3°C and b) at -10°C. Numbers in brackets represent $T_{1\rho}$ parameters and non-bracketed numbers represent T_1 parameters.

5.2.2 2D Relaxation in Natural Cartilage

Figure B.4 in Appendix B shows a typical $T_{1\rho}$ τ-plot in natural cartilage at 3°C using a spin-locking field strength of 10 G. As shown in Appendix B, the decay was well described by the sum of three exponential decays with $T_{1\rho}$ = 1 ms, 5.5 ms and 187 ms. By analyzing such $T_{1\rho}$ τ-plots at 40 time points on the FID, sometimes also referred to as time windows, we effectively are generating a 2D data set of signal magnitude verses t (time along FID) and τ (length of spin-locking pulse). This 2D data set is analysed as described in section 4.1.5 to produce a reconstructed FID for each $T_{1\rho}$ component. In this case, with three $T_{1\rho}$ components, three reconstructed FIDs are obtained as shown in Fig. 5.12a. As discussed in section 4.1.5, this analysis also yields a $T_{1\rho}$ value for each resolved $T_{1\rho}$ component, which represents, the $T_{1\rho}$ averaged over all sampling points along the FID, as obtained from the 2D analysis. In this case the three component $T_{1\rho}$ values are 1 ms, 7 ms, and 200 ms. Each reconstructed FID was analysed using a sum of Gaussian and exponential decays as dictated by the decay behavior, and making use of the approach for analysing multicomponent decay curves discussed in section 4.1.4. The detailed decomposition analysis for each of the three reconstructed FIDs is given in Appendix C.1. The magnetization fractions and associated T_2 values obtained from such analysis are given in Table 5.8.

The magnetization with the fast $T_{1\rho}$ ~1 ms makes up ~ 6 % of the sample total magnetization, and the associated, reconstructed FID is well described by a single Gaussian decay with T_2 ~ 18 μs (S_{1N} component). The magnetization with the intermediate $T_{1\rho}$ ~7 ms makes up ~ 6% of the sample magnetization, and the associated three component reconstructed FID consists of two Gaussians with T_2 ~ 17 μs and 60 μs, and one exponential

with T_2 ~ 2 ms. The observation that these three components, with very different T_2 values, have the same $T_{1\rho}$ ~ 7 ms means that either the three spin reservoirs accidentally have the same $T_{1\rho}$, or these magnetizations are sufficiently strongly coupled to exhibit a common $T_{1\rho}$. The fact that the T_2 values of the three involved spin groups differ considerably suggests that the latter is the case. The magnetization with the long $T_{1\rho}$ ~ 200 ms makes up ~ 88% of the sample magnetization. The associated FID exhibits the curving down at the longer times, on a semi-log plot, characteristic of a sample with $T_2 \geq T_2^*$. In this case only the initial flat portion (on semi-log plot) was fitted to a single exponential to determine the size of this magnetization. The data over the first 1800 μs was used for this purpose (see Fig. 5.12a and Fig. C.1) and the associated T_2 is called T_2^*, Table 5.8.

Considering that $T_2 \sim T_2^*$ of the magnetization L_{1N}, with $T_{1\rho}$ ~ 189 ms, is explicitly longer than T_2 = 2.2 ms of the magnetization L_{N1}, with $T_{1\rho}$ = 7 ms, clearly indicates that two distinct spin groups are involved. From the structure of the reconstructed FIDs we conclude that on the $T_{1\rho}$ time scale spin group L_{N1} is coupled to spin groups S^a_{1N} and S_{2N}. Coupling of spin group L_{2N} or S^b_{1N} to other spin groups is not observed on the $T_{1\rho}$ time scale.

Figure B.5 in Appendix B shows a typical magnetization recovery curve in natural cartilage at 3°C, obtained in a T_{1HH} inversion recovery experiment with the data taken at 7.5 μs time point on the FID. As shown in Figure B.5 and Table B.5, the curve is well described by two exponentials; 2.2% of the magnetization has T_1 = 57 ms and 97.8 % of the magnetization has T_1 = 456 ms. Figure 5.9b shows the reconstructed FIDs from this T_{1HH} experiment in the natural cartilage at 3°C.

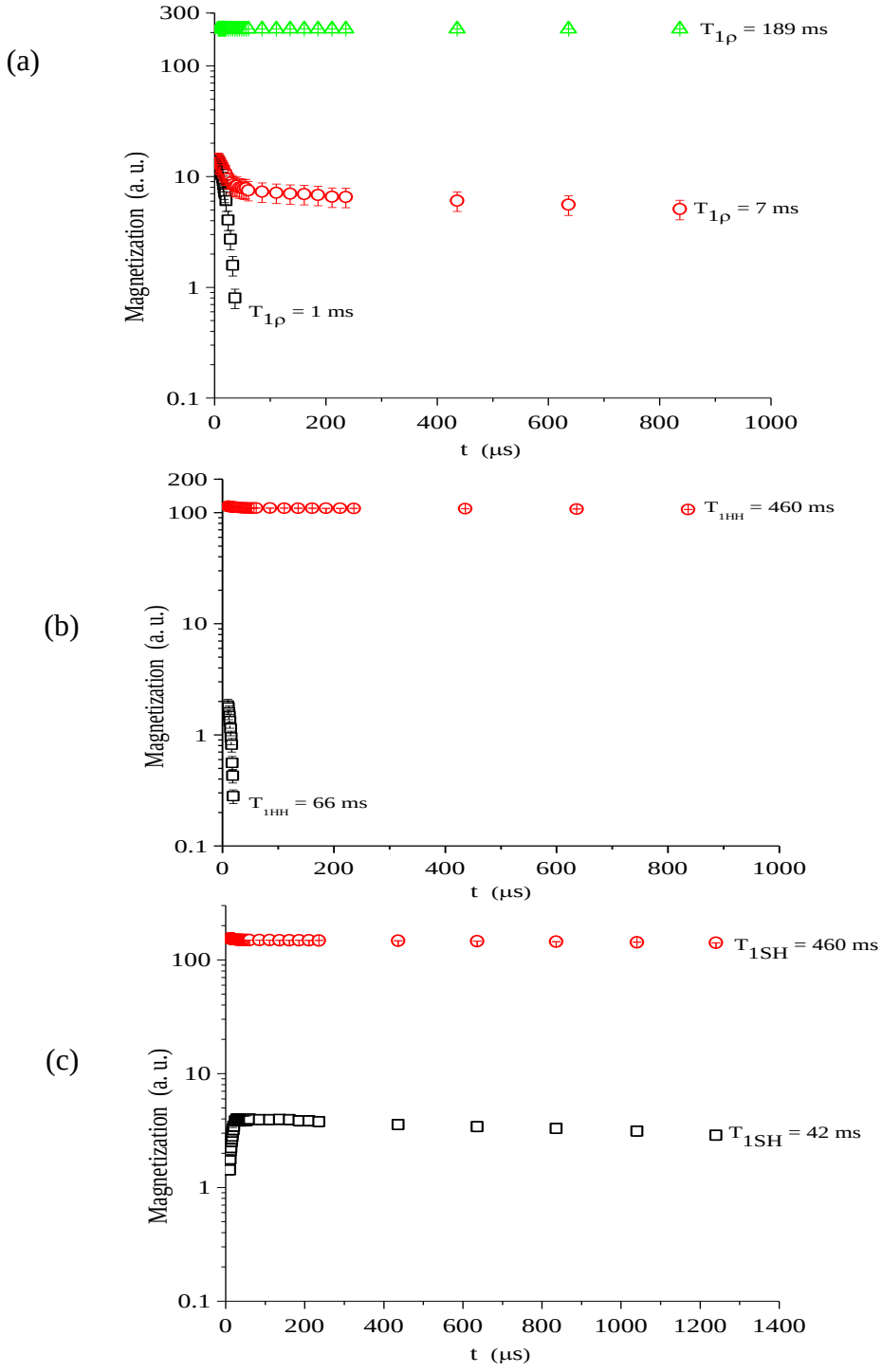

Figure 5.12 Reconstructed FID's for natural cartilage at 3°C. Data was taken to t = 1800 μs and shown in this figure up to 1000 μs in order to show the short T_2 component clearer. a) $T_{1\rho}$, b) T_{1HH} and c) T_{1SH}.

Each reconstructed FID was analyzed using a sum of Gaussian and exponential function as suggested by the shape of the FIDs in Fig. 5.9b and utilizing the approach discussed in section 4.1.4.

Table 5.8 Observed 2D relaxation parameters of the natural articular cartilage at 3^{o}C . The repetition time for all experiments is 6 seconds. The symbols (G) and (E) indicate Gaussian and exponential FID shapes, respectively.

Natural 3^{o}C	**T_1, $T_{1\rho}$ (ms)**	**T_2 (µs)**	**Assignment**	**Magnetization %**
$T_{1\rho}$				
long	189 ± 1	T_2^*	H_2O (L_{1N})	88.0 ± 0.5
medium	7 ± 2	17.0 ± 0.5 (G)	Collagen a (S^a_{2N})	2.5 ± 0.5
		59 ± 8 (G)	CH_3 (S_{2N})	0.5 ± 0.5
		2200 ± 42 (E)	PG + H_2O_{bound} (L_{2N})	3.0 ± 0.5
short	1.0 ± 0.5	18 ± 1 (G)	Collagen b (S^b_{2N})	6.0 ± 0.5
T_{1HH}				
long	460 ± 2	21.5 ± 0.5 (G)	Collagen b (S^b_{2N})	4 ± 0.5
		T_2^*	H_2O (L_{1N})	93.0 ± 0.5
short	66 ± 12	13 ± 5 (G)	Collagen a (S^a_{2N})	3 ± 0.5
T_{1SH}				
long	460 ± 2	21 ± 1 (G)	Collagen b (S^b_{2N})	6.0 ± 0.5
		T_2^*	L_{1N}	94 ± 0.5
short	42 ± 10	20.5 ± 0.5 (G)	Collagen a (S^a_{2N})	(-4.0) ± 0.5
		4800 ± 140 (E)	PG + H_2O_{bound} (L_{2N})	4.0 ± 0.5

The magnetization, with the long T_{1HH} ~ 460 ms, makes up approximately 97% of the sample magnetization, and the associated, reconstructed FID was modeled as the sum of two components; a Gaussian with T_2 ~20 μs (solid) and an exponential with T_2^* (liquid), Figure C.2. The observation of having the solid and liquid components, with two very different T_2, exhibit the same apparent T_1 means that either these two different spin reservoirs accidentally have the same T_1 or magnetization exchange couples their spin -lattice relaxations strongly enough so that a single T_1 is observed.

In the natural cartilage at 3°C, two T_1 components were resolved in the T_{1SH} experiment similar to those seen in the T_{1HH} experiment (Figure B.6 and Table B.6). The results from the 2D analysis are shown in Figures C.3, 5.12c and Table 5.8. The magnetizations with T_1 ~ 460 ms and T_1 ~ 42, show distinctly different reconstructed FID behavior compared to that seen in the reconstructed FIDs in the T_{1HH} results because of different spin preparation. A negative reconstructive FID associated with the magnetization with the short T_1 is a key indicator for exchange coupling between the solid and liquid magnetization components within the cartilage matrix.

The results of the 2D spin- lattice relaxation time measurements for the natural cartilage sample at -10°C are summarized in Figure 5.13, Figures C.4 - C.6 and Table 5.9.

(a)

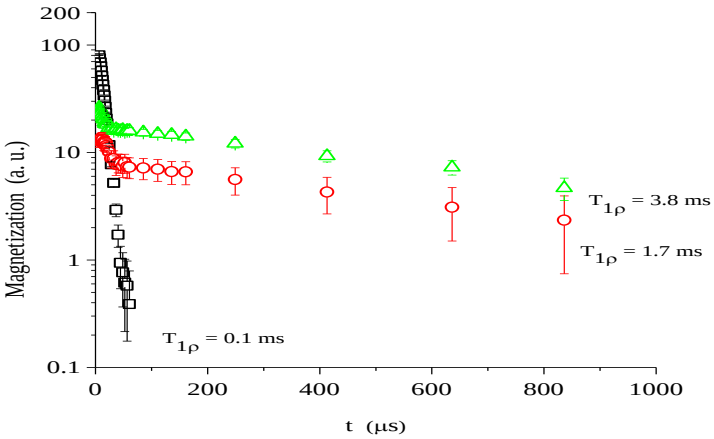

(b)

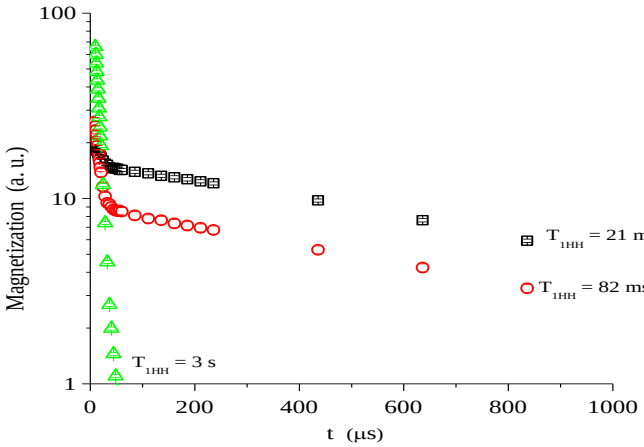

(c)

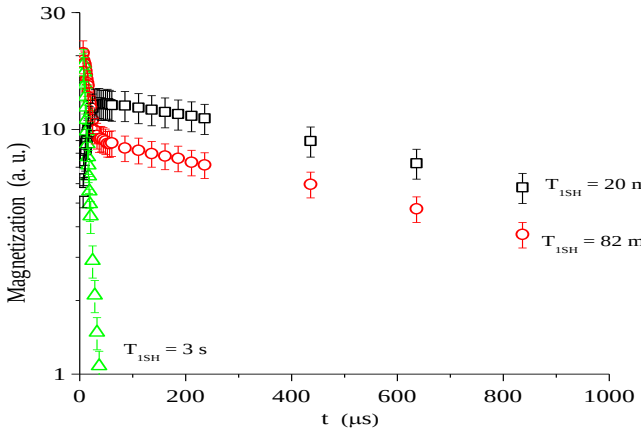

Figure 5.13 Reconstructed FID's for frozen natural cartilage at -10°C. Data was taken to t = 1800 μs and shown in this figure up to 1000 μs in order to show the short T_2 component clearer. a) $T_{1\rho}$,, b) T_{1HH} and c) T_{1SH}.

Table 5.9 Observed 2D Relaxation Parameters of the natural articular cartilage at -10^{o}C . The repetition time for all experiments is 15 seconds. The symbols (G) and (E) indicate Gaussian and exponential FID shapes.

Natural –10^{o}C	**T_1, $T_{1\rho}$ (ms)**	**T_2 (µs)**	**Assignment**	**Magnetization %**
$T_{1\rho}$				
long	4 ± 1	12.0 ± 0.5 (G)	Collagen a (S^{a}_{1N})	8.5 ± 0.5
		740 ± 32 (E)	PG (L_{1N})	13.0 ± 0.5
medium	1.5 ± 0.5	22 ± 1 (G)	Collagen b (S^{b}_{2N})	4.5 ± 0.5
		663 ± 49 (E)	H_2O_{Bound} (L_{2N})	6.0 ± 0.5
short	0.10 ± 0.01	13.5 ± 0.5 (G)	Ice (S_{3N})	68 ± 1
T_{1HH}				
long	3000 ± 1	13.5 ± 0.5 (G)	Ice (S_{3N})	68 ± 12
medium	82 ± 3	14.0 ± 0.5 (G)	Collagen a (S^{a}_{1N})	14.0 ± 2
		845 ± 18 (E)	PG (L_{1N})	11 ± 2
Short-T_{1HH}	21 ± 2	17 ± 1 (G)	Collagen b (S^{b}_{2N})	1.5 ± 0.5
		T_2^{*}	H_2O_{Bound} (L_{2N})	5.5 ± 0.5
T_{1SH}				
long	3000 ± 1	13.5 ± 0.5 (G)	Ice (S_{3N})	43 ± 1
medium	82 ± 8	14.5 ± 0.5 (G)	Collagen a (S_{1N})	24.5 ± 0.5
		899 ± 17 (E)	PG (L_{1N})	18.5 ± 0.5
Short-T_{1SH}	20 ± 3	13.5 ± 0.5 (G)	Collagen b (S_{2N})	(-14.5) ± 0.5
		988 ± 20 (E)	H_2O_{Bound} (L_{2N})	29.0 ± 0.5

Due to the presence of the large water proton reservoir in the natural tissue, which undergoes drastic changes as the water freezes, the reconstructed FIDs at -10^{o}C appear quite different from those at 3^{o}C; i.e., FIDs in Figure 5.13 compared with FIDs in Figure 5.12. One of the most prominent changes is the disappearance of the major magnetization component L_{2N} seen at 3^{o}C (Figure 5.12) and the appearance of the major magnetization component S_{3N} (Figure 5.13, Table 5.9) with T_2 in the range 13-17 μs and T_1 = seconds and $T_{1\rho}$ = 100 μs. This component was assigned to ice protons in the tissue. Excluding the ice signal, two T_1 components, each with a solid-like and liquid-like (T_2 ~ ms) FID, is observed.

Comparing this to the results at -10^{o}C for the deuterated tissue, it is seen that the liquid-like component with short T_{1HH}, as well as T_{1SH}, is clearly of much larger amplitude in the natural tissue than in the deuterated tissue. The larger proportion of the L_{2N} components is assigned to non-freezable bound H_2O.

Exchange Analysis in Natural Articular Cartilage

From Figure 5.13 (and Table 5.9) it is seen that the 13 μs T_2 component (S_{3N}), which has been assigned to ice protons, does not appear to have associated with it any other T_2 component. The collagen a and collagen b signals in all the reconstructed FID's for the natural cartilage tissue have been labeled as S_{1N} and $S_{2N,}$ respectively. The S_{1N} component is observed to be associated with the PG (L_{1N}) component. The S_{2N} component appears to be associated with the long-T_2 liquid component, which is most likely a mixture of PG (L_{1N}) and bound water (L_{2N}) signals. The above is indicative of 4-sites exchange scenario, which involves two collagen groups a and b, PG (L_{2N}) and bound water.

Results of the simulation of the 4-site exchange model for the natural cartilage at -10^{o}C is given for $T_{1\rho}$, T_{1HH} and T_{1SH} experiments in tables D.4 - D.6. For the above-freezing case, (3^{o}C), four-site exchange modeling is indicated and the exchange simulations for all 2D experiments for the deuterated cartilage are presented in Tables D.1 – D.3. In the T_{1SH} experiments the same procedure as used in section 5.2.1 for calculating the inversion factor for each magnetization component from selective inversion experiment, was used.

The simulated 4-site exchange scenario for the 3^{o}C case (natural cartilage) is shown in Figure 5.14a. The simulated 4-site exchange scenario for the -10^{o}C case (natural cartilage) is shown in Figure 5.14b.

Observed Discrepancies between Simulated and Experimental Relaxation Parameters in the Exchange Modelling

Considering the modelling results presented in the exchange analysis tables in Appendix D, it is seen that in general the match between simulation and experiment is not perfect. In this connection a number of factors warrant comment. The first, connected with some of the required experimental relaxation parameters needed to define the intrinsic relaxation/exchange scenario fully, not being observed experimentally, has been mentioned already at the beginning of the subsection “Exchange Analysis in Deuterated Articular Cartilage” in section 5.2.1. A second factor, inherent in the present experiments, is directly related to the fact that cartilage is not a homogeneous material. In particular, cartilage consist of different PG – collagen – water subsystems with in the different zones (layers) within the cartilage sample, with differing structural and dynamical characteristics. In the present 2D

relaxation experiments an average over the different zones is observed for each resolved relaxation parameter.

In view of the above we consider the present exchange results to provide a semi-quantitative representation of the tissue, with the derived relaxation and exchange parameters acting as a guide as to the nature of the true parameters.

(a)

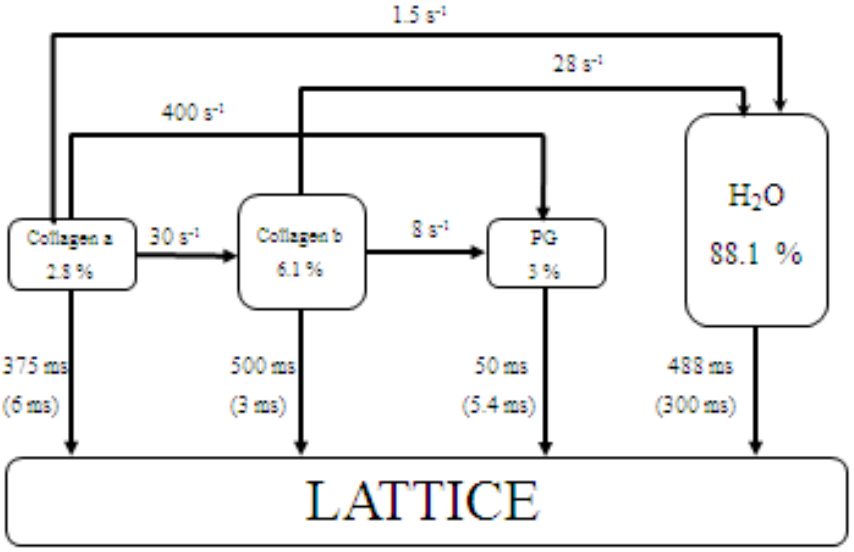

(b)

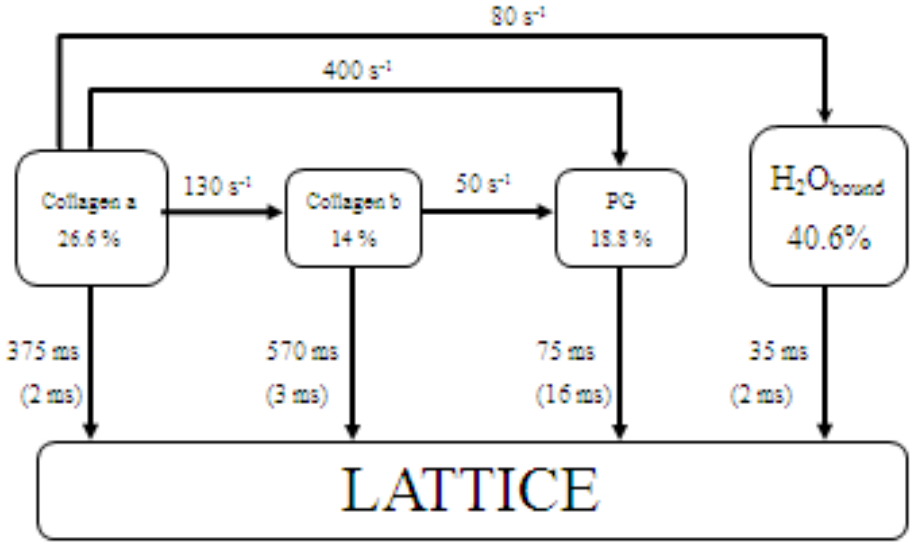

Figure 5.14 Exchange model for natural cartilage, a) at 3°C and b) at -10°C. Numbers in brackets represent $T_{1\rho}$ parameters and non-bracketed numbers represent T_1 parameters.

5.3 High Field Results and Discussion

In this section, a method based on NMR Spectroscopy is developed for the detection of cartilage deterioration. The method is tested and assessed on a commonly used in-vitro model of cartilage degradation using enzymatic depletion of PG with Trypsin: a model which also provides a controlled simulation of osteoarthritis. Although only preliminary results are presented in this study, the method shows potential for the early detection of the onset of cartilage degradation. The aim of the present approach is to look directly at the main structures of ECM, collagen and PG, without reference to water; i.e., to look directly at the component of the tissue being degraded in early OA, as well as at collagen as a reference.

This section presents two approaches for determining PG contents. One is concerned with proton MAS NMR spectroscopy of cartilage, which provides a bench-mark reference for the other approach dealing with CSI spectroscopy, which offers a more practical technique for clinical application. In this preliminary study, only fully- deuterated cartilage samples are considered.

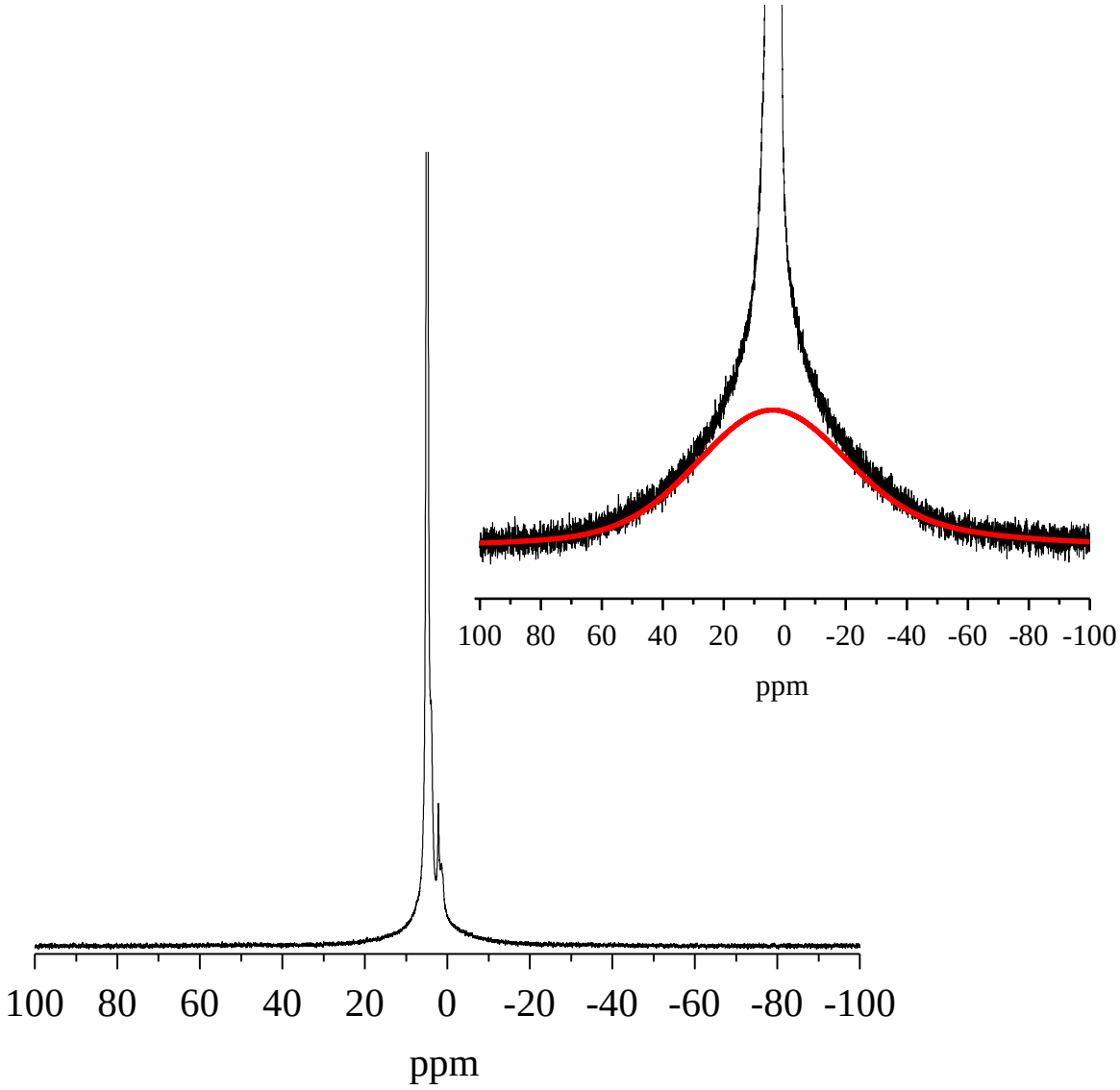

Figure 5.15 A static proton spectrum of deuterated bovine articular cartilage tissue. The inset shows the spectrum with the amplitude x 10. The solid line in the inset represents the two Gaussian fit for the collagen.

Articular cartilage covers the surface of bone in articulating joints. It is made up of a complex network containing mainly collagen fibres, which play an important structural role in maintaining tissue integrity, and proteoglycans, which are highly charged, hygroscopic molecules responsible for the osmotic pressure aspects of the tissue. In cartilage tissue PG molecules are considered to be substantially more mobile than collagen molecules with their proton resonances lying in the motional narrowing and rigid lattice regimes, respectively. The spin groups in the motional narrowing and rigid lattice regimes are also referred to as liquid-like and solid-like groups, respectively. Figure 5.15 shows a static proton spectrum in deuterated bovine articular cartilage tissue. The aim is to define the collagen part. The static spectrum has been analysed using a number of Lorentzian to provide a reasonable representation of the narrow peaks, and two Gaussians to represent the broad peaks. The Lorentzian peaks can then be subtracted from the total spectrum to give us the collagen spectrum. The inset gives a vertically expanded view of the spectrum. The solid line represents a least squares fit of two Gaussians to represent the collagen proton component.

Figure 5.16 shows a ^{1}H MAS NMR spectrum of articular cartilage at 500 MHz and spinning rate of 5 kHz. The larger collagen molecules give rise to signals that are too broad (see Fig. 5.15) to be properly detected with MAS. The labels on the spectral features, the assignments, shown in Figure 5.16 are based on published work by Mucci *et al*., Schiller *et al.*, Xia and Ling *et al*. [107, 109, 121-123].

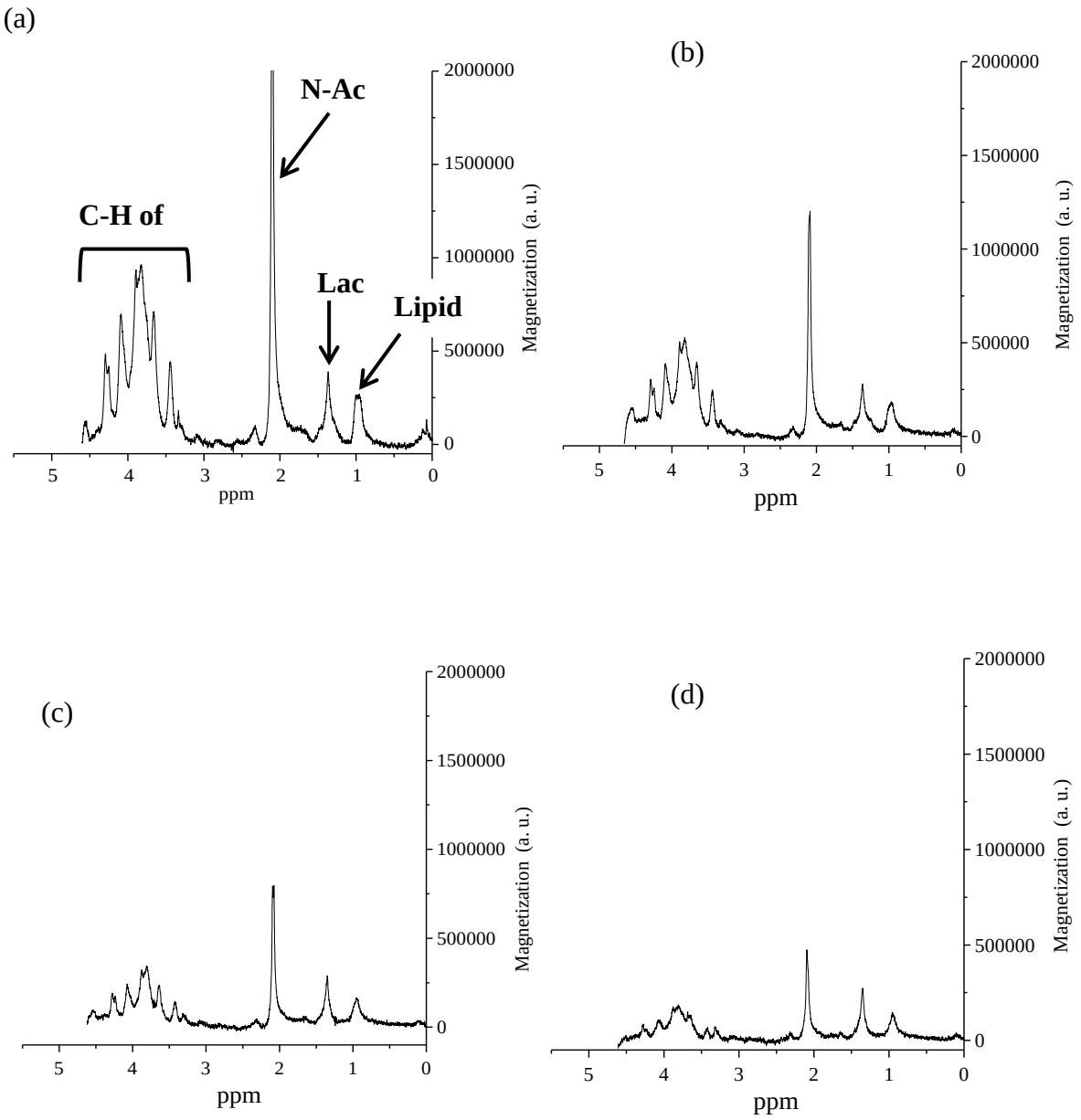

Figure 5.16 ^{1}H MAS NMR spectra of deuterated bovine articular cartilage. (a) 0% PG-depleted AC tissue (normal AC). (b) 14% PG-depleted AC tissue. (c) 38% PG-depleted AC tissue. (d) 68% PG-depleted AC tissue. Lipid consist of a chain of CH_2 groups termenated at one end with a CH_3 group and at the other end with a polar head group.

Treating the tissue with trypsin modifies PG but not collagen. In this section, the aim is to obtain a relationship between the sizes of collagen and PG structural components and to find a marker that shows sensitivity to tissue degradation. Proton MAS provides a resolved PG spectrum, quantifying the sizes of sugar ring, N-Acetyl group, and lactate acid proton groups, while a static spectrum yields the size of the collagen proton spin group, which serves as internal reference for quantifying the amount of PG in the tissue.

Trypsin was used at different concentrations and for different application times to achieve different PG-depletion levels in the cartilage. In this study depletion levels in the range of ~ 10 % to ~ 70 % were used.

A standard curve was tested to determine the accuracy of the reference sample slope of the reference sample to ensure accuracy when plating the actual samples, Figure 5.17. The standard curve will show a specific color range when the dye is added, and it is important to make sure that the samples being tested will fall into this color range. As explained in chapter 4 the process of preparing and plotting the standard curve will be important to establish the standard curve by knowing the exact amount of chondroitin sulphate at each point in the curve. This standard curve was the reference to find out how much PG is left in each depleted sample after digesting the sample with papain. Next we obtained the spectrophotometer reading using 50 µl in three wells. Then, adding 200 µl of the dye we tried to make sure it fell in the standard curve colors range. After taking the spectrophotometer reading at 525

wave length, the average of the three sets of each sample was taken to calculate the PG amount and to make sure that it fell on the standard curve (calculated line). If the spectrophotometer reading was off the standard curve, then dilution of the actual cartilage sample is needed. Not only should the cartilage supernatant be measured, but also the trypsin and the trypsin inhibitor solutions. These should all fall on the standard curve. Following this, the final PG-depletion level can be calculated.

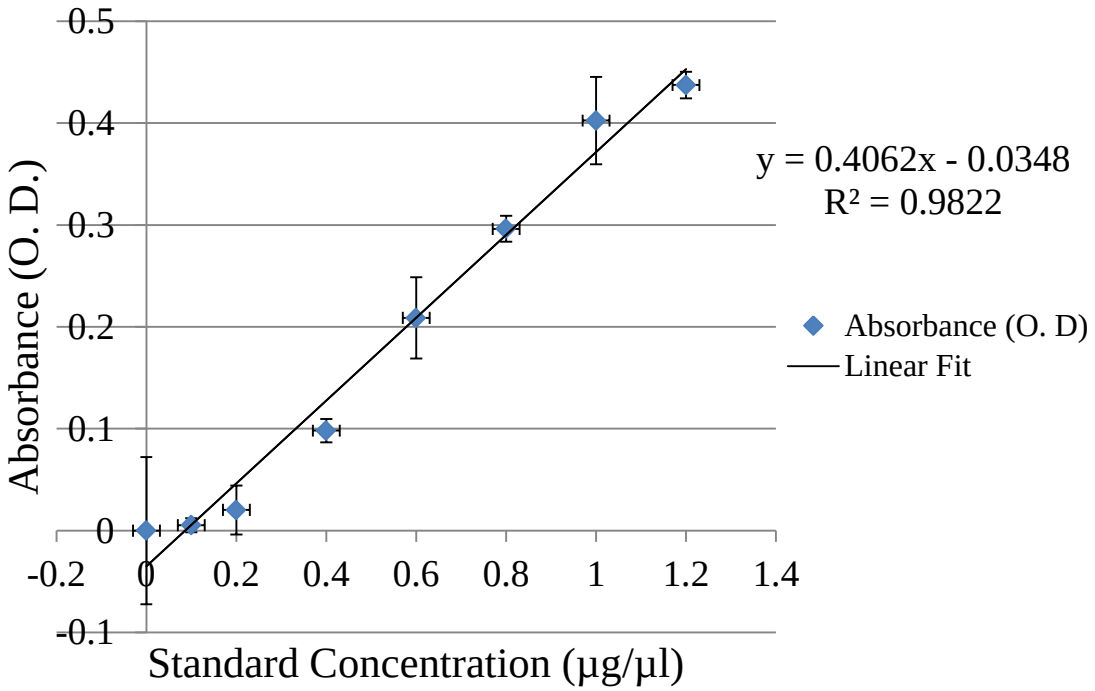

Figure 5.17 Standard curve for media DMMB shows the absorbance reading in optical dencity (O. D.) for each standard concentration in µg.

Table 5.10 gives the ratio of the areas of the three main peaks (whole PG area, N-Acetyl group, and sugar rings (C-S)) to the area of the collagen peak as a function of depletion, while Figure 5.18 shown plots of these ratios.

Table 5.10 PG/Coll, N-Ac/Coll, and C-S/Coll ratios , as determined from the MAS and static experiments , for a series of PG-Depletion levels.

% PG-Depletion	PG/Coll	N-Ac/Coll	C-S/Coll
0	1.0 ± 0.3	1.0 ± 0.3	1.0 ± 0.3
11.93	0.5 ± 0.2	0.5 ± 0.2	0.5 ± 0.2
13.96	0.6 ± 0.2	0.5 ± 0.2	0.6 ± 0.2
14.30	0.6 ± 0.2	0.5 ± 0.2	0.5 ± 0.2
14.33	0.6 ± 0.2	0.4 ± 0.2	0.3 ± 0.1
14.44	0.6 ± 0.1	0.5 ± 0.1	0.6 ± 0.2
15.96	0.6 ± 0.2	0.5 ± 0.2	0.5 ± 0.2
16.29	0.6 ± 0.2	0.5 ± 0.2	0.5 ± 0.2
18.82	0.6 ± 0.2	0.5 ± 0.2	0.6 ± 0.2
20.01	0.4 ± 0.2	0.3 ± 0.1	0.3 ± 0.1
20.07	0.6 ± 0.2	0.5 ± 0.1	0.5 ± 0.2
20.98	0.6 ± 0.1	0.4 ± 0.1	0.5 ± 0.2
24.03	0.4 ± 0.1	0.4 ± 0.1	0.4 ± 0.1
27.32	0.4 ± 0.2	0.3 ± 0.2	0.3 ± 0.1
27.33	0.5 ± 0.2	0.5 ± 0.2	0.4 ± 0.1
35.59	0.5 ± 0.2	0.4 ± 0.1	0.4 ± 0.2
38.09	0.4 ± 0.1	0.3 ± 0.1	0.3 ± 0.05
56.51	0.3 ± 0.1	0.3 ± 0.1	0.2 ± 0.1
68.14	0.2 ± 0.05	0.2 ± 0.05	0.2 ± 0.05

(a)

(b)

(c)

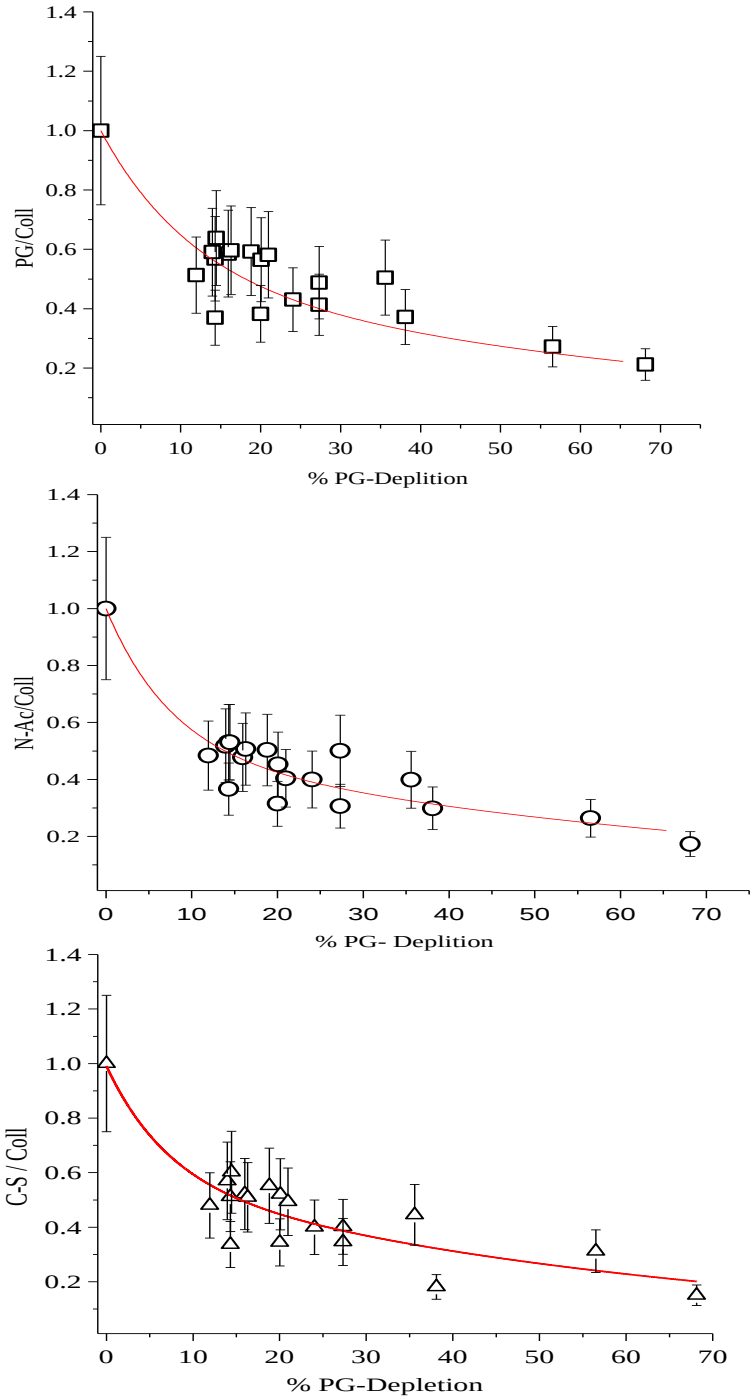

Figure 5.18 Plots of a) PG/Collagen, b) N-Ac/Collagen and c) C-S/Collagen ratios versus PG-depletion. The ratios were determined from the MAS and static experiments as discussed in the text. In each case the ratios were normalized to equal 1 at zero percent PG-depletion. The solid lines represent bi-exponential fits to the data.

Figure 5.19 shows the sensitivity that was calculated from the MAS data. From this graph, we can see that this technique has the potential for high sensitivity particularly over the first 10 % of PG-depletion.

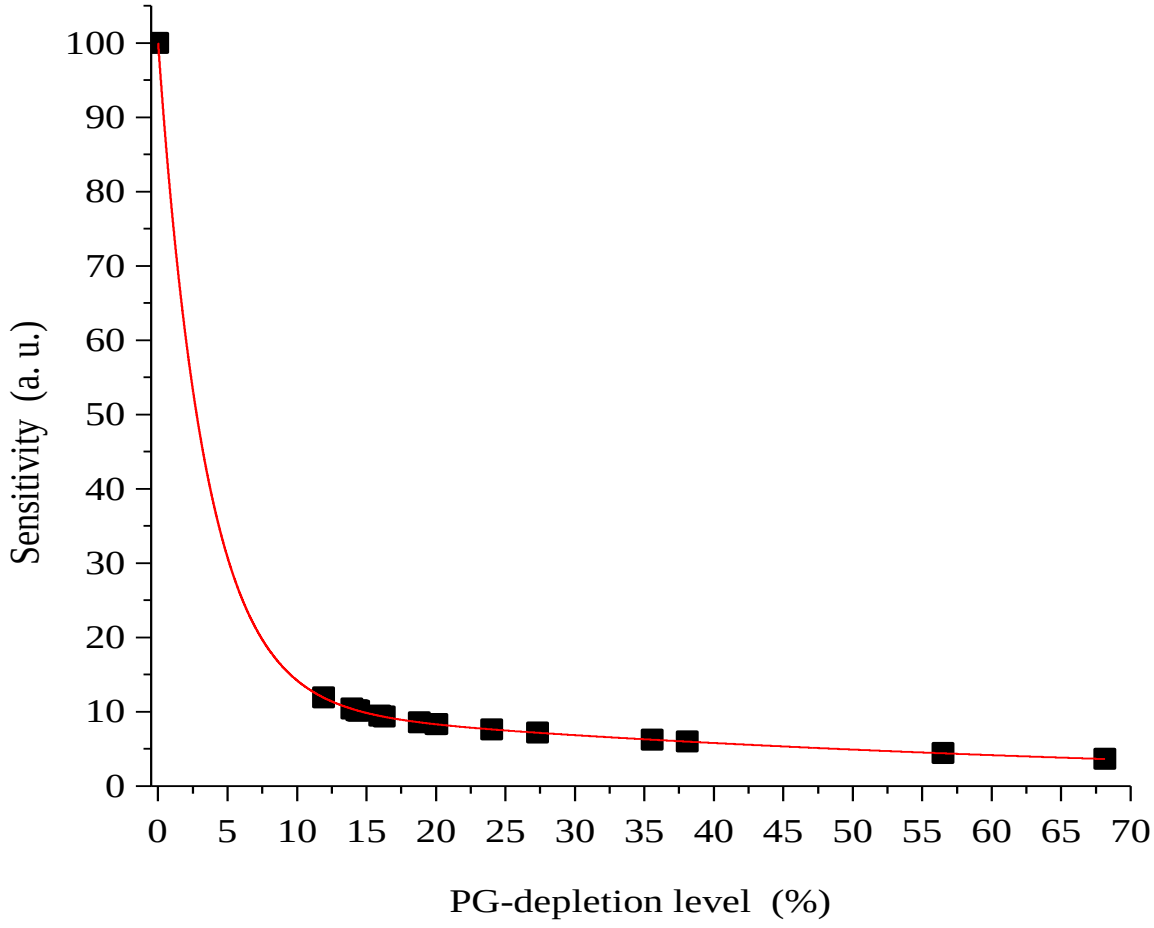

Figure 5.19 PG- depletion sensitivity curve from MAS results. The solid line represent bi-exponential fits to the data.

Although the above combination of MAS and static measurements shows promise as a sensitive depletion method for PG-depletion, the technique is of no practical use for *in vivo* observation of cartilage tissue. A fully stationary technique must be considered with the potential for creating high resolution spectra of PG that define the main spectral features as obtained with MAS.

Chemical shift imaging (CSI) is such technique. This technique provides a high spectral resolution and allows for partial corrections of local field susceptibility and shimming inhomogeneities leading to better spectral resolution. However, while MAS removes dipolar coupling and chemical shift anisotropy, resulting in sharper spectra, CSI does not. Nevertheless, in the case of fast motion of proton spin groups, CSI has been successfully applied in the observation of high resolution spectra of small metabolites in tissue. PG in cartilage is not a small structure, but owing to large and fast segmental motions, relatively sharp spectra of PG can be obtained under stationary conditions using CSI, a circumstance which, could provide a practical method of observation *in vivo*. Such a method is described in the following.

In this work, it is important to emphasize the importance of the effect of PG thermal motions on the spectral resolution. To this end consider the following MAS experiment designed to trace water evaporation in normal deuterated cartilage from full bulk water saturation to total evaporation (Fig. 5.20). The MAS experiment was performed at 5 kHz spinning rate, as described above.

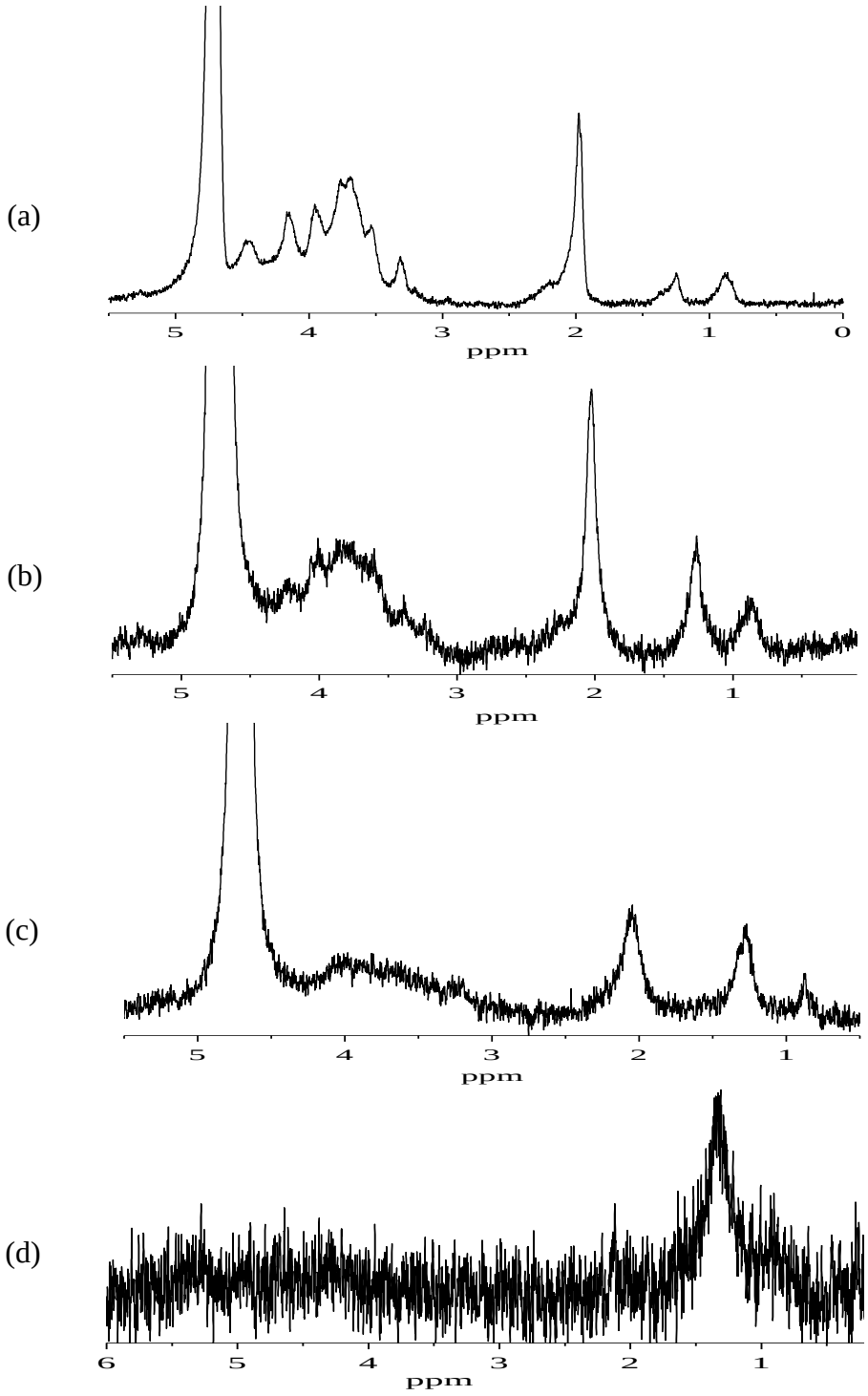

Figure 5.20 Proton MAS spectra in normal, deuterated cartilage at a) 100% hydration, b) 50% hydration, c) 15% hydration and d) 0% hydration.

From the full water saturation case to its final evaporation, the spectral resolution decreases to the point of collapsing into a broad background of collagen- PG spectral structures, despite the 5 kHz MAS condition. This clearly demonstrates the importance of thermal motions in the observation of high resolution PG spectra in cartilage. As demonstrated below, such motions are large enough to even produce well resolved spectra without MAS.

Figure 5.21 shows an example of a 2D proton image (6 mm FOV, 1 mm slice thickness, and 64X64 digital resolutions) of a normal, deuterated bovine cartilage tissue, and its corresponding 1D CSI spectra with a 32 digital resolution (spatial resolutions about 3 mm/32); the CSI scan direction is indicated by an arrow in both diagrams. Similar data were obtained for a series of PG depletion levels ranging from 0% to 68% depletion. Each CSI data set is obtained after correction for shim inhomogeneities and amplitude variation due to imaging gradient imperfections along the 1D imaging direction, utilizing a similar calibration scan on a liquid solution of 22 mM DSS/D_2O. Throughout these scans, water suppression was applied. If any remnants of residual water interference were present, these were removed by post data filtering analysis using least square fitting procedures. Following these correction procedures, a sum total spectrum was created and compared to the global collagen signal, as done for the MAS experiment.

An example of three PG spectra, shown in Figure 5.22, illustrates the variation of the spectral distribution with depletion. The spectra also show sufficient frequency resolution to clearly resolve the peaks at N-Ac and C-S positions. Table 5.11 lists the areas under these peaks for the entire series of spectra obtained for nine depletion levels.

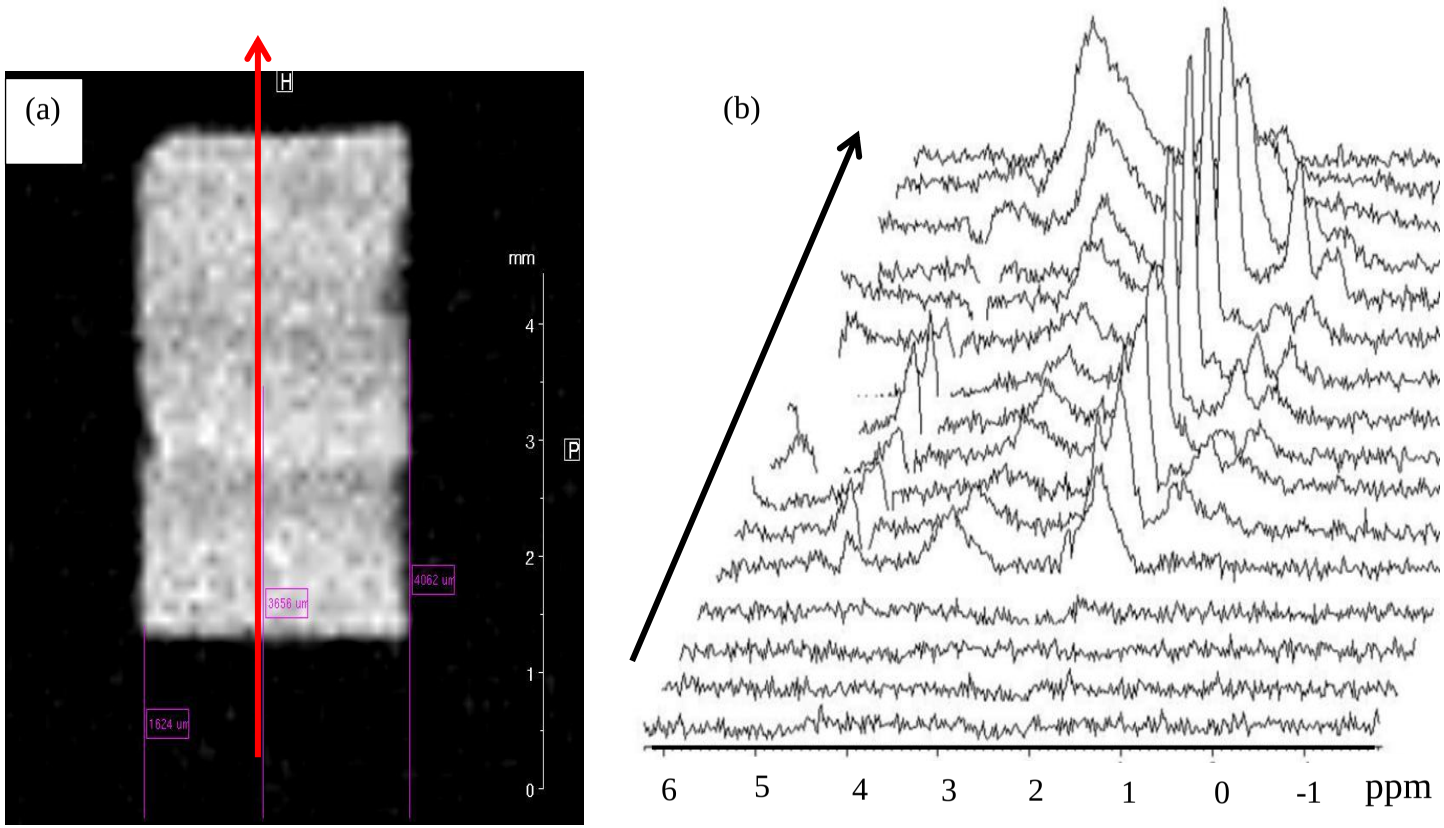

Figure 5.21 (a) CSI image of cartilage discs. The arrows show direction of the CSI scan. (b) Stack plot of 1D CSI.

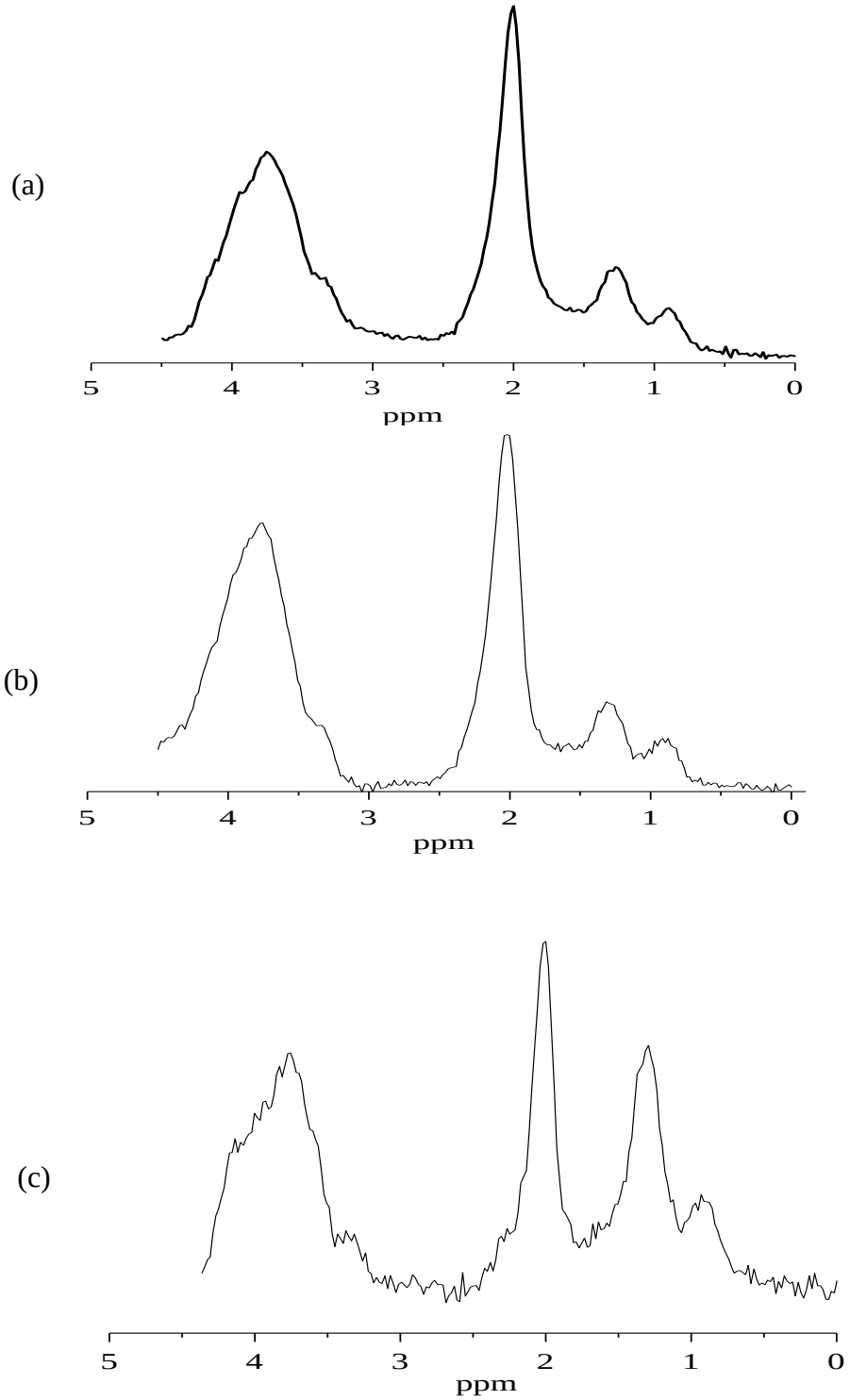

Figure 5.22 CSI spectra for deuterated articular cartilage , (a) 0% PG-depletion, (b) 14% PG-depletion and (c) 40% PG-depletion.

Table 5.11 Spectral area ratios PG/Coll, N-Ac/Coll and C-S/Coll obtained from CSI scans.

% PG-Depletion	PG/Coll	N-Ac/Coll	C-S/Coll
0	1.0 ± 0.3	1.0 ± 0.3	1.0 ± 0.3
0	1.0 ± 0.3	1.1 ± 0.3	1.2 ± 0.3
10.04	0.5 ± 0.2	0.5 ± 0.2	0.5 ± 0.2
10.95	0.5 ± 0.2	0.5 ± 0.2	0.7 ± 0.2
11.273	0.9 ± 0.3	0.9 ± 0.3	1.1 ± 0.3
14.81	0.6 ± 0.2	0.6 ± 0.2	0.6 ± 0.2
27.07	0.4 ± 0.1	0.4 ± 0.2	0.5 ± 0.2
40.24	0.3 ± 0.1	0.3 ± 0.1	0.3 ± 0.1
65.33	0.2 ± 0.05	0.2 ± 0.05	0.2 ± 0.05

A series of nine depletion levels of collagen areas was obtained by subtracting of the cartilage spectrum obtained from a spin echo with a 1 ms echo delay from the spectrum obtained from the FID following a short 90 degree pulse of 5 μs. In each case a repetition time of 5 s was used to avoid saturation effects. The signal from the spin echo was devoid of collagen broad line signal. Each signal was filtered with a 1000 Hz exponential filter and Fourier transformed before subtraction. This approach effectively leaves a collagen line to be analysed for area extraction, as is illustrated in Fig. 5.23. The list of these areas is given in Table 5.12.

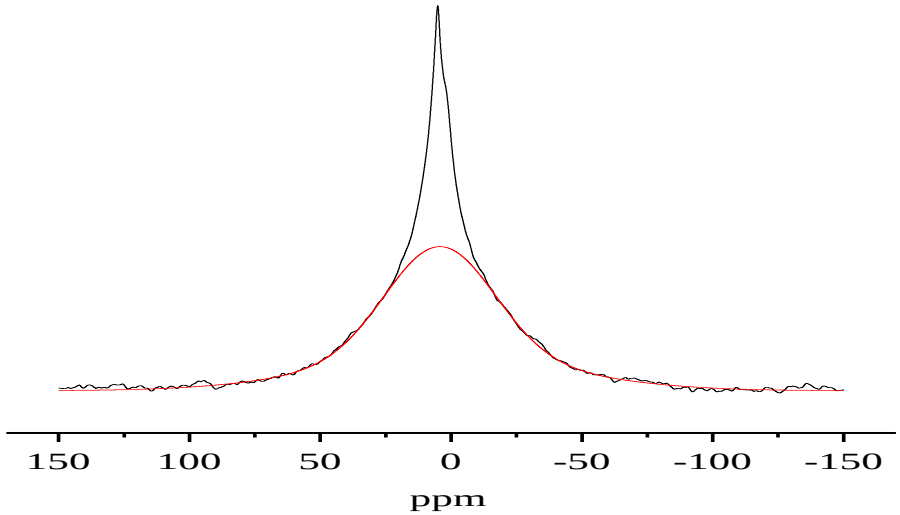

Figure 5.23 Typical collagen area extraction from static spectrum of deuterated articular cartilage.

Table 5.12 Collagen area was extracted from the total polymiric spectral area and all collagen areas in the table were renormlized such that first area entry equal to one.

% PG- Depletion	Collagen Area (a. u.)
0	1.0 ± 0.3
0	0.6 ± 0.2
10.04	1.2 ± 0.3
10.95	1.3 ± 0.4
11.27	0.7 ± 0.2
14.81	0.8 ± 0.3
27.078	1.3 ± 0.4
40.24	0.8 ± 0.2
65.33	2.3 ± 0.6

(a)

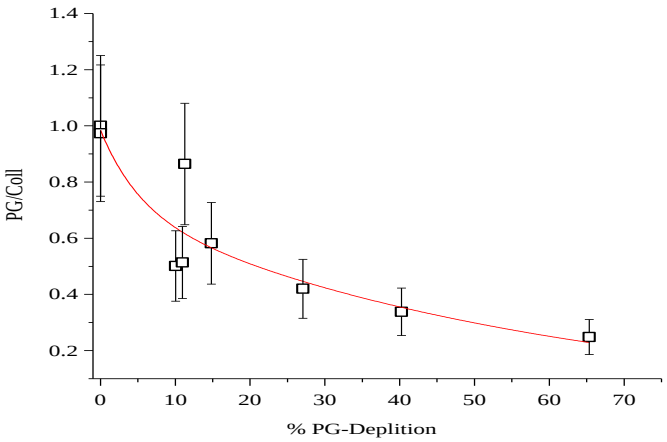

(b)

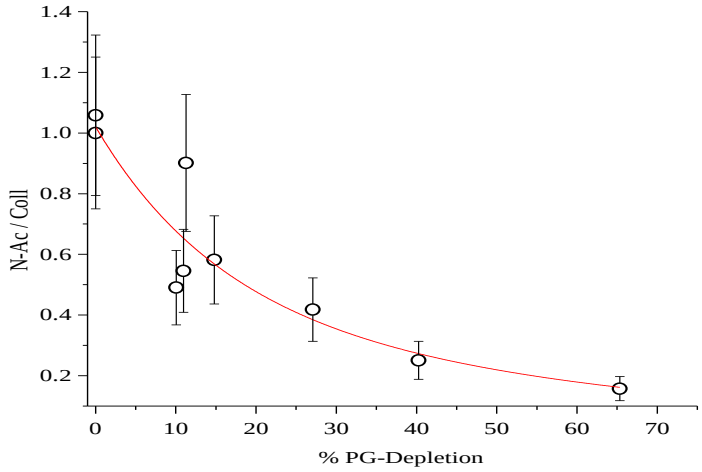

(c)

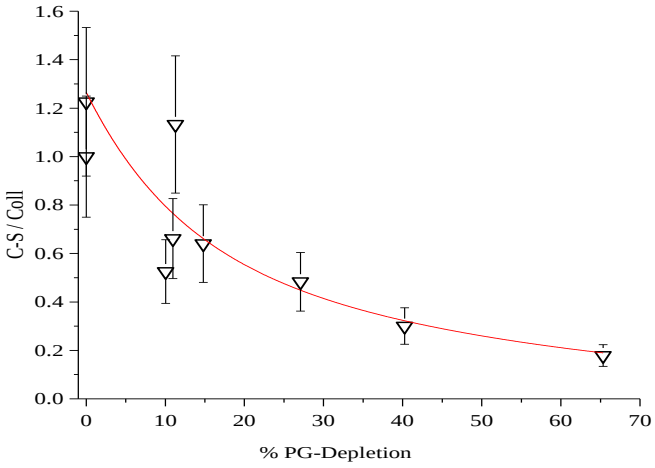

Figure 5.24 Ratio from CSI experiments (a) PG-Collagen ratio , (b) N-Ac –Collagen ratio, (c) C-S – Collagen ratio. The solid lines represent bi-exponential fits to the data.

The final results for the PG-Collagen ratio as a function of the PG depletion level are given in Figure 5.24 and Table 5.11. The average trend of the variation of these ratios with respect to the depletion level is represented by the solid lines. These lines are calculated from a least square fits of the sum of two exponential functions to the data. As for the MAS experiment, this allows for computation of the sensitivity of the various ratios, as defined above, to the PG depletion level, especially at the lower levels of depletion, associated with early detection of PG defects, Fig. 5.25. In the present case Fig 5.25 suggests that the slope of the ratio versus depletion plot is particularly sensitive to depletion in the range 0 - 10% depletion. These results are in keeping with our main goal of presenting an NMR technique with high sensitivity to early onset of cartilage deterioration, and with a realistic potential for clinical application.

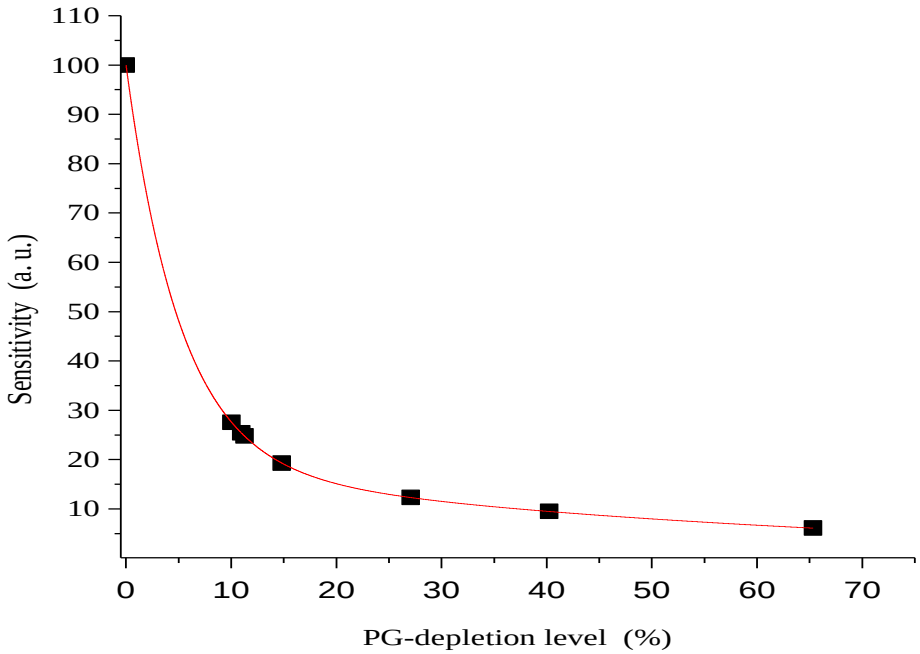

Figure 5.25 PG- depletion sensitivity curve from CSI results. The solid line represent bi-exponential fits to the data.

Chapter 6
CONCLUSIONS AND RECOMENDATIONS

6.1 Conclusions

30 MHz Relaxation and Exchange Modeling

The proton transverse decay was measured and analysed in natural and deuterated bovine articular cartilage at 3^{o}C and at -10^{o}C. These experiments clearly identified collagen, liquid-like PG, water and ice proton spin groups. In addition, in the frozen, deuterated cartilage the HDO ice proton spin group was particularly well defined through its long T_1 ~ 3 seconds and T_2 ~ 80 μs.

Using the 2D time domain NMR spin-lattice relaxation experiments, T_{1HH}, T_{1SH} and $T_{1\rho}$, the FIDs of the T_1 and $T_{1\rho}$ component magnetizations were reconstructed for the four cases, natural and deuterated tissue at 3^{o}C and -10^{o}C. The reconstructed FID for deuterated tissue at -10^{o}C, obtained in the 2D $T_{1\rho}$ experiment, resolved two distinct collagen spin groups, each making up a significant portion of the collagen spin reservoir. This is the first time that these collagen subgroups have been identified and characterized. For each of the four cases, the results from the 2D time domain experiments, combined with the transverse decay results and known sample stoichiometry, were interpreted with a view towards defining a multi-spin group relaxation/exchange model for the tissue. The models were quantified using an exchange analysis/simulation approach. This way, for each case a comprehensive exchange model was derived involving four spin reservoirs, two collagen spin reservoirs (a and b), one mobile PG and one water spin reservoirs (H_2O in natural and

HDO in deuterated cartilage tissue). At -10^{o}C the ice spin group was found to be uncoupled from the remaining spin groups.

The relaxation/exchange models for articular cartilage, reported upon here, provide a more detailed description of cartilage inter-constituent pathways for magnetization exchange, than available in the literature. As such, they are expected to have application in improving MRI-based magnetization transfer protocols in the clinical setting.

500 MHz CSI Experiments

The ratio of the area of the PG/broad-line collagen signal was obtained in cartilage, at various levels of PG depletion, by combining a CSI sequence (no spinning) to define the high resolution PG signal, with a simple broad-line sequence (no spinning) to obtain the collagen signal. In effect this gives the absolute PG content (PG/collagen ratio) in a static setting (e.g., *in vivo*, clinical setting). The PG/collagen ratios obtained this way were found to compare well to those using MAS in place of CSI, demonstrating that this combination of CSI signals and broadline collagen signal may have practical application in the clinical setting. In addition, CSI was successfully used in a 2D imaging experiment of deuterated cartilage, and in combination with broadline spectra for collagen demonstrates proof-of-concept for using this approach to determine the PG/collagen ratio in the MRI setting. To our knowledge this represents the first time that the CSI signal - collagen signal ratio has been investigated in PG depletion cartilage tissue.

6.2 Recommendations

To circumvent the averaging effect of the apparent relaxation parameters over the cartilage zones in cartilage plugs it should prove useful to develop samples which contain only one type of cartilage zone; i.e., physically separate the zones of a cartilage plug. This will allow the study of relaxation and magnetization exchange for each separate zone type.

The CSI-based approach for PG/collagen ratio in the MRI setting can be improved upon by using faster field gradients to detect collagen, also with CSI. This would involve modification of the gradient switching circuitry. The above proof–of –concept experiment needs to be repeated using natural cartilage rather than deuterated cartilage to demonstrate applicability in the clinical setting.

Appendix A
Proteoglycan Structure

Proteoglycan structure and components molecular weights were discussed in section 3.13. In this Appendix a brief description of the main sugar ring chains, that build up the proteoglycan, is presented. Figure A.1 shows the polysaccharide structure and sulfate positions of Hyaluronic acid, Chondroitin Sulfate, and Keratin Sulfate [124].

Hyaluronic acid (HA) is the major long chain that contains non-sulfated glycosaminoglycan and binds proteoglycan monomers via linked proteins. The repeating disaccharide of HA is shown in Fig. A.1a.

Chondroitin Sulfate exists in three different forms A, B and C, depending on the sulfate ester position, and are shown in Fig. A1c, A1d and A1e, respectively. Chondroitin sulfate A and B are also called chondroitin-4 and chondroitin-6.

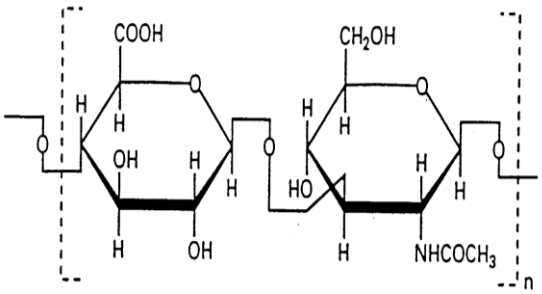

(a) Hyaluronic acid.

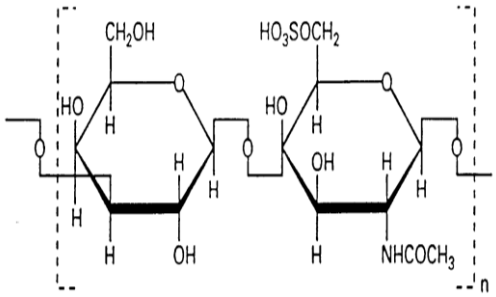

(b) Keratin Sulfate.

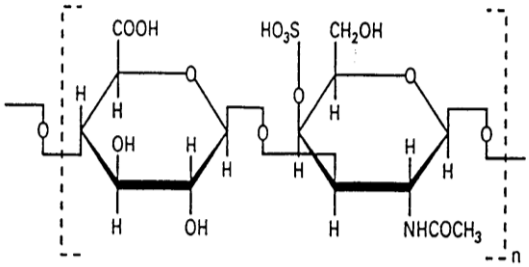

(c) Chondroitin Sulfate (A).

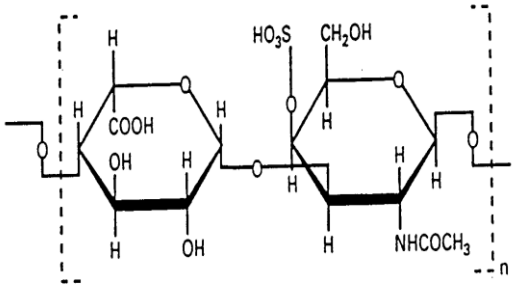

(d) Chondroitin Sulfate (B).

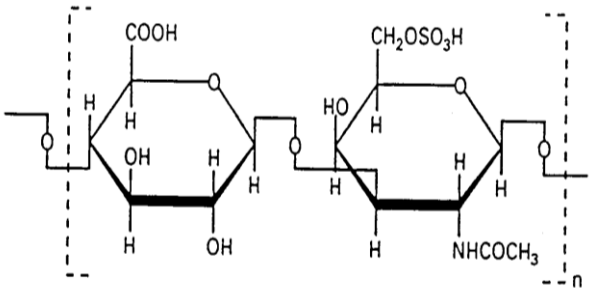

(e) Chondroitin Sulfate (C).

Figure A. 1 Repeating disaccharide units in glycosaminoglycan chains. a) Hyaluronic acid, b) Keratin Sulfate, c), d), and e) different forms of Chondroition Sulfate.

Appendix B

Examples of Multicomponent Relaxation Decay Curves

In this Appendix a few examples are given of the procedure (section 4.14) used to decide on the number of magnetization components relevant for a particular multicomponent analysis.

B.1 $T_{1\rho}$ of deuterated cartilage at 3°C

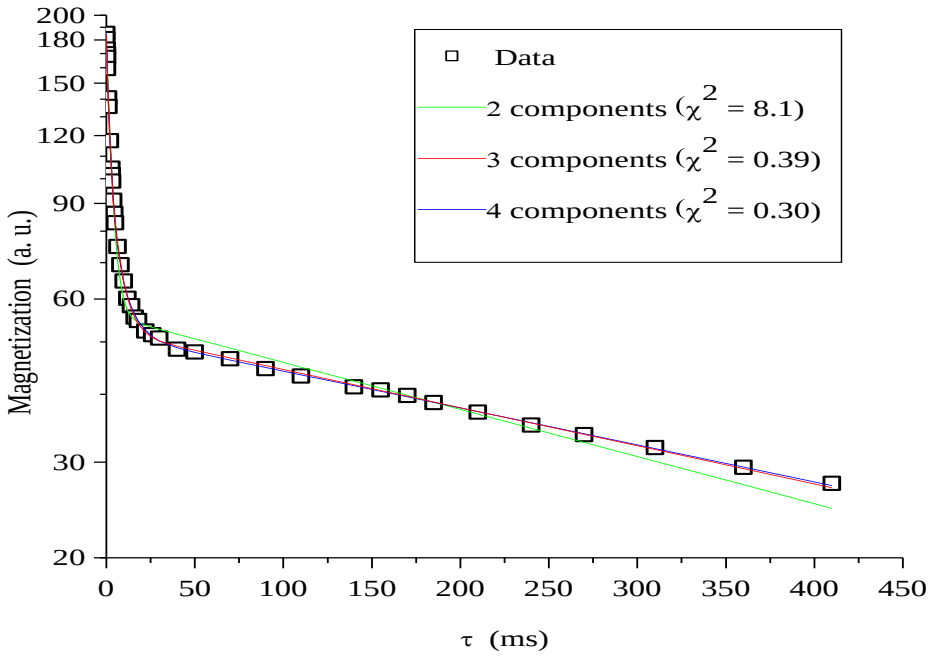

Figure B. 1 $T_{1\rho}$ relaxation curve of deuterated cartilage for a time window of 7.5 μs on the FID at 3°C, showing 2, 3 and 4 component fits. The best-fit parameters and the corresponding χ^2 values are shown in Table B.1.

Table B. 1 The best-fit parameters, $T_{1\rho}$ and magnetization fractions, as well as χ^2 values for 2, 3 and 4 component decompositions of $T_{1\rho}$ decay curve given in Figure B.1.

Components of natural $T_{1\rho}$ (t = 7.5 µs), (3^oC)		$T_{1\rho}$ (ms)	Magnetization	χ^2
Two component	$T_{1\rho Short}$	3.1 ± 0.1	125.6 ± 1.6	8.10
	$T_{1\rho Long}$	500.2 ± 37.6	56 ± 1	
Three components	$T_{1\rho Short}$	1.3 ± 0.8	66.2 ± 3.8	0.39
	$T_{1\rho Medium}$	6.2 ± 0.3	69.3 ± 3.9	
	$T_{1\rho Long}$	662.4 ± 20.5	51.6 ± 8.4	
Four components	$T_{1\rho Short}$	0.7 ± 0.2	26.8 ± 8.4	0.30
	$T_{1\rho Medium1}$	2.8 ± 0.5	79.3 ± 6.4	
	$T_{1\rho Medium2}$	10.2 ± 2.0	31.7 ± 9.5	
	$T_{1\rho Long}$	658.4 ± 22.3	50.5 ± 0.5	

B.2 T_{1HH} of deuterated cartilage at 3^oC

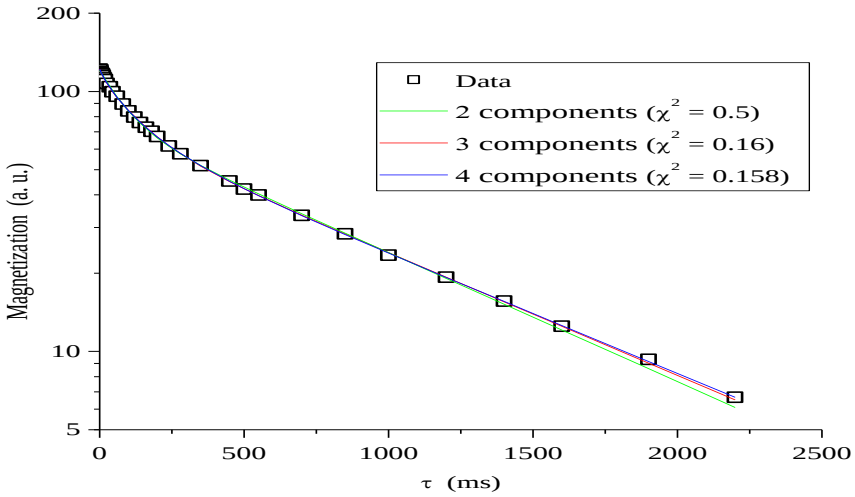

Figure B. 2 T_{1HH} relaxation curve of deuterated cartilage for a time window of 7.5 µs on the FID at 3^oC, showing 2, 3 and 4 component fits. The best-fit parameters and the corresponding χ^2 values are shown in Table B.2

Table B. 2 The best-fit parameters, T_{1HH} and magnetization fractions, as well as χ^2 values for 2, 3 and 4 component decompositions of T_{1HH} decay curve given in Figure B.2.

Components of natural T_{1HH} (t = 7.5 μs), (3°C)		T_{1HH} (ms)	Magnetization	χ^2
Two component	T_{1Short}	101.3 ± 0.1	45.5 ± 1.1	0.50
	T_{1Long}	874.7 ± 16.7	75.3 ± 1.2	
Three components	T_{1Short}	20.7 ± 6.3	5.9 ± 1.4	0.16
	$T_{1Medium}$	129.6 ± 51	44.5 ± 1.2	
	T_{1Long}	919.4 ± 14.5	71.2 ± 1.1	
Four components	T_{1Short}	12.9 ± 9.4	26.8 ± 8.4	0.16
	$T_{1Medium1}$	80.9 ± 64.5	79.3 ± 6.4	
	$T_{1Medium2}$	181.5 ± 117.3	31.7 ± 9.5	
	T_{1Long}	942.7 ± 354	50.5 ± 0.5	

B.3 T_{1SH} of deuterated cartilage at 3°C

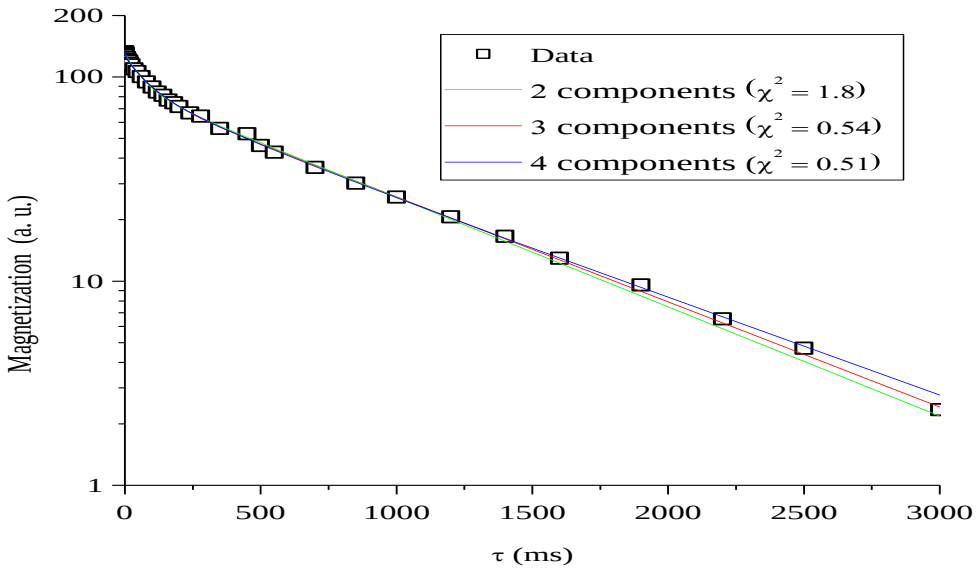

Figure B. 3 T_{1SH} relaxation curve of deuterated cartilage for a time window of 28.5 μs on the FID at 3°C, showing 2, 3 and 4 component fits. The best-fit parameters and the corresponding χ^2 values are shown in Table B.3.

Table B. 3 The best-fit parameters, T_{1SH} and magnetization fractions, as well as χ^2 values for 2, 3 and 4 component decompositions of T_{1SH} decay curve given in Figure B.3.

Components of natural T_{1SH} (t = 28.5 μs), (3°C)		T_{1SH} (ms)	Magnetization	χ^2
Two component	T_{1Short}	72.2 ± 5.1	41.7 ± 1.5	1.8
	T_{1Long}	810.9 ± 21.2	88.1 ± 1.6	
Three components	T_{1Short}	2.9 ± 6.3	6.5 ± 0.7	0.54
	$T_{1Medium}$	91.9 ± 4.8	41.9 ± 1.1	
	T_{1Long}	843.4 ± 14.8	84.7 ± 1.2	
Four components	T_{1Short}	2.4 ± 0.7	5.9 ± 0.7	0.51
	$T_{1Medium1}$	75.6 ± 13.6	34.4 ± 8.3	
	$T_{1Medium2}$	308.2 ± 284.7	18.1 ± 10.0	
	T_{1Long}	910.5 ± 88.2	74.7 ± 15.6	

B.4 $T_{1\rho}$ of natural cartilage at 3°C

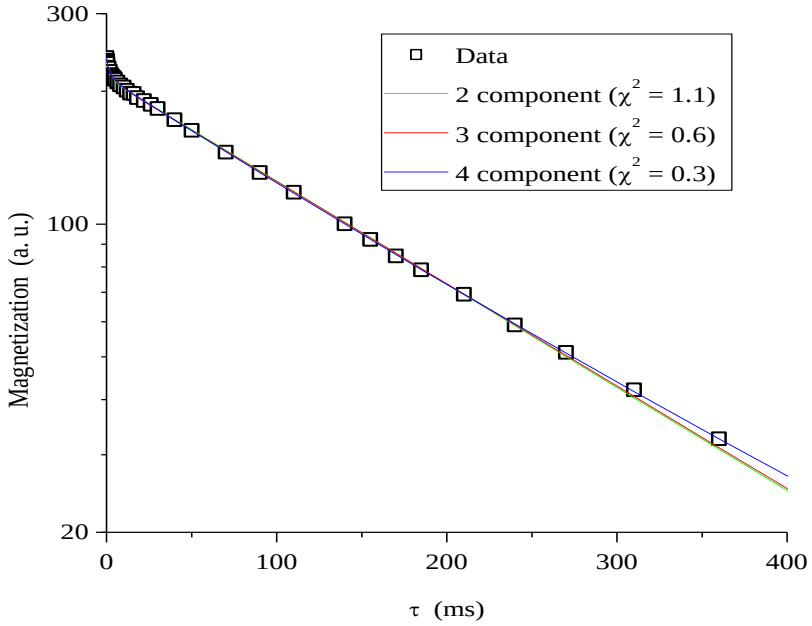

Figure B. 4 $T_{1\rho}$ relaxation curve of natural cartilage for a time window of 7.5 μs on the FID at 3°C, showing 2, 3 and 4 component fits. The best-fit parameters and the corresponding χ^2 values are shown in Table B.4.

Table B. 4 $T_{1\rho}$ The best-fit parameters, T_{1HH} and magnetization fractions, as well as χ^2 values for 2, 3 and 4 component decompositions of T_{1HH} decay curve given in Figure B.4.

Components of natural $T_{1\rho}$ (t = 7.5 µs), (3^oC)		$T_{1\rho}$ (ms)	Magnetization	χ^2
Two component	$T_{1\rho Short}$	2.5 ± 0.6	22.3 ± 0.6	1.1
	$T_{1\rho Long}$	185.7 ± 0.9	214.1 ± 0.4	
Three components	$T_{1\rho Short}$	0.9 ± 0.2	12.5 ± 2.6	0.6
	$T_{1\rho Medium}$	5.6 ± 1.5	12.6 ± 2.5	
	$T_{1\rho Long}$	187.1 ± 0.9	213.1 ± 0.6	
Four components	$T_{1\rho Short}$	0.6 ± 2.8	8.2 ± 2.8	0.3
	$T_{1\rho Medium1}$	3.3 ± 0.7	15.1 ± 2.7	
	$T_{1\rho Medium2}$	124.1 ± 156.3	145.9 ± 51.0	
	$T_{1\rho Long}$	90.9 ± 156.7	245.0 ± 128.4	

B.5 T_{1HH} of natural cartilage at 3°C

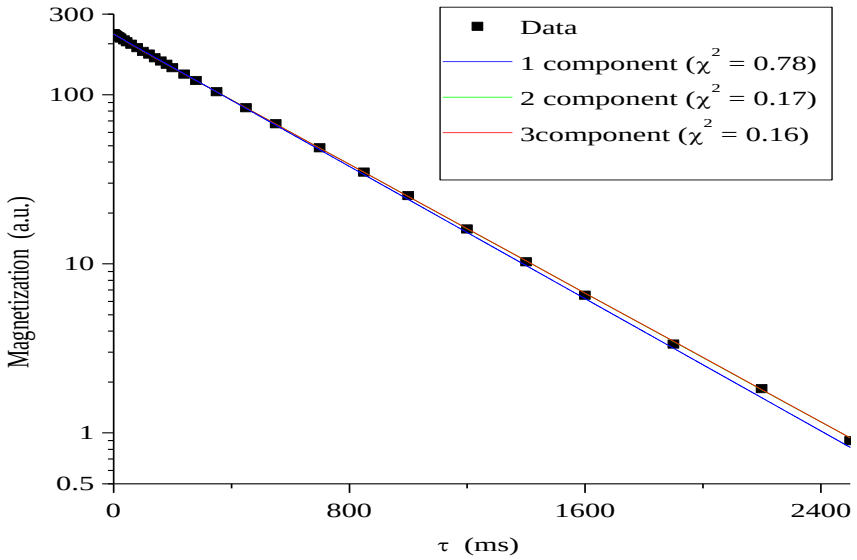

Figure B. 5 T_{1HH} relaxation curve of natural cartilage for a time window of 7.5 μs on the FID at 3°C, showing 1, 2 and 3 component fits. The best-fit parameters and the corresponding χ^2 values are shown in Table B.5.

Table B. 5 T_{1HH} The best-fit parameters, T_{1HH} and magnetization fractions, as well as χ^2 values for 1, 2 and 3 component decompositions of T_{1HH} decay curve given in Figure B.5.

Components of natural T_{1HH} (τ = 7.5 µs), (3^oC)		T_1 (ms)	Magnetization	χ^2
one component	T_1	444.04 ± 1.8	228.4 ± 0.2	0.83
Two components	T_{1Short}	57.2± 12.6	5.03 ± 0.7	0.17
	T_{1Long}	456 ± 2	224.3 ± 0.7	
Three components	T_{1Short}	7.2 ± 88.8	0.11 ± 1.0	0.16
	$T_{1Medium}$	60.8 ± 26.3	4.9 ± 0.9	
	T_{1Long}	456.1 ± 2.1	224.3 ± 2.1	

B.6 T_{1SH} of natural cartilage at 3°C

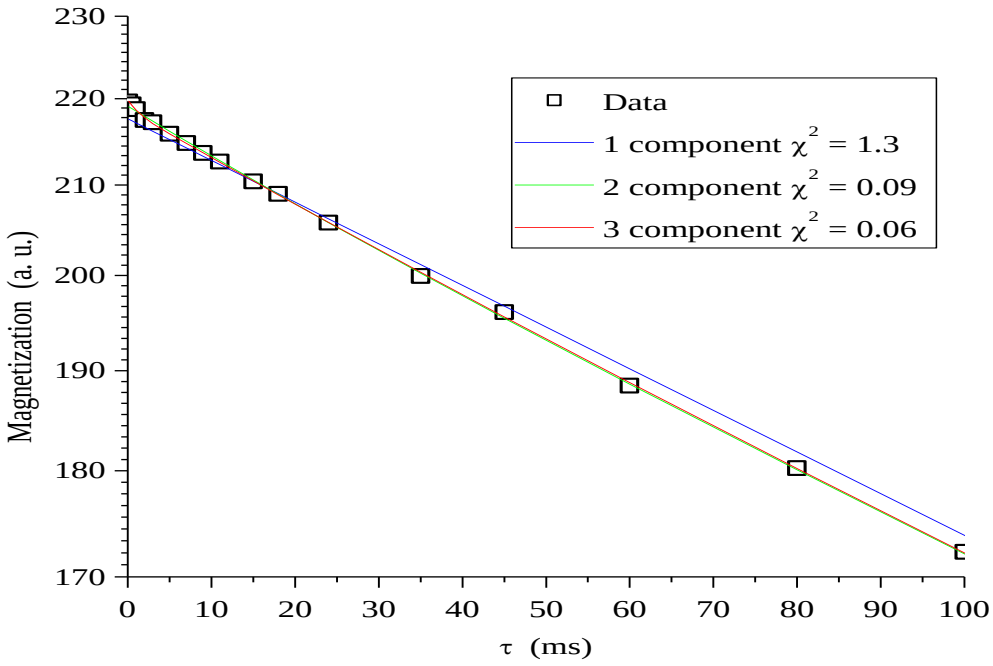

Figure B. 6 T_{1SH} relaxation curve of natural cartilage for a time window of 30.5 µs on the FID at 3°C, showing 1, 2 and 3 component fits. The best-fit parameters and the corresponding χ^2 values are shown in Table B.6.

Table B. 6 The best-fit parameters, T_{1SH} and magnetization fractions, as well as χ^2 values for 1, 2 and 3 component decompositions of T_{1SH} decay curve given in Figure B.7.

Components of natural T_{1SH} (τ = 30.5 μs), (3°C)	T_1 (ms)		Magnetization	χ^2
one component	T_1	445.3± 2.3	217.6 ± 0.3	1.3
Two components	T_{1Short}	44.2± 5.1	6.1 ± 0.3	0.09
	T_{1Long}	460.1 ± 1.2	213.1 ± 0.3	
Three components	T_{1Short}	1.2 ± 2.9	1.2 ± 0.6	0.06
	$T_{1Medium}$	56.5 ± 7.1	6.1 ± 0.4	
	T_{1Long}	461.5 ± 1.8	212.5 ± 0.4	

Appendix C

2D Reconstructed FIDs Fitting

This appendix presents the details for least-squares fitting for all reconstructed FIDs presented in section 5.2

C.1 Reconstructed FIDs from $T_{1\rho}$ experiment in natural cartilage at 3°C

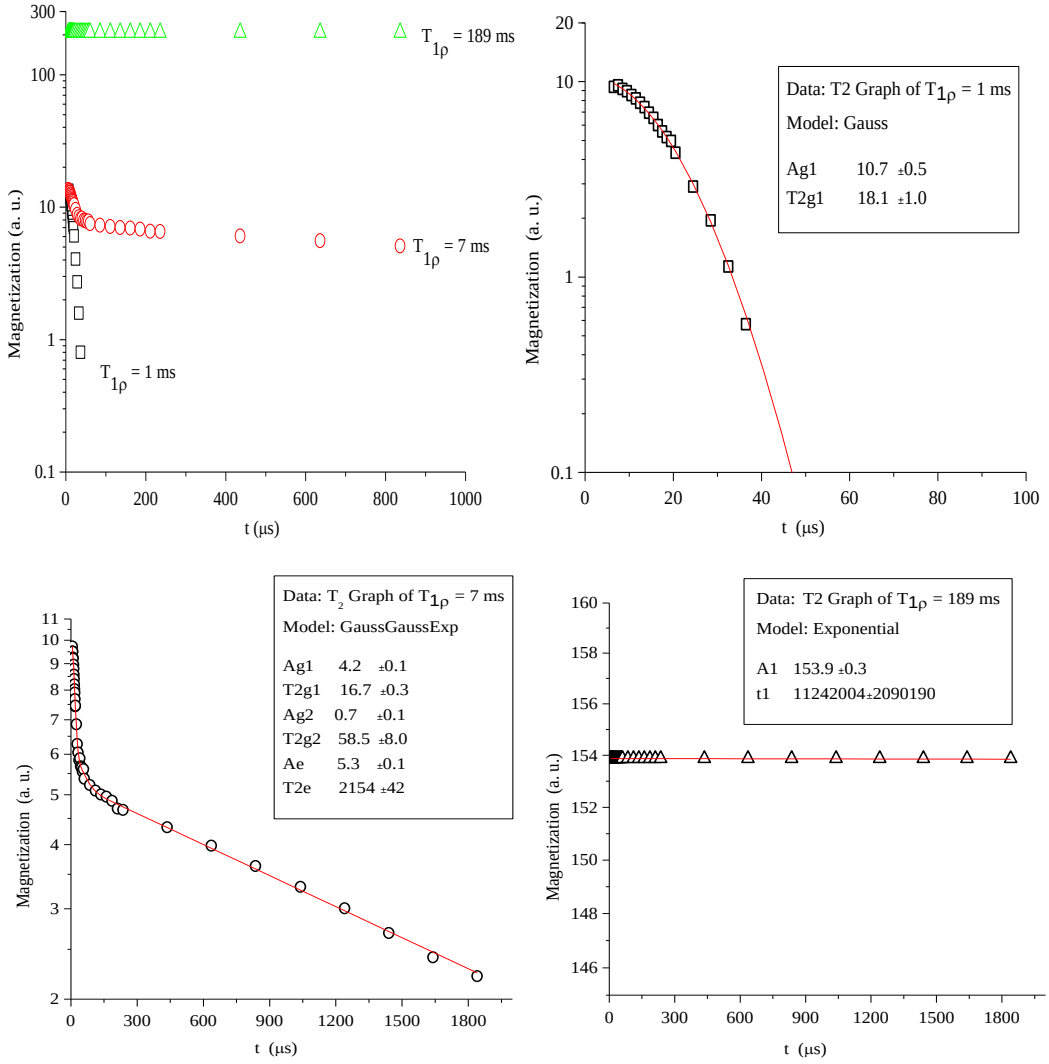

Figure C. 1 Reconstructed FID's from 2D-$T_{1\rho}$ experiment in natural cartilage at 3°C with the best-fit line and associated best-fit parameters indicated for each separate, reconstructed FID.

C.2 Reconstructed FIDs from T_{1HH} experiment in natural cartilage at 3°C

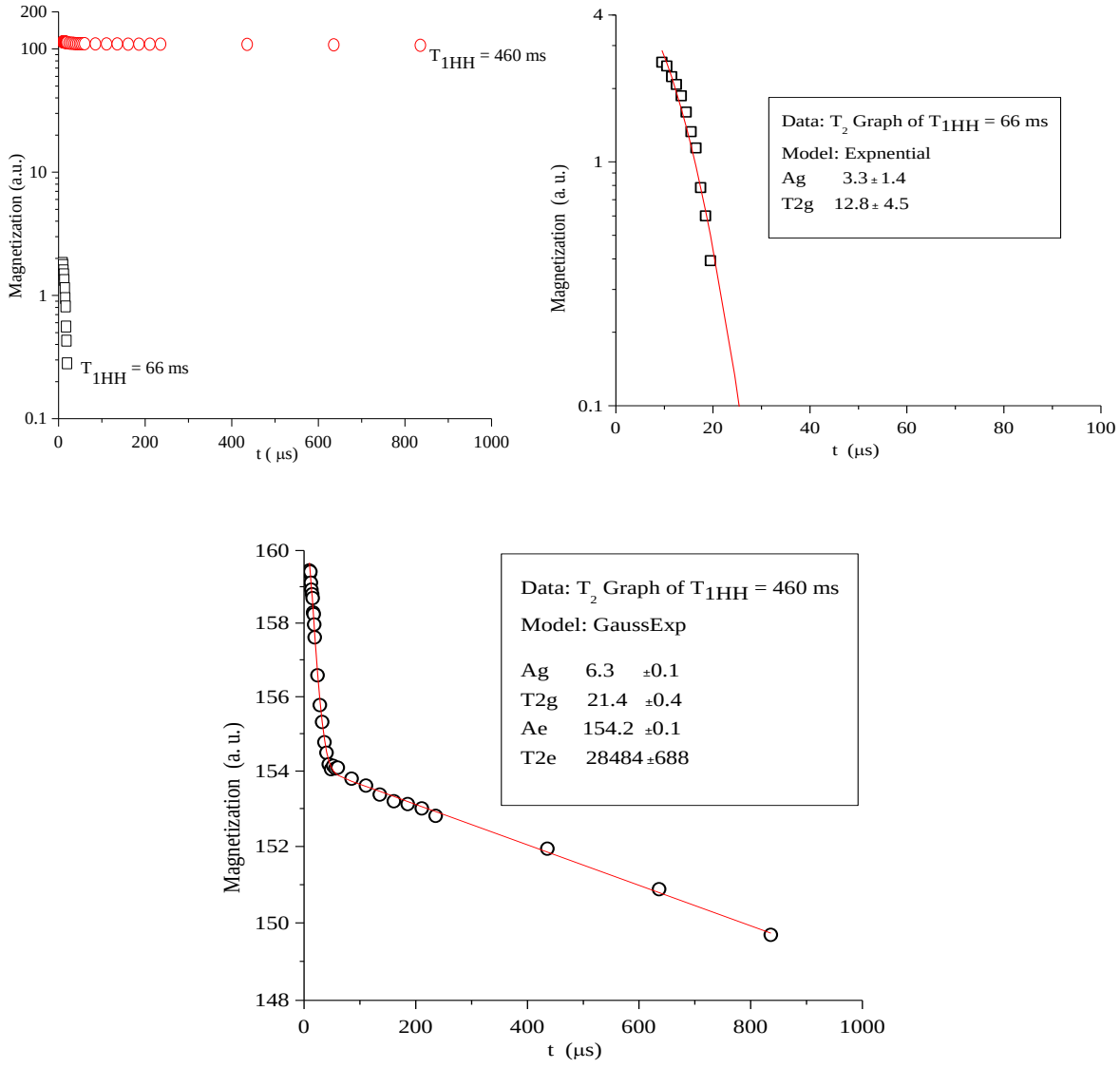

Figure C. 2 Reconstructed FID's from 2D-T_{HH} experiment in natural cartilage at 3°C with the best-fit line and associated best-fit parameters indicated for each separate, reconstructed FID.

C.3 Reconstructed FIDs from T_{1SH} experiment in natural cartilage at 3°C

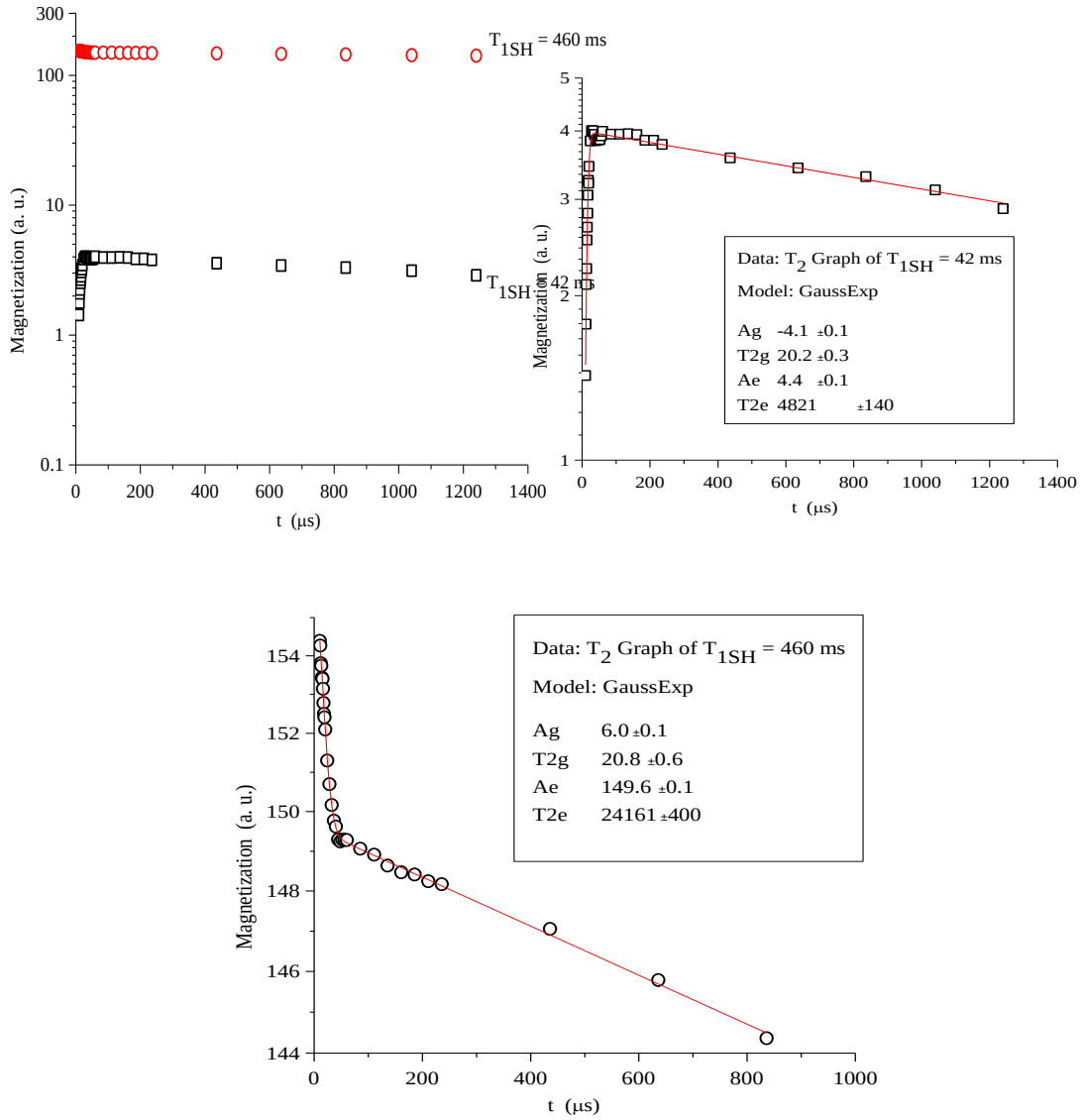

Figure C. 3 Reconstructed FID's from 2D-T_{SH} experiment in natural cartilage at 3°C with the best-fit line and associated best-fit parameters indicated for each separate, reconstructed FID.

C.4 Reconstructed FIDs from $T_{1\rho}$ experiment in natural cartilage at -10°C

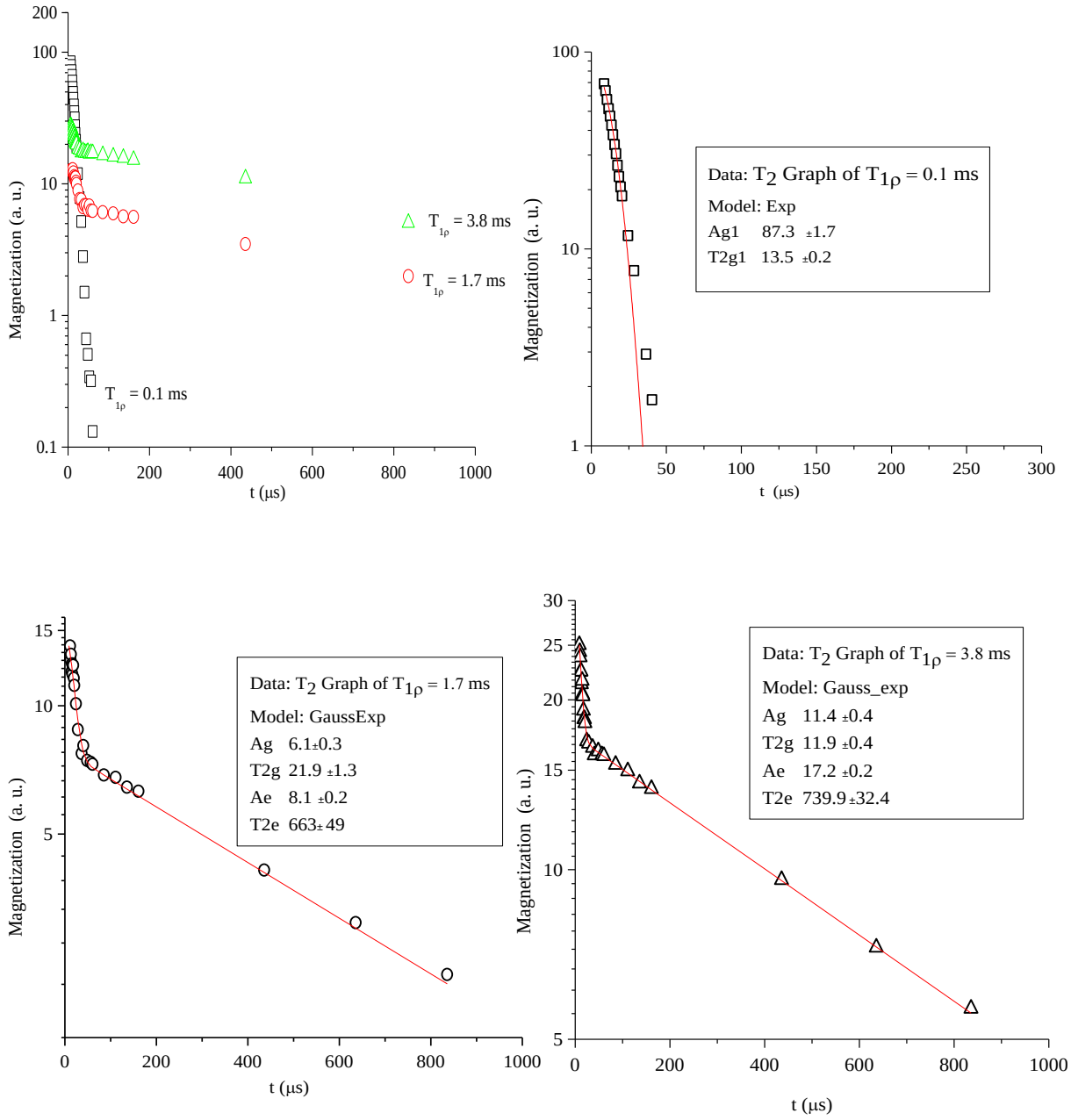

Figure C.4 Reconstructed FID's from 2D-$T_{1\rho}$ experiment in natural cartilage at -10°C with the best-fit line and associated best-fit parameters indicated for each separate, reconstructed FID.

C.5 Reconstructed FIDs from T_{HH} experiment in natural cartilage at -10°C

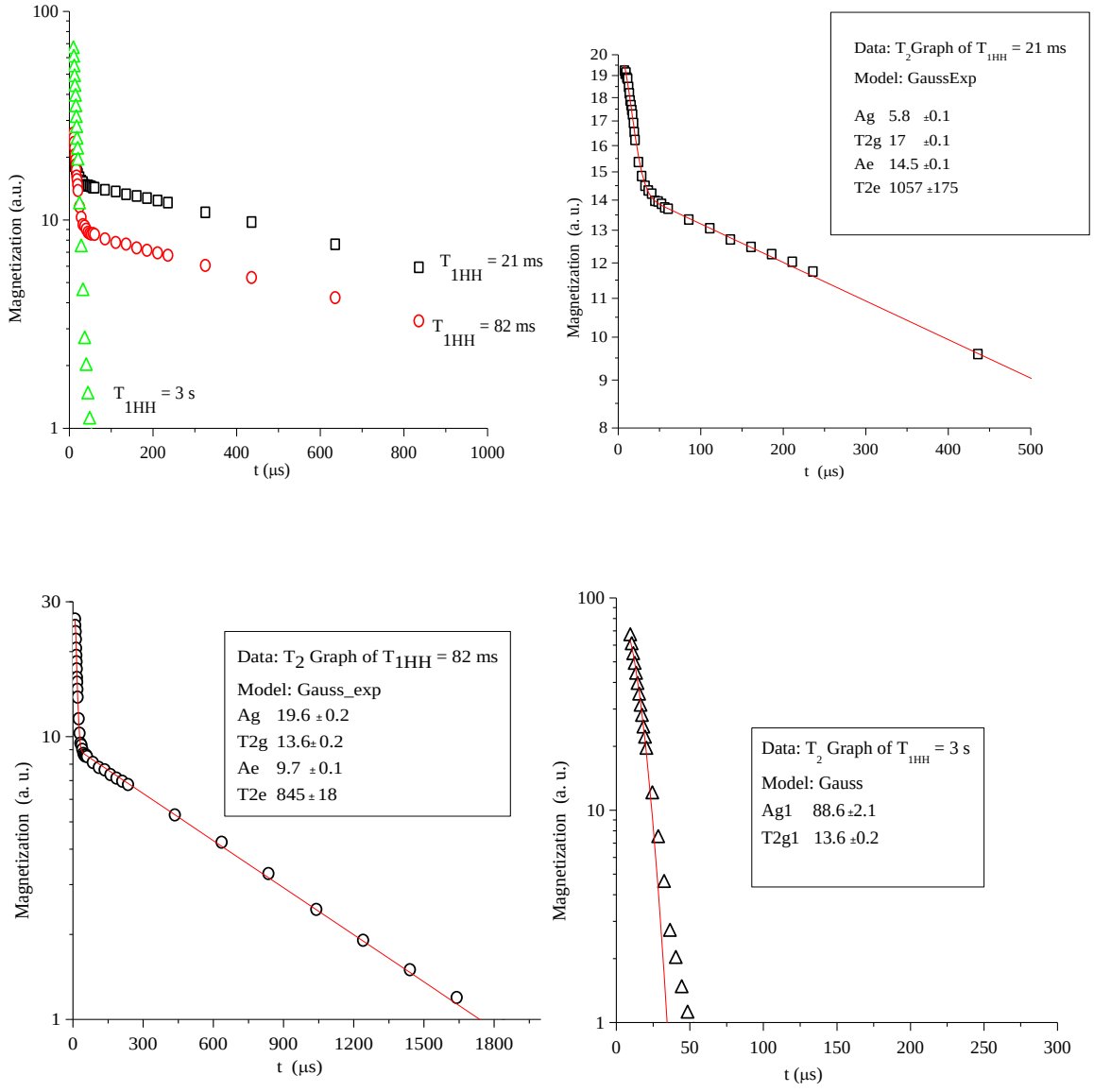

Figure C. 5 Reconstructed FID's from 2D-T_{HH} experiment in natural cartilage at -10°C with the best-fit line and associated best-fit parameters indicated for each separate, reconstructed FID.

C.6 Reconstructed FIDs from T_{SH} experiment natural cartilage at -10°C

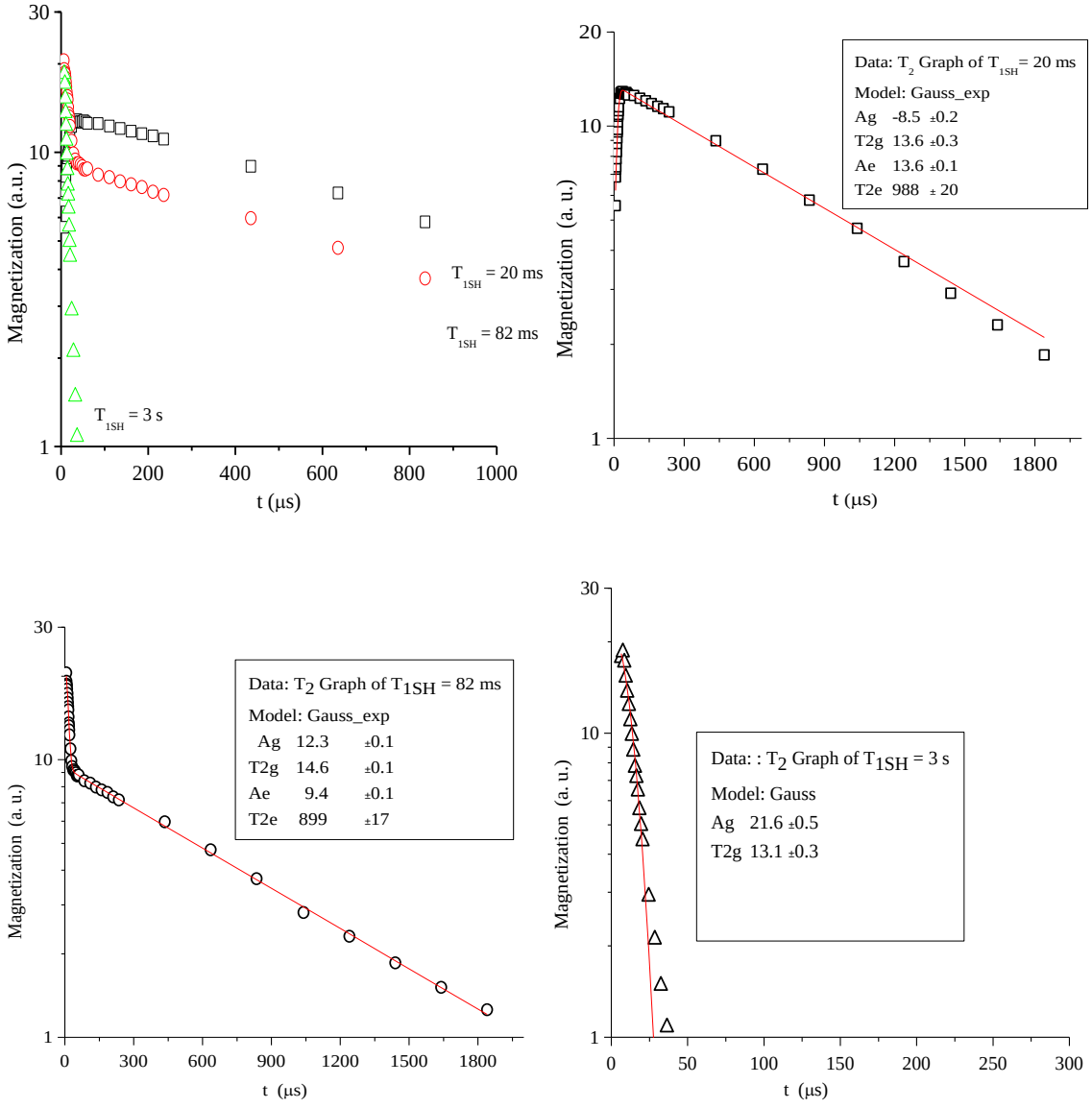

Figure C. 6 Reconstructed FID's from 2D-T_{1SH} experiment in natural cartilage at -10°C with the best-fit line and associated best-fit parameters indicated for each separate, reconstructed FID.

C.7 Reconstructed FIDs from $T_{1\rho}$ experiment in deuterated cartilage at 3°C

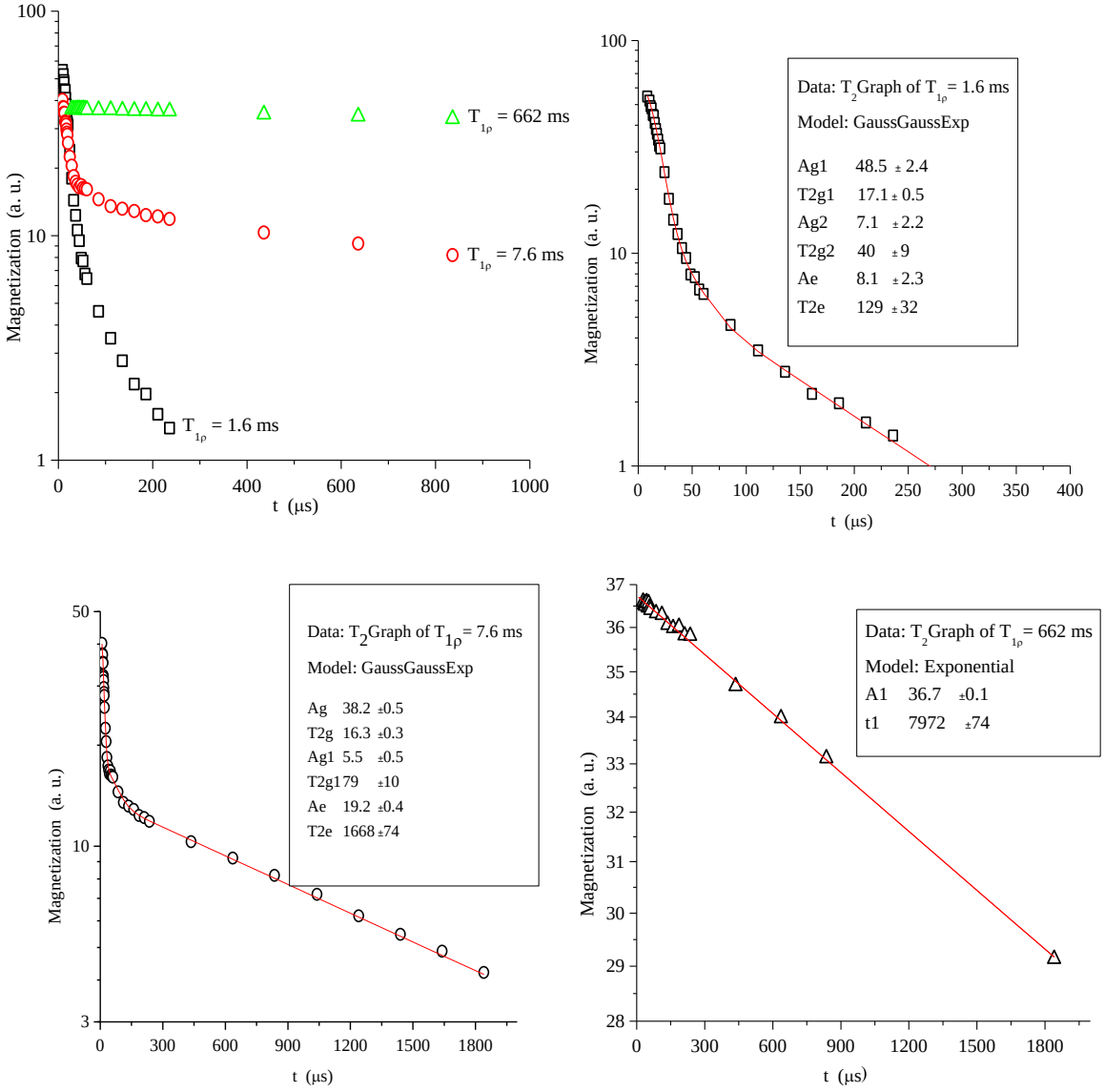

Figure C. 7 Reconstructed FID's from 2D-$T_{1\rho}$ experiment in deuterated cartilage at 3°C with the best-fit line and associated best-fit parameters indicated for each separate, reconstructed FID.

C.8 Reconstructed FIDs from T_{HH} experiment in deuterated cartilage at 3°C

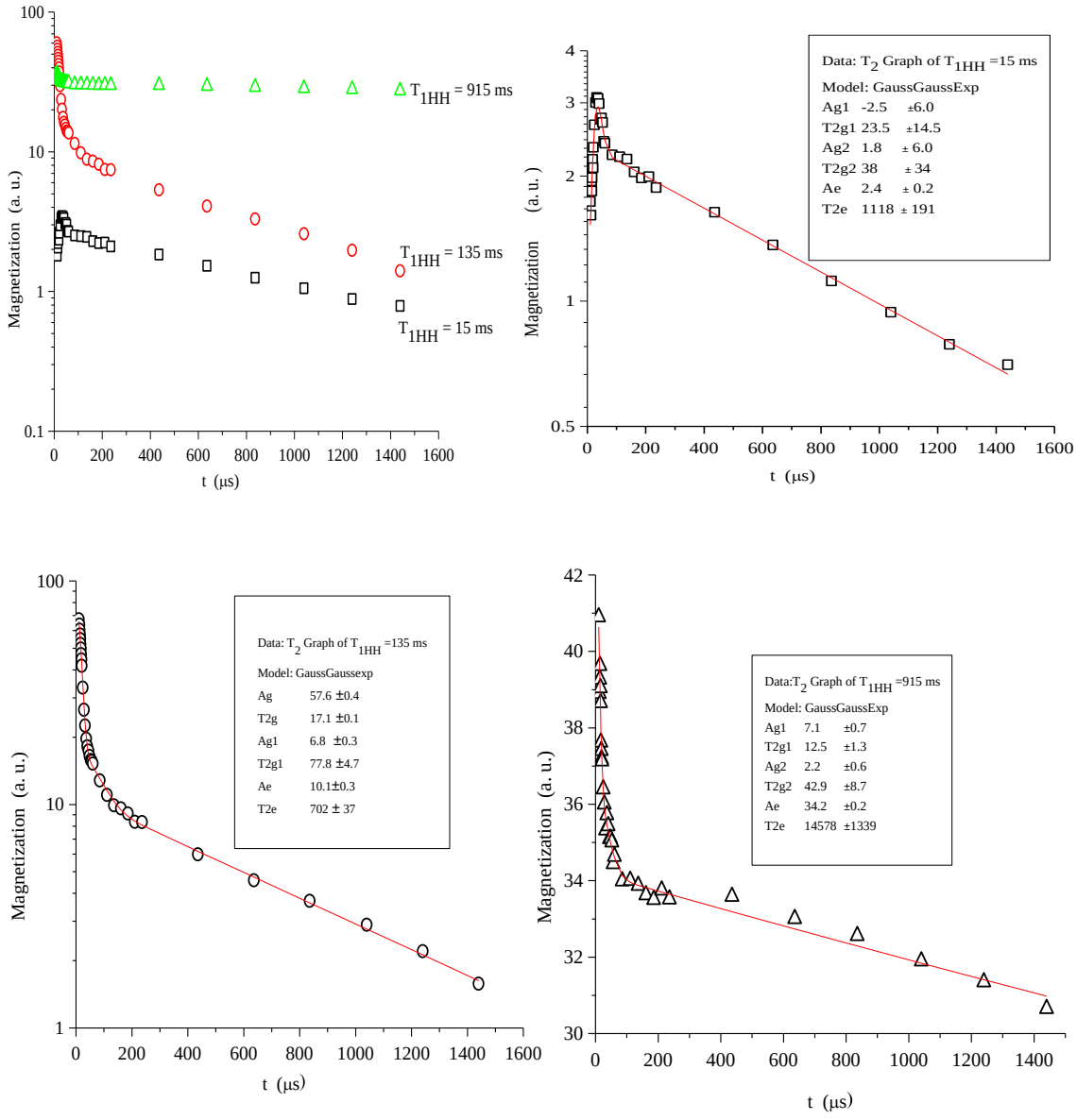

Figure C. 8 Reconstructed FID's from 2D-T_{HH} experiment in deuterated cartilage at 3°C with the best-fit line and associated best-fit parameters indicated for each separate, reconstructed FID.

C.9 Reconstructed FIDs from T_{SH} experiment in deuterated cartilage at 3°C

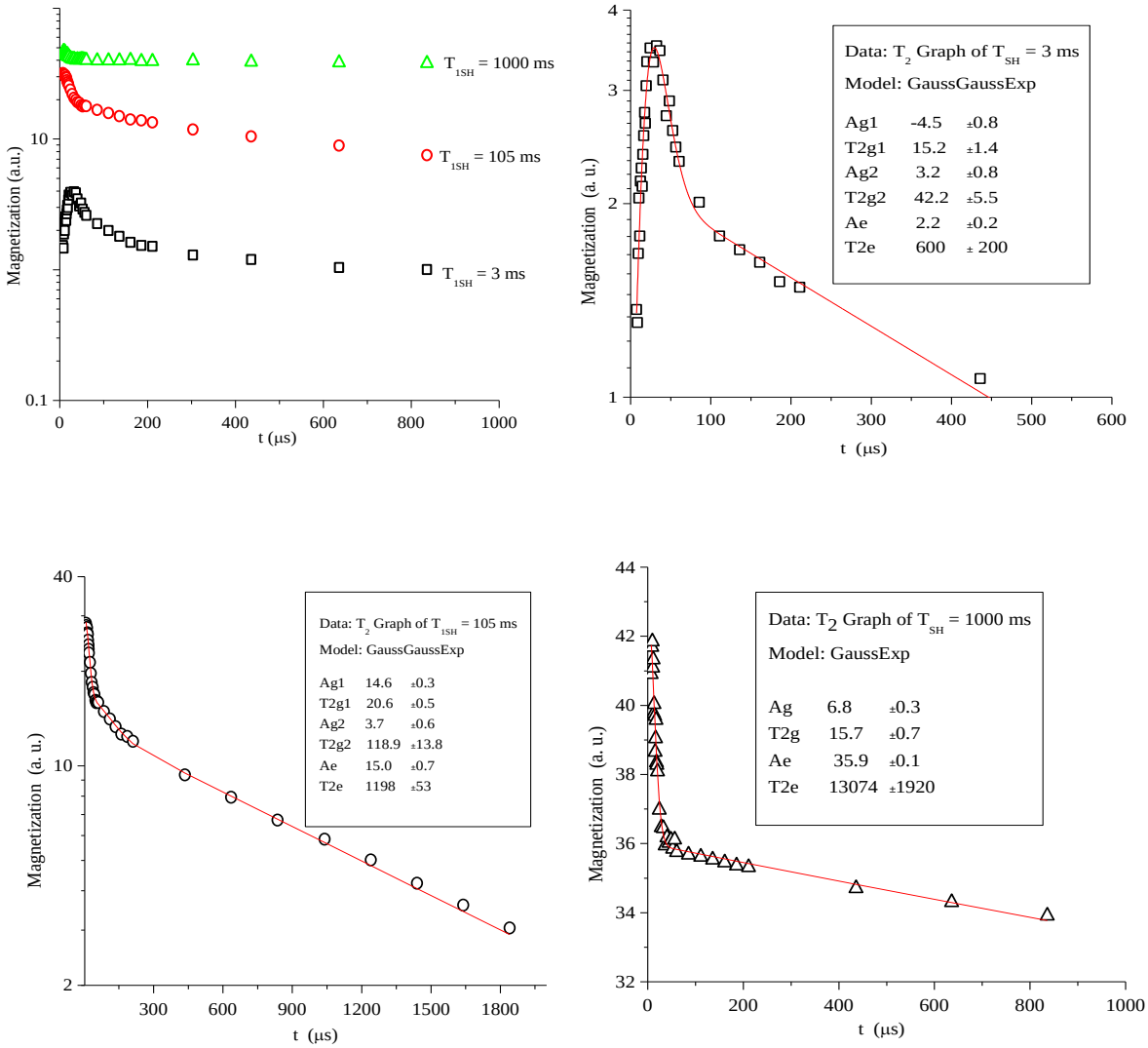

Figure C. 9 Reconstructed FID's from 2D-T_{SH} experiment in deuterated cartilage at 3°C with the best-fit line and associated best-fit parameters indicated for each separate, reconstructed FID.

C.10 Reconstructed FIDs from $T_{1\rho}$ experiment in deuterated cartilage at -10°C

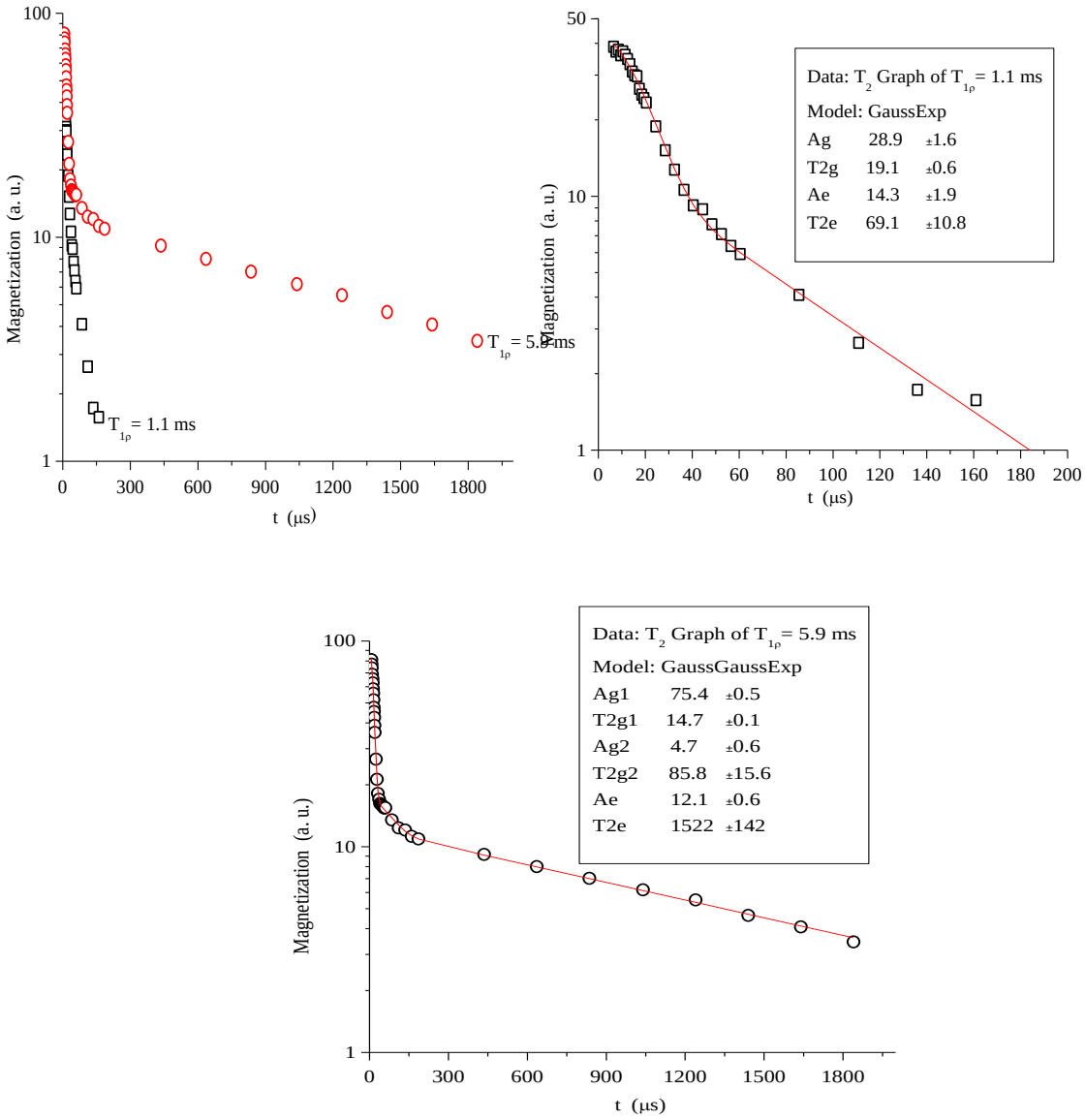

Figure C. 10 Reconstructed FID's from 2D-$T_{1\rho}$ experiment in deuterated cartilage at -10°C with the best-fit line and associated best-fit parameters indicated for each separate, reconstructed FID.

C.11 Reconstructed FIDs from T_{HH} experiment in deuterated cartilage at -10°C

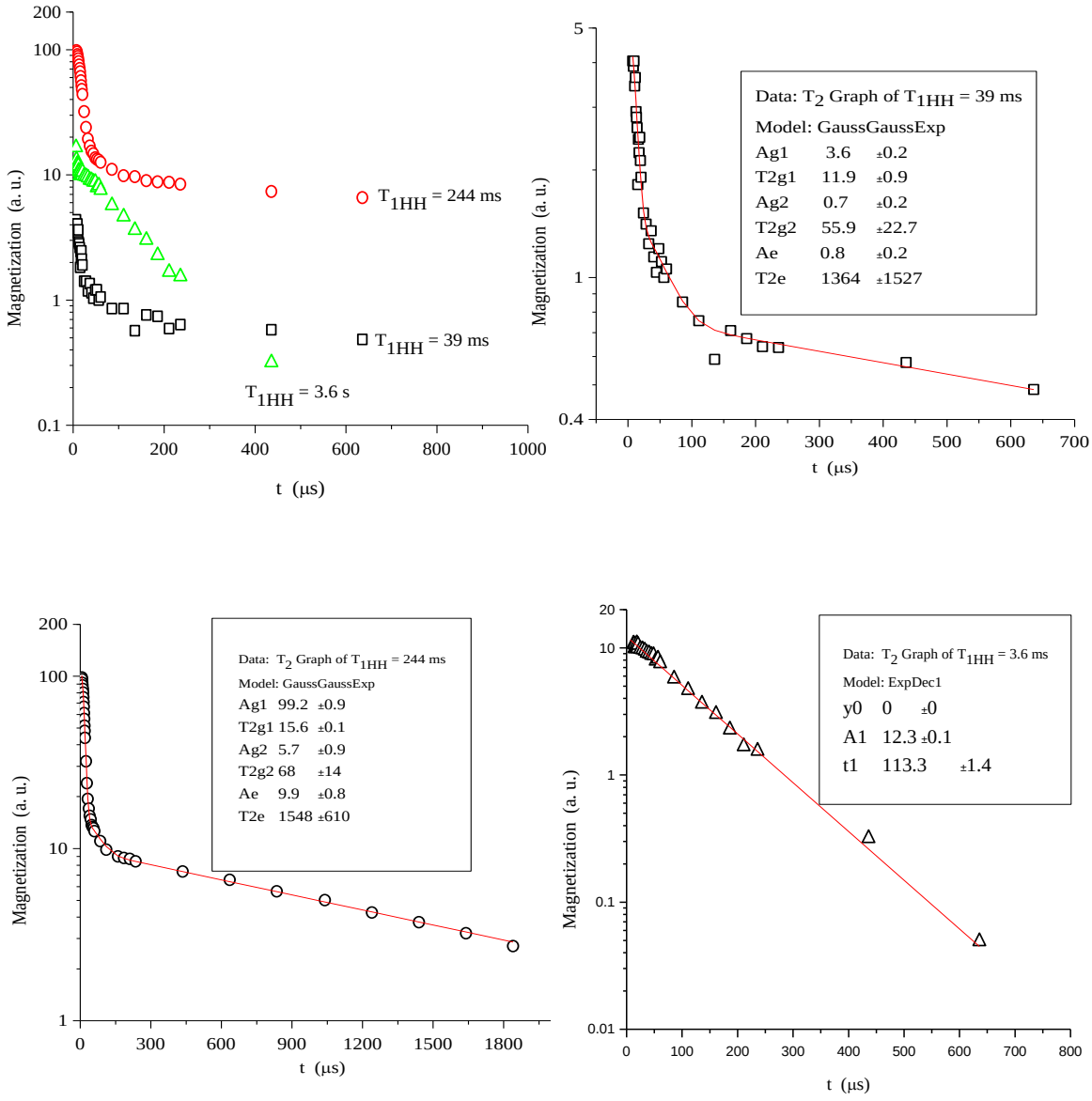

Figure C. 11 Reconstructed FID's from 2D-T_{HH} experiment in deuterated cartilage at -10°C with the best-fit line and associated best-fit parameters indicated for each separate, reconstructed FID.

C.12 Reconstructed FIDs from T_{SH} experiment in deuterated cartilage at -10°C

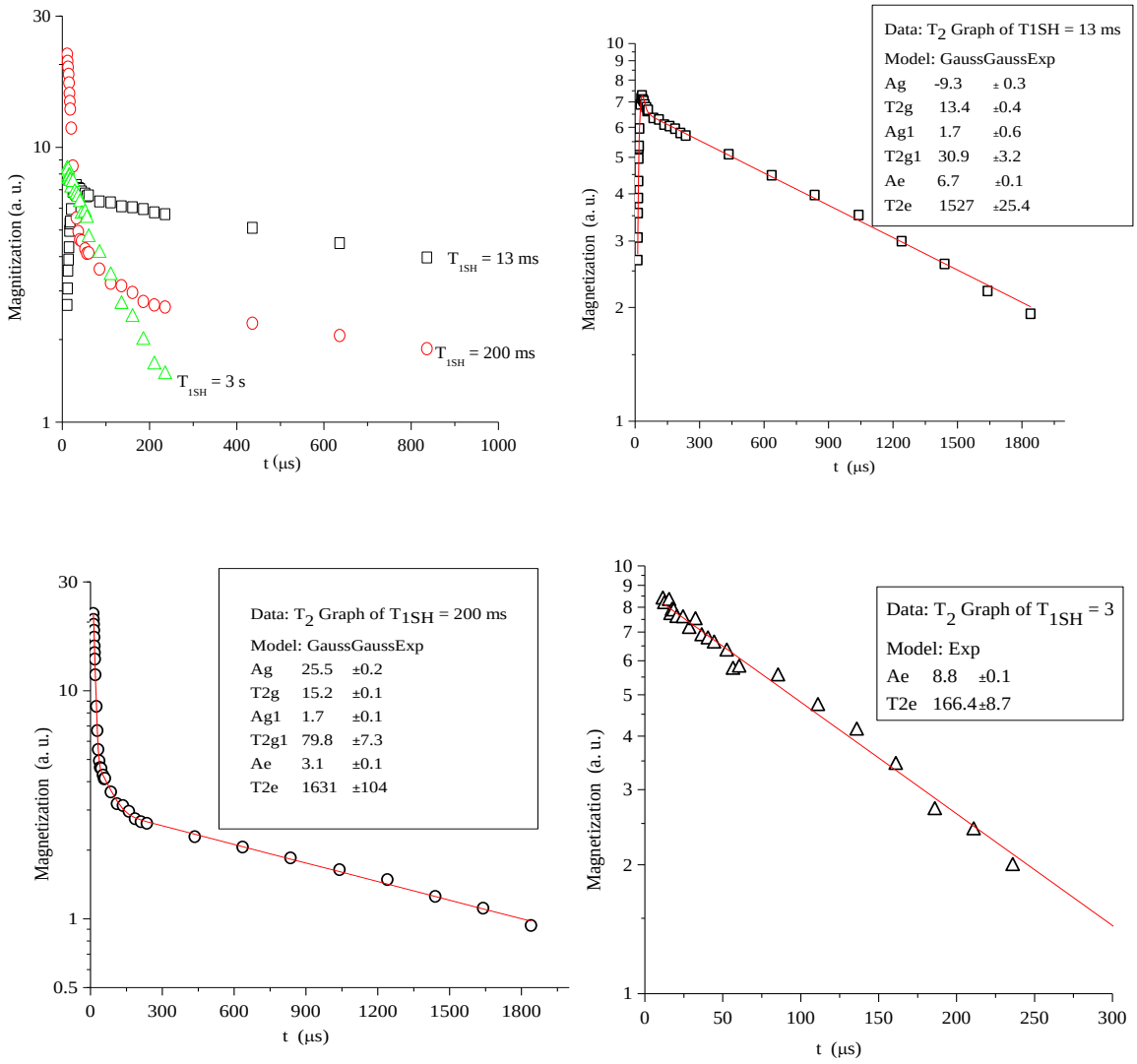

Figure C. 12 Reconstructed FID's from 2D-T_{HH} experiment in deuterated cartilage at -10°C with the best-fit line and associated best-fit parameters indicated for each separate, reconstructed FID.

Appendix D

Exchange Analysis Tables

In this Appendix all simulation tables for exchange analyses for natural and deuterated articular cartilage at 3°C and -10°C from section 5.2 are presented.

D.1 Natural Cartilage at 3°C

Table D. 1 Exchange analysis results from $T_{1\rho}$ experiment of natural cartilage at 3°C. The left table shows the experimental and calculated values for each parameter. The right table shows the rate values for exchange rates (k_{ij}), intrinsic times (T_x) and intrinsic reservoir sizes (P_x). Experimental relaxation times in brackets were not observed in this experiment, and were assigned the same values as the calculated/simulated relaxation time.

Parameter	Calculated	Experimental
T^{++}	1 ms	1 ms
T^{+-}	2.5 ms	(2) ms
T^{-+}	5.5 ms	7 ms
T^{--}	189 ms	189 ms
$(C_a+C_b)^{++}$	0	6.1 %
$(C_c+ C_d)^{++}$	0	0
$(C_a+C_b)^{+-}$	4.6 %	0
$(C_c+ C_d)^{+-}$	-0.6 %	0
$(C_a+C_b)^{-+}$	3.8 %	2.8 %
$(C_c+ C_d)^{-+}$	3.1 %	3%
$(C_a+C_b)^{--}$	0.4 %	0
$(C_c+ C_d)^{--}$	88.6 %	88.1%

Rates	Values
k_{ab}	30 s^{-1}
k_{bc}	8 s^{-1}
k_{cd}	0 s^{-1}
k_{ad}	1.5 s^{-1}
k_{ac}	400 s^{-1}
k_{bd}	28 s^{-1}
T_a	6 ms
T_b	3 ms
T_c	5.4 ms
T_d	300 ms
P_a	2.8 %
P_b	6.1 %
P_c	3 %
P_d	88.1 %

Table D. 2 Exchange analysis results from T_{1HH} experiment of natural cartilage at 3°C.The left table shows the experimental and calculated values for each parameter. The right table shows the rate values for exchange rates (k_{ij}), intrinsic times (T_x) and intrinsic reservoir sizes (P_x). Experimental relaxation times in brackets were not observed in this experiment, and were assigned the same values as the calculated/simulated relaxation time.

Parameter	Calculated	Experimental
T^{++}	1.5 ms	(3) ms
T^{+-}	15 ms	(12) ms
T^{-+}	47 ms	42 ms
T^{--}	466 ms	466 ms
$(C_a+C_b)^{++}$	0	0
$(C_c+ C_d)^{++}$	0	0
$(C_a+C_b)^{+-}$	-0.2 %	0
$(C_c+ C_d)^{+-}$	0.1 %	0
$(C_a+C_b)^{-+}$	2.3 %	3 %
$(C_c+ C_d)^{-+}$	0.4 %	0
$(C_a+C_b)^{--}$	6.8 %	4 %
$(C_c+ C_d)^{--}$	90.5 %	93 %

Rates	Values
k_{ab}	30 s^{-1}
k_{bc}	8 s^{-1}
k_{cd}	0
k_{ad}	1.5 s^{-1}
k_{ac}	400 s^{-1}
k_{bd}	28 s^{-1}
T_a	400 ms
T_b	500 ms
T_c	50 ms
T_d	488 ms
P_a	2.8 %
P_b	6.1 %
P_c	3 %
P_d	88.1 %

Table D. 3 Exchange analysis results from T_{1SH} experiment of natural cartilage at 3°C.The left table shows the expermintal and calculated values for each parameter. The right table shows the rate values for exhange rates (k_{ij}), intrinsic times (T_x) and intrinsic resirvoir sizes (P_x). Experimental relaxation times in brackets were not observed in this experiment, and were assigned the same values as the calculated/simulated relaxation time.

Parameter	Calculated	Experimental
T^{++}	2 ms	(3) ms
T^{+-}	15 ms	(12) ms
T^{-+}	47 ms	42 ms
T^{--}	465 ms	466 ms
$(C_a+C_b)^{++}$	-0.7 %	0
$(C_c+ C_d)^{++}$	0.7 %	0
$(C_a+C_b)^{+-}$	-1.5 %	0
$(C_c+ C_d)^{+-}$	1.6 %	0
$(C_a+C_b)^{-+}$	-2 %	-4 %
$(C_c+ C_d)^{-+}$	2.7%	4 %
$(C_a+C_b)^{--}$	6.9 %	6 %
$(C_c+ C_d)^{--}$	92 %	94 %

Rates	Values
k_{ab}	30 s^{-1}
k_{bc}	8 s^{-1}
k_{cd}	0
k_{ad}	1.5 s^{-1}
k_{ac}	400 s^{-1}
k_{bd}	28 s^{-1}
T_a	375 s^{-1}
T_b	500 s^{-1}
T_c	50 s^{-1}
T_d	488 s^{-1}
P_a	2.8 %
P_b	6.1 %
P_c	3 %
P_d	88.1 %

D.2 Natural Cartilage at -10°C

Table D. 4 Exchange analysis results from $T_{1\rho}$ experiment of natural cartilage at -10°C. The left table shows the expermintal and calculated values for each parameter. The right table shows the rate values for exhange rates (k_{ij}), intrinsic times (T_x) and intrinsic resirvoir sizes (P_x). Experimental relaxation times in brackets were not observed in this experiment, and were assigned the same values as the calculated/simulated relaxation time.

Parameter	Calculated	Experimental
T^{++}	0.7 ms	(1) ms
T^{+-}	1.8 ms	1.7 ms
T^{-+}	2 ms	(3) ms
T^{--}	3.4 ms	3.8 ms
$(C_a+C_b)^{++}$	4.5 %	0
$(C_c+ C_d)^{++}$	-3.3 %	0
$(C_a+C_b)^{+-}$	3 %	14 %
$(C_c+ C_d)^{+-}$	20 %	18.8 %
$(C_a+C_b)^{-+}$	-2.3 %	0
$(C_c+ C_d)^{-+}$	3.3 %	0
$(C_a+C_b)^{--}$	35 %	26.6 %
$(C_c+ C_d)^{--}$	39 %	40.6 %

Rates	Values
k_{ab}	60 s^{-1}
k_{bc}	56 s^{-1}
k_{cd}	0
k_{ad}	80 s^{-1}
k_{ac}	400 s^{-1}
k_{bd}	0
T_a	2.3 ms
T_b	3.5 ms
T_c	16 ms
T_d	2 ms
P_a	26.6 %
P_b	14 %
P_c	18.8 %
P_d	40.6 %

Table D. 5 Exchange analysis results from T_{1HH} experiment of natural cartilage at -10°C. The left table shows the experimental and calculated values for each parameter. The right table shows the rate values for exchange rates (k_{ij}), intrinsic times (T_x) and intrinsic reservoirs sizes(P_x). Experimental relaxation times in brackets were not observed in this experiment, and were assigned the same values as the calculated/simulated relaxation time.

Parameter	Calculated	Experimental
T^{++}	0.9 ms	(1.5) ms
T^{+-}	2 ms	(3) ms
T^{-+}	18 ms	20 ms
T^{--}	83.6 ms	82 ms
$(C_a+C_b)^{++}$	-0.1 %	0
$(C_c+ C_d)^{++}$	0.1 %	0
$(C_a+C_b)^{+-}$	0	0
$(C_c+ C_d)^{+-}$	0	0
$(C_a+C_b)^{-+}$	-5 %	4.7 %
$(C_c+ C_d)^{-+}$	13 %	17.3 %
$(C_a+C_b)^{--}$	46 %	44 %
$(C_c+ C_d)^{--}$	41 %	34 %

Rates	Values
k_{ab}	130 s^{-1}
k_{bc}	46 s^{-1}
k_{cd}	0
k_{ad}	30 s^{-1}
k_{ac}	400 s^{-1}
k_{bd}	0
T_a	375 ms
T_b	570 ms
T_c	75 ms
T_d	34 ms
P_a	26.6 %
P_b	14 %
P_c	18.8 %
P_d	40.6 %

Table D. 6 Exchange analysis results from T_{1SH} experiment of natural cartilage at -10^{o}C.The left table shows the expermintal and calculated values for each parameter. The right table shows the rate values for exhange rates (k_{ij}), intrinsic times (T_x) and intrinsic resirvoir sizes (P_x). Experimental relaxation times in brackets were not observed in this experiment, and were assigned the same values as the calculated/simulated relaxation time.

Parameter	Calculated	Experimental
T^{++}	0.9 ms	(1.5) ms
T^{+-}	2.8 ms	(3) ms
T^{-+}	18 ms	20 ms
T^{--}	83 ms	82 ms
$(C_a+C_b)^{++}$	-7 %	0
$(C_c+ C_d)^{++}$	7.5 %	0
$(C_a+C_b)^{+-}$	-2 %	0
$(C_c+ C_d)^{+-}$	2 %	0
$(C_a+C_b)^{-+}$	-14 %	-26 %
$(C_c+ C_d)^{-+}$	31 %	50 %
$(C_a+C_b)^{--}$	41.4 %	42.1 %
$(C_c+ C_d)^{--}$	41 %	33 %

Rates	Values
k_{ab}	130 s^{-1}
k_{bc}	46 s^{-1}
k_{cd}	0
k_{ad}	30 s^{-1}
k_{ac}	400 s^{-1}
k_{bd}	0
T_a	375 ms
T_b	570 ms
T_c	74 ms
T_d	35 ms
P_a	26.6 %
P_b	14 %
P_c	18.8 %
P_d	40.6 %

D.3 Deuterated Cartilage at 3°C

Table D. 7 Exchange analysis results from $T_{1\rho}$ experiment of deuterated cartilage at 3°C. The left table shows the experimental and calculated values for each parameter. The right table shows the rate values for exchange rates (k_{ij}), intrinsic times (T_x) and intrinsic reservoirs sizes (P_x). Experimental relaxation times in brackets were not observed in this experiment, and were assigned the same values as the calculated/simulated relaxation time.

Parameter	Calculated	Experimental
T^{++}	0.7 ms	(1) ms
T^{+-}	2 ms	1.6 ms
T^{-+}	7.7 ms	7.6 ms
T^{--}	517 ms	660 ms
$(C_a+C_b)^{++}$	0.3 %	0
C_c^{++}	-0.3 %	0
C_d^{++}	0	0
$(C_a+C_b)^{+-}$	41.2 %	44.4 %
C_c^{+-}	-0.7 %	-0.6 %
C_d^{+-}	0	0
$(C_a+C_b)^{-+}$	23.9 %	18.8 %
C_c^{-+}	10.5 %	11.1 %
C_d^{-+}	0	0
$(C_a+C_b)^{--}$	0	0
C_c^{--}	0	0
C_d^{--}	25.1 %	25.5 %

Rates	Values
k_{ab}	30 s^{-1}
k_{bc}	0
k_{cd}	0
k_{ad}	0.5 s^{-1}
k_{ac}	400 s^{-1}
k_{bd}	0
T_a	7.3 ms
T_b	2 ms
T_c	19.8 ms
T_d	666 ms
P_a	21.7 %
P_b	43.9 %
P_c	9.4 %
P_d	25 %

Table D. 8 Exchange analysis results from T_{1HH} experiment of deuterated cartilage at 3°C. The left table shows the experimental and calculated values for each parameter. The right table shows the rate values for exchange rates (k_{ij}), intrinsic times (T_x) and intrinsic reservoirs sizes (P_x). Experimental relaxation times in brackets were not observed in this experiment, and were assigned the same values as the calculated/simulated relaxation time.

Parameter	Calculated	Experimental
T^{++}	1 ms	(3) ms
T^{+-}	15 ms	15 ms
T^{-+}	195 ms	135 ms
T^{--}	915 ms	915 ms
$(C_a+C_b)^{++}$	-0.1 %	0
C_c^{++}	0.1 %	0
C_d^{++}	0	0
$(C_a+C_b)^{+-}$	-0.4 %	-2 %
C_c^{+-}	1 %	3.3 %
C_d^{+-}	0	0
$(C_a+C_b)^{-+}$	63 %	55.5 %
C_c^{-+}	8.2 %	8.9 %
C_d^{-+}	-2.4 %	0
$(C_a+C_b)^{--}$	2.4 %	6.7 %
C_c^{--}	0.3 %	0
C_d^{--}	27.4 %	28 %

Rates	Values
k_{ab}	30 s^{-1}
k_{bc}	0
k_{cd}	0
k_{ad}	0.5 s^{-1}
k_{ac}	400 s^{-1}
k_{bd}	0
T_a	335 ms
T_b	475 ms
T_c	40 ms
T_d	1500 ms
P_a	21.7 %
P_b	43.9 %
P_c	9.4 %
P_d	25 %

Table D. 9 Exchange analysis results from T_{1SH} experiment of deuterated cartilage at 3°C.The left table shows the experimental and calculated values for each parameter. The right table shows the rate values for exchange rates (k_{ij}), intrinsic times (T_x) and intrinsic reservoirs sizes (P_x). Experimental relaxation times in brackets were not observed in this experiment, and were assigned the same values as the calculated/simulated relaxation time.

Parameter	Calculated	Experimental
T^{++}	1 ms	3 ms
T^{+-}	15 ms	(15) ms
T^{-+}	196 ms	105 ms
T^{--}	1000 ms	1000 ms
$(C_a+C_b)^{++}$	-6 %	-5 %
C_c^{++}	6 %	4.9 %
C_d^{++}	0	0
$(C_a+C_b)^{+-}$	-1 %	0
C_c^{+-}	2 %	0
C_d^{+-}	0	0
$(C_a+C_b)^{-+}$	40 %	22.5 %
C_c^{-+}	5 %	8.9 %
C_d^{-+}	-1.5 %	0
$(C_a+C_b)^{--}$	4.5 %	9.2 %
C_c^{--}	0.6 %	0
C_d^{--}	49.4 %	49 %

Rates	Values
k_{ab}	30 s^{-1}
k_{bc}	0
k_{cd}	0
k_{ad}	0.5 s^{-1}
k_{ac}	400 s^{-1}
k_{bd}	0
T_a	335 ms
T_b	475 ms
T_c	40 ms
T_d	1723 ms
P_a	21.7 %
P_b	43.9 %
P_c	9.4 %
P_d	25 %

D.4 Deuterated Cartilage at -10°C

Table D. 10 Exchange analysis results from $T_{1\rho}$ experiment of deuterated cartilage at -10°C. The left table shows the experimental and calculated values for each parameter. The right table shows the rate values for exchange rates (k_{ij}), intrinsic times (T_x) and intrinsic reservoirs sizes (P_x). Experimental relaxation times in brackets were not observed in this experiment, and were assigned the same values as the calculated/simulated relaxation time.

Parameter	Calculated	Experimental
T^+	1.2 ms	(1) ms
T^0	1.8 ms	1.1 ms
T^-	5.7 ms	5.9 ms
$(C_a+C_b)^+$	2.6 %	0
C_c^+	-2.2 %	0
$(C_a+C_b)^0$	22 %	24.6 %
C_c^0	-11 %	0
$(C_a+C_b)^-$	63.1 %	65.5 %
C_c^-	15 %	9.9 %

Rates	Values
k_{ab}	30 s^{-1}
k_{bc}	40 s^{-1}
k_{ca}	400 s^{-1}
T_a	7 ms
T_b	3.5 ms
T_c	20 ms
P_a	29 %
P_b	58.5 %
P_c	12.5 %

Table D. 11 Exchange analysis results from T_{1HH} experiment of deuterated cartilage at -10°C. The left table shows the experimental and calculated values for each parameter. The right table shows the rate values for exchange rates (k_{ij}), intrinsic times (T_x) and intrinsic reservoirs sizes (P_x). Experimental relaxation times in brackets were not observed in this experiment, and were assigned the same values as the calculated/simulated relaxation time.

Parameter	Calculated	Experimental
T^+	7 ms	(13) ms
T^0	24 ms	39 ms
T^-	233 ms	244 ms
$(C_a+C_b)^+$	-0.2 %	0
C_c^+	0.2 %	0
$(C_a+C_b)^0$	-0.6 %	3 %
C_c^0	1.2 %	1.1 %
$(C_a+C_b)^-$	88.4 %	79.3 %
C_c^-	10.9 %	8.8 %

Rates	Values
k_{ab}	30 s^{-1}
k_{bc}	40 s^{-1}
k_{ca}	400 s^{-1}
T_a	370 ms
T_b	500 ms
T_c	50 ms
P_a	29 %
P_b	58.5 %
P_c	12.5 %

Table D. 12 Exchange analysis results from T_{1SH} experiment of deuterated cartilage at -10^{o}C. The left table shows the experimental and calculated values for each parameter. The right table shows the rate values for exchange rates (k_{ij}), intrinsic times (T_x) and intrinsic reservoirs sizes (P_x) Experimental relaxation times in brackets were not observed in this experiment, and were assigned the same values as the calculated/simulated relaxation time.

Parameter	Calculated	Experimental
T^+	8 ms	13 ms
T^0	24 ms	(39) ms
T^-	241 ms	244 ms
$(C_a+C_b)^+$	-12 %	-26.7 %
C_c^+	12 %	23.5 %
$(C_a+C_b)^0$	-2 %	0
C_c^0	4 %	0
$(C_a+C_b)^-$	86.5 %	92.8 %
C_c^-	10.6 %	10.4 %

Rates	Values
k_{ab}	30 s^{-1}
k_{bc}	40 s^{-1}
k_{ca}	400 s^{-1}
T_a	400 ms
T_b	500 ms
T_c	50 ms
P_a	29 %
P_b	58.5 %
P_c	12.5 %

Glossary of Terms

AC : Articular Cartilage

B_0 : External magnetic field

BSA : Bovine Serum Albumin

BBP : Bloembergen, Purcell and Pound

C^+ : Apparent magnetization fraction for the short relaxation time component

C^- : Apparent magnetization fraction for the long relaxation time component

CPMG: Carr-Purcell-Meiboom-Gill sequence for T_2 measurements

CS : Chondroitin Sulfate

CSI : Chemical Shift Imaging

D_2O : Deuterium oxide (heavy water)

DMMB: Dimethylmethyene blue

GAG : Glycosaminoglycans

FID : Free Induction Decay

$F^{(q)}(x(t))$: spin lattice interaction function

$\mathcal{H}$: Hamiltonian

HA : Hyaluronic Acid

$\mathcal{H}_D$: Dipole-dipole interaction Hamiltonian

$\mathcal{H}_{CS}$ **:** Chemical shift interaction Hamiltonian

$\mathcal{H}_{J}$ **:** J coupling Hamiltonian

$\mathcal{H}_{Z}$ **:** Zeeman interaction Hamiltonian

I **:** Nuclear Spin angular momentum operator

$J^{|q|}(|q|\omega)$**:** Spectral density function

$\mathbf{k_{ij}}$ **:** Magnetization exchange rate from site *i* to site *j*

KEL-F: Kellogg and Fluoropolymer, $(C_2ClF_3)_n$

KS **:** Keratin Sulfate

λ^+ **:** Apparent relaxation rate for short relaxation time component

λ^- **:** Apparent relaxation rate for long relaxation time component

M **:** Net magnetization vector

MAS : Magic Angle Spinning

$\mathbf{m_i(\tau)}$**:** The reduced magnetization of the i^{th} site at time τ

MRI : Magnetic Resonance Imagining

NMR: Nuclear Magnetic Resonance

OA **:** Osteoarthritis

OD **:** Optical Density

PBS **:** Phosphate Buffer Saline

PG : Proteoglycan

T_1 : Spin-lattice relaxation time

T_{1HH} : Spin-lattice relaxation measured with non-selective excitation pulse sequence

$T_{1\rho}$: Spin-lattice relaxation time in the rotating frame

T_{1SH} : Spin-lattice relaxation time measured with selective excitation pulse sequence

T_2 FID: Spin-spin relaxation time from FID experiment using single 90^o pulse excitation

T_2^* : T_2 obtained using the T_2 FID pulse sequence, but where the measured T_2 is significantly shortened, relative to the true sample T_2, due to inhomogeneities in the external magnetic field

T_2 CPMG: Spin-spin relaxation time measured using the CPMG train sequence

2D-TD: Two dimensional time domain

TMJ : Temporomandibular joint

τ : Correlation time

μ : Nuclear dipole magnetic moment

ω_o : Larmor Frequency

References

[1] M.A.R. Freeman, *Adult articular cartilage*, Pitman Medical, Tunbridge Wells, England.1979.

[2] M. Venn and A. Maroudas, "Chemical composition and swelling of normal and osteoarthrotic femoral head cartilage. I. Chemical composition", *Annals of the Rheumatic Diseases*, **36**, (2) 1977, pp. 121-129.

[3] P. Torzilli, K. Takebe, A. Burstein, J. Zika, and K. Heiple, "The material properties of immature bone", *Journal of Biomechanical Engineering*, **104**, (1) 1982, pp. 12-20.

[4] P.A. Torzilli, J.M. Arduino, J.D. Gregory, and M. Bansal, "Effect of proteoglycan removal on solute mobility in articular cartilage", *Journal of Biomechanics*, **30**, (9) 1997, pp. 895-902.

[5] A. Abragam, *The Principles of Nuclear Magnetism*, Clarendon Press, Oxford.1962.

[6] C.P. Slichter, *Principles of magnetic resonance*, Springer-Verlag, Berlin.1990.

[7] U. Haeberlen, *High resolution NMR spectroscopy in solids*, Max-Planck-Institut für Medizinische Forschung, Heidelberg, Germany.1976.

[8] E. Fukushima and S.B. Roeder, *Experimental pulse NMR: a nuts and bolts approach*, Addison-Wesley, Reading, MA.1981.

[9] G.P. Jones, "Spin-lattice relaxation in the rotating frame: weak-collision case", *Physical Review*, **148**, (1) 1966, pp. 332.

[10] N. Bloembergen, E.M. Purcell, and R.V. Pound, "Relaxation effects in nuclear magnetic resonance absorption", *Physical Review*, **73**, (7) 1948, pp. 679-712.

[11] E. Stejskal and J.D. Memory, *High resolution NMR in the solid state: fundamentals of CP/MAS*, Cambridge University Press, .1994.

[12] H. Peemoeller, "NMR spin grouping", *Bulletin of Magnetic Resonance*, **11**, (1/2) 1989, pp. 19-30.

[13] J. Zimmerman and W.E. Brittin, "Nuclear magnetic resonance studies in multiple phase systems: lifetime of a water molecule in an adsorbing phase on silica gel", *The Journal of Physical Chemistry*, **61**, (10) 1957, pp. 1328-1333.

[14] S.H. Koenig, "Molecular basis of magnetic relaxation of water protons of tissue", *Academic Radiology*, **3**, (7) 1996, pp. 597-606.

[15] S.H. Koenig and R.D. Brown III, "A molecular theory of relaxation and magnetization transfer: Application to cross-linked BSA, a model for tissue", *Magnetic Resonance in Medicine*, **30**, (6) 1993, pp. 685-695.

[16] H.T. Edzes and E.T. Samulski, "The measurement of cross- relaxation effects in the proton NMR spin- lattice relaxation of water in biological systems: Hydrated collagen and muscle", *Journal of Magnetic Resonance*, **31**, (2) 1978, pp. 207-229.

[17] R.R. Ernst, *Principles of nuclear magnetic resonance in one and two dimensions*, Clarendon Press, Oxford.1987.

[18] M.J. Hinek, *2D time domain NMR study of wood*, University of Waterloo, Waterloo.1997.

[19] D.A. Oleskevich, N. Ghahramany, W.P. Weglarz, and H. Peemoeller, "Interfacial Spin–Spin Coupling in Wood by 2D Time-Domain NMR", *Journal of Magnetic Resonance, Series B*, **113**, (1) 1996, pp. 1-8.

[20] W.T. Vetterling, S.A. Teukolsky, and W.H. Press, *Numerical recipes: example book C (The Art of Scientific Computing)*, Press Syndicate of the University of Cambridge, 1992.

[21] E. Andrew, A. Bradbury, and R. Eades, "Nuclear magnetic resonance spectra from a crystal rotated at high speed", *Nature*, **182**, (4650) 1958, pp. 1659.

[22] I. Lowe, "Free induction decays of rotating solids", *Physical Review Letters*, **2**, (7) 1959, pp. 285.

[23] T.R. Brown, B.M. Kincaid, and K. Ugurbil, "NMR chemical shift imaging in three dimensions", *Proceedings of the National Academy of Sciences of the United States of America*, **79**, (11) 1982, pp. 3523-3526.

[24] C. Malveau, B. Diter, P. Tekely, and D. Canet, "Chemical shift imaging in rotating solids by radiofrequency field gradients", *Journal of Magnetic Resonance*, **134**, (1) 1998, pp. 171-175.

[25] E. Adalsteinsson, J. Star-Lack, C.H. Meyer, and D.M. Spielman, "Reduced spatial side lobes in chemical-shift imaging", *Magnetic Resonance in Medicine*, **42**, (2) 1999, pp. 314-323.

[26] P. Sajda, S. Du, T.R. Brown, R. Stoyanova, D.C. Shungu, X. Mao, and L.C. Parra, "Nonnegative matrix factorization for rapid recovery of constituent spectra in magnetic resonance chemical shift imaging of the brain", *IEEE Transactions on Medical Imaging*, **23**, (12) 2004, pp. 1453-1465.

[27] V.C. Mow, A. Ratcliffe, and A.R. Poole, "Cartilage and diarthrodial joints as paradigms for hierarchical materials and structures", *Biomaterials*, **13**, (2) 1992, pp. 67-97.

[28] R. Stockwell, G. Meachim, and M. Freeman, *Adult articular cartilage*, Pitman Medical, Kent, England.1979.

[29] D. Huster, L. Naji, J. Schiller, and K. Arnold, "Dynamics of the biopolymers in articular cartilage studied by magic angle spinning NMR", *Applied Magnetic Resonance*, **27**, (3-4) 2004, pp. 471-487.

[30] A.L. Mescher, *Junqueira's basic histology: text & atlas*, McGraw-Hill Medical, New York.2010.

[31] N.T. Colburn, *Review of Rheumatology*, Springer Science & Business Media, .2011.

[32] G.N. Ramachandran, *Treatise on collagen*, Academic Press, New York.1967.

[33] V.C. Hascall and J.H. Kimura, "Proteoglycans: isolation and characterization", *Methods in enzymology*, **82 Pt A**, 1982, pp. 769-800.

[34] M. Paulsson and D. Heinegard, "Noncollagenous cartilage proteins current status of an emerging research field", *Collagen and related research*, **4**, (3) 1984, pp. 219-229.

[35] D. Evered and J. Whelan, *Functions of the Proteoglycans*, Wiley, .1986.

[36] J.R. Hassell, J.H. Kimura, and V.C. Hascall, "Proteoglycan core protein families", *Annual Review of Biochemistry*, **55**, (1) 1986, pp. 539-567.

[37] K.E. Kuettner, R. Schleyerbach, and V.C. Hascall, *Articular cartilage biochemistry*, Raven Press, New York.1986.

[38] D. Heinegård and M. Paulsson, "Cartilage", *Methods in enzymology*, **145**, 1987, pp. 336-363.

[39] T.C. Laurent and J.R.E. Fraser, "The properties and turnover of hyaluronan", *Functions of the Proteoglycans,* **124**, 1986, pp. 9-29.

[40] M.T. Bayliss, M. Venn, A. Maroudas, and S.Y. Ali, "Structure of proteoglycans from different layers of human articular cartilage", *The Biochemical journal,* **209**, (2) 1983, pp. 387-400.

[41] H. Muir, S. Carney, and L. Hall, "Effects of tiaprofenic acid and other NSAIDs on proteoglycan metabolism in articular cartilage explants", *Drugs,* **35**, (1) 1988, pp. 15-23.

[42] P.J. Roughley and E.R. Lee, "Cartilage proteoglycans: structure and potential functions", *Microscopy Research and Technique,* **28**, (5) 1994, pp. 385-397.

[43] B. Schmitt, Š Zbýň, D. Stelzeneder, V. Jellus, D. Paul, L. Lauer, P. Bachert, and S. Trattnig, "Cartilage quality assessment by using glycosaminoglycan chemical exchange saturation transfer and 23Na MR imaging at 7 T", *Radiology,* **260**, (1) 2011, pp. 257-264.

[44] S.L. Carney and H. Muir, "The structure and function of cartilage proteoglycans", *Physiological Reviews,* **68**, (3) 1988, pp. 858-910.

[45] V.C. Mow, M.H. Holmes, and W.M. Lai, "Fluid transport and mechanical properties of articular cartilage: a review", *Journal of Biomechanics,* **17**, (5) 1984, pp. 377-394.

[46] T.E. Hardingham, A.J. Fosang, and J. Dudhia, "Domain structure in aggregating proteoglycans from cartilage", *Biochemical Society Transactions,* **18**, (5) 1990, pp. 794-796.

[47] V.C. Hascall, "Interaction of cartilage proteoglycans with hyaluronic acid", *Journal of Supramolecular Structure,* **7**, (1) 1977, pp. 101-120.

[48] P.A. Bottomley, T.H. Foster, R.E. Argersinger, and L.M. Pfeifer, "A review of normal tissue hydrogen NMR relaxation times and relaxation mechanisms from 1- 100 MHz: Dependence on tissue type, NMR frequency, temperature, species, excision, and age", *Medical Physics,* **11**, (4) 1984, pp. 425-448.

[49] G. Adam, C. Nolte-ernsting, A. Prescher, M. Bühne, K. Bruchmüller, W. Küpper, and R.W. Günther, "Experimental hyaline cartilage lesions: Two-dimensional spin-echo versus three-dimensional gradient-echo MR imaging", *Journal of Magnetic Resonance Imaging,* **1**, (6) 1991, pp. 665-672.

[50] D. Burstein, M.L. Gray, A.L. Hartman, R. Gipe, and B.D. Foy, "Diffusion of small solutes in cartilage as measured by nuclear magnetic resonance (NMR) spectroscopy and imaging", *Journal of Orthopaedic Research*, **11**, (4) 1993, pp. 465-478.

[51] G. Bacic, K.J. Liu, F. Goda, P.J. Hoopes, G.M. Rosen, and H.M. Swartz, "MRI contrast enhanced study of cartilage proteoglycan degradation in the rabbit knee", *Magnetic Resonance in Medicine,* **37**, (5) 1997, pp. 764-768.

[52] R.G. Allen, D. Burstein, and M.L. Gray, "Monitoring glycosaminoglycan replenishment in cartilage explants with gadolinium-enhanced magnetic resonance imaging", *Journal of Orthopaedic Research,* **17**, (3) 1999, pp. 430-436.

[53] M. Ghiassi-Nejad, P.A. Torzilli, H. Peemoeller, and M.M. Pintar, "Proton spin– spin relaxation study of molecular dynamics and proteoglycan hydration in articular cartilage", *Biomaterials,* **21**, (20) 2000, pp. 2089-2095.

[54] P.J. Lattanzio, K.W. Marshall, A.Z. Damyanovich, and H. Peemoeller, "Macromolecule and water magnetization exchange modeling in articular cartilage", *Magnetic Resonance in Medicine,* **44**, (6) 2000, pp. 840-851.

[55] T.J. Swift and O.G. Fritz Jr, "A proton spin-echo study of the state of water in frog nerves", *Biophysical Journal,* **9**, (1) 1969, pp. 54-59.

[56] C.F. Hazlewood, D.C. Chang, B.L. Nichols, and D.E. Woessner, "Nuclear magnetic resonance transverse relaxation times of water protons in skeletal muscle", *Biophysical Journal,* **14**, (8) 1974, pp. 583-606.

[57] V. Vasilescu, E. Katona, V. Simplaceanu, and D. Demco, "Water compartments in the myelinated nerve. III. Pulsed NMR result", *Experientia,* **34**, (11) 1978, pp. 1443-1444.

[58] P. Belton and R. Ratcliffe, "NMR and compartmentation in biological tissues", *Progress in Nuclear Magnetic Resonance Spectroscopy*, **17**, 1985, pp. 241-279.

[59] R.M. Henkelman, G.J. Stanisz, J.K. Kim, and M.J. Bronskill, "Anisotropy of NMR properties of tissues", *Magnetic Resonance in Medicine,* **32**, (5) 1994, pp. 592-601.

[60] Y. Xia, "Relaxation anisotropy in cartilage by NMR microscopy (μMRI) at 14-μm resolution", *Magnetic Resonance in Medicine,* **39**, (6) 1998, pp. 941-949.

[61] S. Zheng and Y. Xia, "On the measurement of multi-component T 2 relaxation in cartilage by MR spectroscopy and imaging", *Magnetic Resonance Imaging,* **28**, (4) 2010, pp. 537-545.

[62] M.D. Crema, F.W. Roemer, M.D. Marra, D. Burstein, G.E. Gold, F. Eckstein, T. Baum, T.J. Mosher, J.A. Carrino, and A. Guermazi, "Articular Cartilage in the Knee: Current MR Imaging Techniques and Applications in Clinical Practice and Research", *Radiographics,* **31**, (1) 2011, pp. 37-61.

[63] N. Wang and Y. Xia, "Dependencies of multi-component T_2 and $T_{1\rho}$ relaxation on the anisotropy of collagen fibrils in bovine nasal cartilage", *Journal of Magnetic Resonance,* **212**, (1) 2011, pp. 124-132.

[64] B.J. Dardzinski, T.J. Mosher, S. Li, M.A. Van Slyke, and M.B. Smith, "Spatial variation of T_2 in human articular cartilage", *Radiology,* **205**, (2) 1997, pp. 546-550.

[65] Y. Xia, J.B. Moody, and H. Alhadlaq, "Orientational dependence of T_2 relaxation in articular cartilage: A microscopic MRI (μMRI) study", *Magnetic Resonance in Medicine,* **48**, (3) 2002, pp. 460-469.

[66] E. Lammentausta, P. Kiviranta, M. Nissi, M. Laasanen, I. Kiviranta, M. Nieminen, and J. Jurvelin, "T_2 relaxation time and delayed gadolinium-enhanced MRI of cartilage (dGEMRIC) of human patellar cartilage at 1.5 T and 9.4 T: Relationships with tissue mechanical properties", *Journal of Orthopaedic Research,* **24**, (3) 2006, pp. 366-374.

[67] N. Wang and Y. Xia, "Depth and orientational dependencies of MRI T(2) and T(1rho) sensitivities towards trypsin degradation and Gd-DTPA(2-) presence in articular cartilage at microscopic resolution", *Magnetic Resonance Imaging,* **30**, (3) 2012, pp. 361-370.

[68] V. Mlynarik, P. Szomolanyi, R. Toffanin, F. Vittur, and S. Trattnig, "Transverse relaxation mechanisms in articular cartilage", *Journal of Magnetic Resonance,* **169**, (2) 2004, pp. 300-307.

[69] R.G. Bryant, D.A. Mendelson, and C.C. Lester, "The magnetic- field dependence of proton spin relaxation in tissues", *Magnetic Resonance in Medicine,* **21**, (1) 1991, pp. 117-126.

[70] U. Duvvuri, R. Reddy, S.D. Patel, J.H. Kaufman, J.B. Kneeland, and J.S. Leigh, "$T_{1\rho}$ - relaxation in articular cartilage: Effects of enzymatic degradation", *Magnetic Resonance in Medicine*, **38**, (6) 1997, pp. 863-867.

[71] R.R. Regatte, S.V. Akella, A. Borthakur, J.B. Kneeland, and R. Reddy, "Proteoglycan depletion–induced changes in transverse relaxation maps of cartilage: comparison of T_2 and $T_{1\rho}$", *Academic Radiology*, **9**, (12) 2002, pp. 1388-1394.

[72] L.S. Lohmander, M.W. Lark, L. Dahlberg, L.A. Walakovits, and H. Roos, "Cartilage matrix metabolism in osteoarthritis: markers in synovial fluid, serum, and urine", *Clinical Biochemistry*, **25**, (3) 1992, pp. 167-174.

[73] A. Damyanovich, J. Staples, and K. Marshall, "1 H NMR investigation of changes in the metabolic profile of synovial fluid in bilateral canine osteoarthritis with unilateral joint denervation", *Osteoarthritis and Cartilage*, **7**, (2) 1999, pp. 165-172.

[74] T.L. Ceckler, S.D. Wolff, V. YIP, S.A. Simon, and R.S. Balaban, "Dynamic and chemical factors factors affecting water proton relaxation by macromolecules", *Journal of Magnetic Resonance*, **98**, (3) 1992, pp. 637-645.

[75] G.D. Fullerton, E. Nes, M. Amurao, A. Rahal, L. Krasnosselskaia, and I. Cameron, "An NMR method to characterize multiple water compartments on mammalian collagen", *Cell Biology International*, **30**, (1) 2006, pp. 66-73.

[76] F. Loix, F.M.F. Simões, and B. Loret, "Articular cartilage with intra and extrafibrillar waters – Simulations of mechanical and chemical loadings by the finite element method", *Computer Methods in Applied Mechanics and Engineering*, **197**, (51-52) 2008, pp. 4840-4857.

[77] D.K. Kim, T.L. Ceckler, V.C. Hascall, A. Calabro, and R.S. Balaban, "Analysis of water- macromolecule proton magnetization transfer in articular cartilage", *Magnetic Resonance in Medicine*, **29**, (2) 1993, pp. 211.

[78] D. Tzou, S. Lee, and H.N. Yeung, "Temperature dependence and phase transition of proton relaxation of hydrated collagen in intact beef tendon specimens via cross-relaxation spectroscopy", *Magnetic Resonance in Medicine*, **37**, (3) 1997, pp. 359-365.

[79] G.D. Fullerton and M.R. Amurao, "Evidence that collagen and tendon have monolayer water coverage in the native state", *Cell Biology International*, **30**, (1) 2006, pp. 56-65.

[80] C.L. Haskin, G.D. Fullerton, and I.L. Cameron, "Freezing, Flow and Proton NMR Properties of Water Compartments in the Temporomandibular Disc," *Water and the Cell*, Springer, , 2006, pp. 341-352.

[81] D. Huster, J. Schiller, and K. Arnold, "Comparison of collagen dynamics in articular cartilage and isolated fibrils by solid-state NMR spectroscopy", *Magnetic Resonance in Medicine*, **48**, (4) 2002, pp. 624-632.

[82] D. Huster, J. Schiller, and K. Arnold, "Dynamics of collagen in articular cartilage studied by solid-state NMR methods," *Cartilage and Osteoarthritis*, Springer, , 2004, pp. 303-318.

[83] H. Saito and M. Yokoi, "A ^{13}C NMR study on collagens in the solid state: hydration/dehydration-induced conformational change of collagen and detection of internal motions", *Journal of Biochemistry*, **111**, (3) 1992, pp. 376-382.

[84] J. Schiller, J. Arnhold, and K. Arnold, "Nuclear magnetic resonance and mass spectrometric studies on the action of proteases on pig articular cartilage", *Zeitschrift für Naturforschung C*, **53**, (11-12) 1998, pp. 1072-1080.

[85] P. Lattanzio, K.W. Marshall, A.Z. Damyanovich, and H. Peemoeller, "Characterization of proteoglycan depletion in articular cartilage using two-dimensional time domain nuclear magnetic resonance", *Magnetic Resonance in Medicine*, **54**, (6) 2005, pp. 1397-1402.

[86] H.R. Moody, C.P. Brown, J. Bowden, R.W. Crawford, D. McElwain, and A. Oloyede, "In vitro degradation of articular cartilage: does trypsin treatment produce consistent results?", *Journal of Anatomy*, **209**, (2) 2006, pp. 259-267.

[87] R.M. Henkelman, X. Huang, Q. Xiang, G.J. Stanisz, S.D. Swanson, and M.J. Bronskill, "Quantitative interpretation of magnetization transfer", *Magnetic Resonance in Medicine*, **29**, (6) 1993, pp. 759-766.

[88] J.J. Tessier, N. Dillon, T.A. Carpenter, and L.D. Hall, "Interpretation of magnetization transfer and proton cross-relaxation spectra of biological tissues", *Journal of Magnetic Resonance, Series B*, **107**, (2) 1995, pp. 138-144.

[89] R.S. Adler, S.D. Swanson, and H.N. Yeung, "A Three- Component Model for Magnetization Transfer. Solution by Projection-Operator Technique, and Application to Cartilage", *Journal of Magnetic Resonance, Series B,* **110**, (1) 1996, pp. 1-8.

[90] D.F. Gochberg, R.P. Kennan, and J.C. Gore, "Quantitative studies of magnetization transfer by selective excitation and T 1 recovery", *Magnetic Resonance in Medicine,* **38**, (2) 1997, pp. 224-231.

[91] G. Morris and A. Freemont, "Direct observation of the magnetization exchange dynamics responsible for magnetization transfer contrast in human cartilage in vitro", *Magnetic Resonance in Medicine,* **28**, (1) 1992, pp. 97-104.

[92] T. Nightingale, A. Mackay, R.H. Pearce, K.P. Whittall, and B. Flak, "A model of unloaded human intervertebral disk based on NMR relaxation", *Magnetic Resonance in Medicine,* **43**, (1) 2000, pp. 34-44.

[93] M.T. Nieminen, J. Rieppo, J. Töyräs, J.M. Hakumäki, J. Silvennoinen, M.M. Hyttinen, H.J. Helminen, and J.S. Jurvelin, "T_2 relaxation reveals spatial collagen architecture in articular cartilage: a comparative quantitative MRI and polarized light microscopic study", *Magnetic Resonance in Medicine,* **46**, (3) 2001, pp. 487-493.

[94] D.A. Reiter, P. Lin, K.W. Fishbein, and R.G. Spencer, "Multicomponent T2 relaxation analysis in cartilage", *Magnetic Resonance in Medicine,* **61**, (4) 2009, pp. 803-809.

[95] L.M. Broche, G.P. Ashcroft, and D.J. Lurie, "Detection of osteoarthritis in knee and hip joints by fast field-cycling NMR", *Magnetic Resonance in Medicine,* **68**, (2) 2011, pp. 358–362.

[96] X. Li, C.B. Ma, T.M. Link, D. Castillo, G. Blumenkrantz, J. Lozano, J. Carballido-Gamio, M. Ries, and S. Majumdar, "In vivo T 1ρ and T 2 mapping of articular cartilage in osteoarthritis of the knee using 3T MRI", *Osteoarthritis and cartilage,* **15**, (7) 2007, pp. 789-797.

[97] C. Ficat and A. Maroudas, "Cartilage of the patella. Topographical variation of glycosaminoglycan content in normal and fibrillated tissue", *Annals of the Rheumatic Diseases,* **34**, (6) 1975, pp. 515-519.

[98] Y. Kusaka, W. Gründer, H. Rumpel, K. Dannhauer, and K. Gersonde, "MR microimaging of articular cartilage and contrast enhancement by manganese ions", *Magnetic Resonance in Medicine,* **24**, (1) 1992, pp. 137-148.

[99] McKeag, Smith, Edminster, Laird, Clark and Herron. , "Estimating the severity of osteoarthritis with magnetic resonance spectroscopy", *Seminars in arthritis and rheumatism* Elsevier 1992, pp.227-238.

[100] A. Werner and W. Gründer, "Calcium-induced structural changes of cartilage proteoglycans studied by 1H NMR relaxometry and diffusion measurements", *Magnetic Resonance in Medicine,* **41**, (1) 1999, pp. 43-50.

[101] J. Schiller, L. Naji, D. Huster, J. Kaufmann, and K. Arnold, "1H and13C HR-MAS NMR investigations on native and enzymatically digested bovine nasal cartilage", *Magnetic Resonance Materials in Physics, Biology and Medicine,* **13**, (1) 2001, pp. 19-27.

[102] M. Borel, P. Pastoureau, J. Papon, J.C. Madelmont, N. Moins, J. Maublant, and E. Miot-Noirault, "Longitudinal profiling of articular cartilage degradation in osteoarthritis by high-resolution magic angle spinning 1H NMR spectroscopy: experimental study in the meniscectomized guinea pig model", *Journal of Proteome Research,* **8**, (5) 2009, pp. 2594-2600.

[103] H.A. Scheidt, S. Schibur, A. Magalhaes, E.R. de Azevedo, T.J. Bonagamba, O. Pascui, R. Schulz, D. Reichert, and D. Huster, "The mobility of chondroitin sulfate in articular and artificial cartilage characterized by ^{13}C magic-angle spinning NMR spectroscopy", *Biopolymers,* **93**, (6) 2010, pp. 520-532.

[104] L. Naji, J. Kaufmann, D. Huster, J. Schiller, and K. Arnold, "13 C NMR relaxation studies on cartilage and cartilage components", *Carbohydrate Research,* **327**, (4) 2000, pp. 439-446.

[105] J. Schiller, S. Benard, S. Reichl, J. Arnhold, and K. Arnold, "Cartilage degradation by stimulated human neutrophils: reactive oxygen species decrease markedly the activity of proteolytic enzymes", *Chemistry & Biology,* **7**, (8) 2000, pp. 557-568.

[106] J. Schiller and D. Huster, "New methods to study the composition and structure of the extracellular matrix in natural and bioengineered tissues", *Biomatter,* **2**, (3) 2012, pp. 115-131.

[107] W. Ling, R.R. Regatte, M.E. Schweitzer, and A. Jerschow, "Characterization of bovine patellar cartilage by NMR", *NMR in Biomedicine,* **21**, (3) 2008, pp. 289-295.

[108] H.A. Alhadlaq, Y. Xia, J.B. Moody, and J.R. Matyas, "Detecting structural changes in early experimental osteoarthritis of tibial cartilage by microscopic magnetic resonance imaging and polarised light microscopy", *Annals of the Rheumatic Diseases,* **63**, (6) 2004, pp. 709-717.

[109] Y. Xia, "Heterogeneity of cartilage laminae in MR imaging", *Journal of Magnetic Resonance Imaging,* **11**, (6) 2000, pp. 686-693.

[110] H. Muir, P. Bullough, and A. Maroudas, "The distribution of collagen in human articular cartilage with some of its physiological implications", *The Journal of Bone and Joint Surgery,* **52**, (3) 1970, pp. 554-563.

[111] O. Gonen, J.B. Murdoch, R. Stoyanova, and G. Goelman, "3D multivoxel proton spectroscopy of human brain using a hybrid of 8th-order hadamard encoding with 2D chemical shift imaging", *Magnetic Resonance in Medicine,* **39**, (1) 1998, pp. 34-40.

[112] S. Meiboom and D. Gill, "Modified spin-echo method for measuring nuclear relaxation times", *Review of Scientific Instruments,* **29**, (8) 1958, pp. 688-691.

[113] H.Y. Carr and E.M. Purcell, "Effects of diffusion on free precession in nuclear magnetic resonance experiments", *Physical Review,* **94**, (3) 1954, pp. 630.

[114] D.W. Marquardt, "An Algorithm for Least- Squares Estimation of Nonlinear Parameters", *Journal of the Society for Industrial & Applied Mathematics,* **11**, (2) 1963, pp. 431-441.

[115] J. Stanley and H. Peemoeller, "Characterization of polyproline-water system by NMR spin grouping and exchange analysis", *Journal de Physique II,* **1**, (12) 1991, pp. 1491-1503.

[116] W. Weglarz and H. Peemoeller, "Observation of coupling across the ice–water interface by 2D time domain NMR", *Journal of Magnetic Resonance,* **124**, (2) 1997, pp. 484-485.

[117] M. Niknam, J. Liang, J. Walia, and H. Peemoeller, "Chemical exchange and spectral coalescence in low-hydration MCM-41 studied by proton NMR", *Microporous and Mesoporous Materials*, **162**, 2012, pp. 136-142.

[118] H. Peemoeller and M. Pintar, "Two-dimensional time-evolution approach for resolving a composite free-induction decay", *Journal of Magnetic Resonance*, **41**, (2) 1980, pp. 358-360.

[119] W. Weglarz and H. Haranczyk, "CracSpin-the computer code for the two dimensional decomposition of nuclear relaxation function", *Inst. Fizyki, Uniwersytet Jagiellonski, Cracow (Poland)*, **29**, (14) 1994, pp.

[120] R.W. Farndale, C.A. Sayers, and A.J. Barrett, "A Direct Spectrophotometric Microassay for Sulfated Glycosaminoglycans in Cartilage Cultures", *Connective Tissue Research*, **9**, (4) 1982, pp. 247-248.

[121] A. Mucci, L. Schenetti, and N. Volpi, "^{1}H and ^{13}C nuclear magnetic resonance identification and characterization of components of chondroitin sulfates of various origin", *Carbohydrate Polymers*, **41**, (1) 2000, pp. 37-45.

[122] J. Schiller, L. Naji, D. Huster, J. Kaufmann, and K. Arnold, "H-1 and C-13 HR-MAS NMR investigations on native and enzymatically digested bovine nasal cartilage", *Magnetic Resonance Materials in Physics Biology and Medicine*, **13**, (1) 2001, pp. 19-27.

[123] W. Ling, R.R. Regatte, M.E. Schweitzer, and A. Jerschow, "Characterization of bovine patellar cartilage by NMR", *NMR in biomedicine*, **21**, (3) 2008, pp. 289-295.

[124] W.M. Rhee and R.A. Berg, "Glycosaminoglycan-synthetic polymer conjugates", *United State Patent*, **5**, (476) 1995, pp. 666.